NORTHWESTERN UNIVERSITY

Quasicrystalline Thin Films: Growth, Structure and Interface

A DISSERTATION

SUBMITTED TO THE GRADUATE SCHOOL

IN PARTIAL FULFILLMENT OF THE REQUIREMENTS

for the degree

DOCTOR OF PHILOSOPHY

Field of Materials Science and Engineering

By

Edy Widjaja

EVANSTON, ILLINOIS

June 2004

ABSTRACT

Quasicrystalline Thin Films: Growth, Structure and Interface

Edy Widjaja

Quasicrystals are orientation-ordered structures with classically forbidden rotation symmetries (e.g. 5-fold and 10-fold rotation axes) which are incompatible with periodic translational ordering. Quasicrystalline materials exhibit properties that are very different from conventional metallic materials.

Two systems of quasicrystalline alloys have been studied in this thesis work: decagonal Al-Cu-Fe-Cr and icosahedral Al-Cu-Fe. Thin films were grown by magnetron sputtering system on various substrates and studied by Transmission Electron Microscopy, X-ray Photoelectron Spectroscopy, Scanning Electron Microscopy and Energy Dispersive X-ray Spectroscopy.

The growth mode at room and elevated temperatures has been investigated in-situ and ex-situ. An microstructural evolution study during the phase transformation to the quasicrystalline state has also been performed. Epitaxial quasicrystalline thin films have been successfully grown on crystalline substrates. A

coincidence reciprocal lattice planes model was developed to describe the interface of quasicrystals and crystals.

Approved by

Professor Laurence D. Marks

Department of Materials Science and Engineering

Northwestern University, Evanston, IL 60201, USA

Acknowledgements

God is good. Everything was made possible through the grace and mercy of the Triune God. Being the Truth, He is the one who made the search for the truth possible and wonderful. *Not to us, O LORD, not to us but to your name be the glory, because of your love and faithfulness.*

In more than four years of my graduate school, there have been many people who contributed to my life in so many ways. There were people in Marks' research group and Department of Materials Science and Engineering, whose contribution made this dissertation possible. I had many mentors, co-workers and fellow-learners. There were friends who kept me sane and gave me encouragement to persevere. They were people who made the days and nights and weekends in the lab bearable, even beautiful. They gave a sense of purpose when the busyness and frustration kicked in; they pointed to the beauty of searching for the truth; they were after all: friends. And some will remain as great friends for a much distant future.

I would like to express my gratitude to the people who have contributed much during the years of my graduate life. They have contributed in many ways that it is impossible to list all of them, nor that it is possible to list everybody to whom

I owe my gratitude. Here are a few of them, for what I will remember them best for:

- Professor Laurence Marks, my thesis adviser: whose *'Just do it!'* and *'Figure it out'* have made me a better student and scientist. Thanks for teaching me how to think.
- Sujanto Widjaja, my beloved brother: who instigated and accompanied my journey to PhD-ville. Thanks for being the big brother. Thanks for your guidance and constant encouragement.
- Dad and Mom: for being a reason for perseverance. *Children's children are a crown to the aged, and parents are the pride of their children*
- Professor Scott Barnett, first year thesis adviser: for leading me into the beauty of the world of thin films.
- My dissertation committee members (Profs. Laurence D. Marks, Scott Barnett, David Dunand, Leon Keer): for having faith in me and allowing me to be a member of the PhD-ville.
- Arun Subramanian, a colleague, a friend and a fellow-sojourner: for discussion and assistance, for spending dark-nights in SPEAR room, for proofreading many of my papers and for a constant encouragement. *I'm like a shooting star, I've come so far, I can't go back to where I used to be.*

- Ian Widlow: for teaching me about UHV system and magnetron sputtering, for being a good model of a safety officer.
- Dr. Ilwon Kim: for introducing me thin film depositions in my first year.
- Dr. Natasha Erdman: for teaching me the delicacy of TEM sample preparation.
- Monica Salud: for acquainting me with SPEAR.
- Chris Own: for working together in the first year of quasicrystals project, for being available for all my computer-related problems.
- Yingmin Wang: for asking a few but very important and intriguing questions about my research.
- Dr. Lisen Cheng: for teaching me TEM skills and for the one year of working together on SPEAR.
- Dr. Xing Zhong Li: for teaching me all I need to know about quasicrystals and for the TEM training.
- Ann Chiaramonti: for lending me bike to run many errands and for giving away free stuff that sit happily on my table.
- Arno Merkle: for co-working on baby-sitting SINBAD and taking white-light interferometer data, for being available for lunch anywhere anytime.
- Courtney Lanier: for making life in my research group much more cheerful, for constant supply of chocolates and for chauffeuring me. *Nice!*

- Dr. Wen An Chiou: for assistance in TEM and for making days in EPIC very enjoyable.
- Professor Yip Wah Chung: for provoking thoughts about my research and career.
- Joanna and Sharon: for assisting me in many academic/non-academic issues through out the years.
- Jim Poulos and Ken Eberly: for curing H-9000 when it is misbehaving.
- Yashusi Mizutani, Dr. Jin-won Jung, Dr. Arup Saha: for all the years of group study and tackling homeworks.
- Duane Goodner and Stephan Gerstl: for infinite number of lunches we had together.
- Dr. Kitty Lee: for being there from the beginning of the journey, for encouragement and faith in me.
- Dr. Kitty Lee, Dr. Martin Yan, Dr. Luzy Zhang: for walking the journey together.
- Shawn Nicholson, Mr. and Mrs. Beem: for introducing 'America' to me.
- Sarmauli Manurung and Maya Alamsaputra: for hours of phone call, for listening and making God real in daily life, for love and encouragement. For being a big and a little sister.
- Matt Sterenberg: for keeping me sane and accountable, for Mr. Blue and for introducing me to the world of desserts. *Thank you very much indeed!*

- Scott Norris: for excessive handshakes and hugs, for being there at tough times and for patience. *Is that cow brain?*
- Young-cheol Yoon: for big lunches and bigger dinners, for asking tough questions in my life. *How y'doin?*
- Louis Luangkesorn and Randy Claussen: for advices, for getting me to think about life of integrity, for introducing the world of camping and for being big brothers.
- Pastor and Mrs. Bergfalk: for love and prayers, for spiritual guidance.
- The Edens: Dave, Deanna, Rebekah, Sara and Hannah: for being a family for me, for love and prayers, for all the great times and for giving me the three best girls in my life.
- Small groups (Engelhart 2000, Randy's and Liz', Kinnears', Calvary's, Heart and Mind): for listening, for prayers and encouragements, for being real, and for lots of good time together.
- GCF girls (KEC, HST, PH, HL, YI, CL, GY, CC and others): for flavoring my life, for emphatic ears and for being prayer warriors. Thanks for being the best part in my last 18 months. *You have touched my life in a way I have never been touched before. In what way is it again?*
- POFTUI94 (MRNS, LS, AS, and others): for gift of friendship, for being co-walkers of faith, for constant '*when will you be done?*'
- PMKJ: for accountibility and prayers, for challenging me in *what's next.*

- The Simpsons: the family who constantly provides laughters and lessons in life. *Doh!*
- To many whom I cannot list. To those who contributed tremendously in my first 2-3 years of my graduate life, to whom the cruel time has eroded from my mind, to whom I neglect in my forgetfulness or ignorance.

Contents

List of Tables

List of Figures

CHAPTER 1

Introduction

1.1. Quasicrystals

Plato introduced a three dimensional (3D) analogue to the pentagon, the icosahedron, as one of the divine geometrical forms now known as the Platonic solids. It is characterized by fivefold, threefold and twofold rotational symmetries (Fig 1.1). Examples of pentagonal and icosahedral symmetries abound in nature, particularly in biological systems. Despite their prevalence in nature, these rotational symmetries are absent in crystals. Fundamental arguments demonstrate that they are incompatible with translational periodicity (Kittel 1976; Vainshtein 1981). Twinned assemblies of crystallites can produce diffraction patterns with a pseudo-fivefold symmetry; a careful examination, however, shows that all spots can be indexed to the crystal phases. An example is shown in Fig. 1.2.

Shechtman et al. (1984a) surprised the scientific community by reporting the existence of a metallic solid, $Al_{86}Mn_{14}$, that produced an electron diffraction pattern, shown in Fig. 1.3, with sharp spots arrayed in a tenfold rotationally symmetric arrangement. Sharp spots in electron diffraction are traditionally taken to indicate translational periodicity. Further diffraction studies confirmed that this new phase demonstrated the full rotational symmetry of the icosahedral point group.

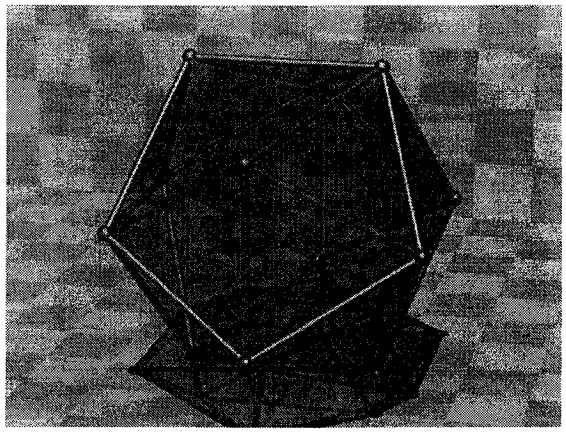

Figure 1.1. An icosahedron

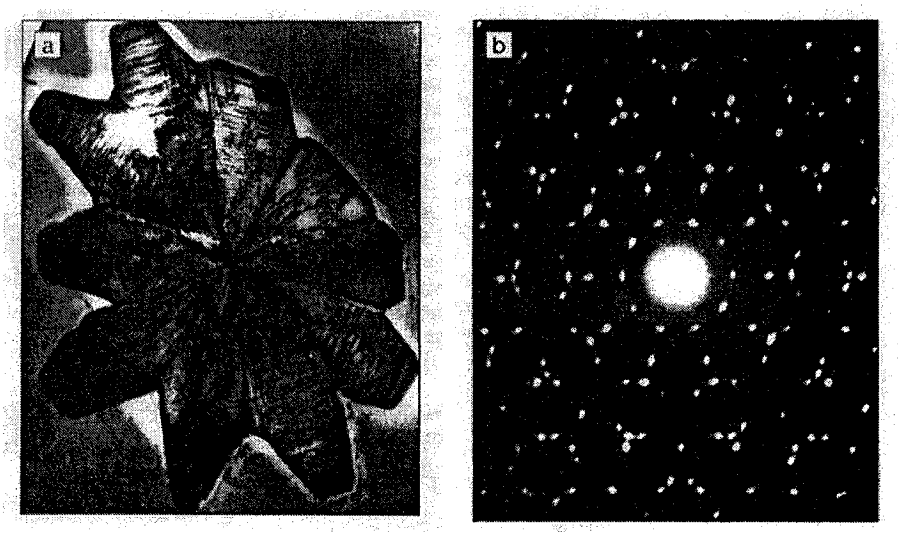

Figure 1.2. Quasi five-fold pattern from twin crystals. a) TEM bright field b) Quasi 5-fold diffraction pattern (Shechtman and Lang 1997)

Since then, the icosahedral phase, sometimes called i-phase or ψ-phase, has been found in a variety of systems. It appears to be a candidate for the most common structure in 3d transition metal alloys (Kelton 1993). Other phases

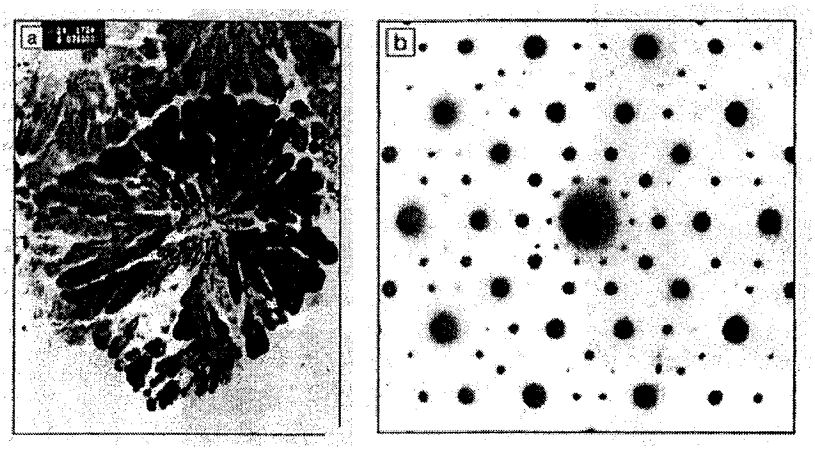

Figure 1.3. Icosahedral grain in Al-Mn alloys a) TEM bright field b) 5-fold diffraction pattern. (Shechtman 1990)

that produce similarly sharp diffraction patterns with different, but still classically forbidden, symmetries have been also discovered. One other notable phase is the decagonal phase, having one periodic axis orthogonal to two non-periodic axes. Collectively, these non-periodic phases are called quasicrystals - a term coined by Levine and Steinhardt (1984) as an abbreviation for quasi-periodic crystals.

Quasicrystals are well-ordered structures with classically forbidden rotation symmetries (e.g. fivefold and 10-fold rotation axes) which are incompatible with traditional periodic lattice ordering. They are metallic alloys, often but not necessarily aluminum-rich. They are quite abundant and quasicrystalline phases have even been observed in steels. In the years immediately following their discovery in 1984, much research focused upon the mathematical aspects, crystallography, atomic and electronic structure, and the issue of whether quasicrystalline phases really represented a new class of materials. The subject of technological applications

has only recently raised substantial interest in the course of a systematic investigation of the properties (Gahler et al. 2000). This was made possible through the ability to grow large single quasicrystals. Today commercial products are on the market which are competitive due to their special combination of properties (Dubois 2000).

1.1.1. Structure of Quasicrystals

1.1.1.1. One Dimensional Quasicrystals. Quasicrystals constitute a new class of condensed matter characterized by a non-crystallographic orientational symmetry. Additionally they are also quasiperiodic. The most familiar example of a one dimensional (1D) quasiperiodic function is the Fibonacci series, resulting originally from the solution to an idealized problem related to the proliferation of rabbits. Representing a baby rabbit by S and an adult rabbit by L, and applying the simple substitution rule that each month a baby rabbit will reach adulthood, will result in the sequence S|L|SL|LSL|SLLSL|... With repeated iterations, the ratio L/S equals precisely τ, the golden mean [$\tau = (1+\sqrt{5})/2$].

A 1D example is shown in Fig. 1.4. The 1D quasicrystal (Fibonacci-sequence) is generated by the projection of a strip of a two dimensional (2D) lattice with slope τ relative to the 2D lattice vector. In a similar way 2D and three dimensional (3D) quasilattices can be obtained projecting strips of five dimensional and six

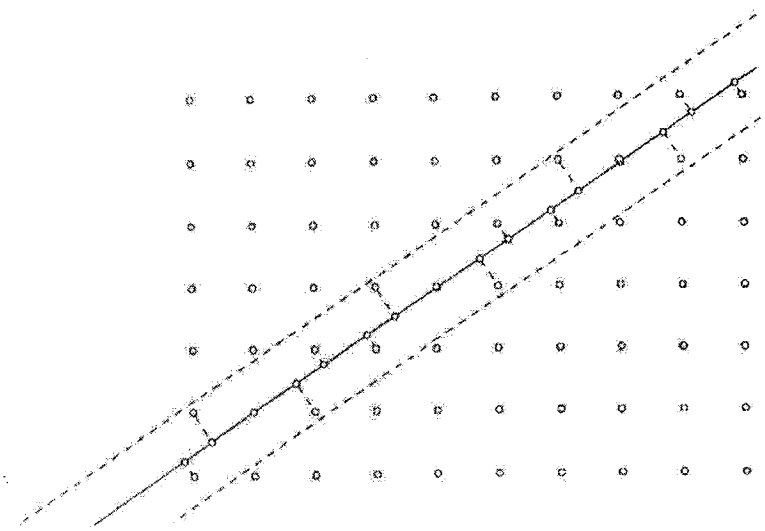

Figure 1.4. A one-dimensional quasicrystals generated by projecting a two-dimensional periodic lattice. (Senechal 1995)

dimensonal periodic lattices, respectively [1]. If the irrational golden number τ is approximated by the rational ratio of two consecutive Fibonacci numbers, such as $F_{n+1}/F_n = 1/0,\ 1/1,\ 2/1,\ (F_{n+1} = F_n + F_{n-1})$ then a crystalline phase called an approximant is produced.

1.1.1.2. Three Dimensional Quasicrystals: Icosahedral. The icosahedral phase forms most readily in aluminum-3d transition (Al-TM) and titanium-3d

[1]It has been demonstrated (Duneau and Katz 1985; Elser 1985, 1986; Kalugin et al. 1985; Gahler and Rhyner 1986; Conway and Knowles 1986; Whittaker and Whittaker 1988) that all quasiperiodic tilings may be obtained by selected projection of the respective nd periodical lattices. The nd space V in which the lattices are embedded can be decomposed into two mutually orthogonal subspaces $V=(V_E,V_I)$. If the nd lattice is inclined with an irrational slope relative to V_E the projection of a strip of the nd lattice upon V_E gives an aperiodic structure. The selection rule, which determines the strip (window function), can be derived from the projection of the nd lattice upon V_I. All lattice points which come to lie inside of the projected nd unit cell (acceptance volume) belong to the strip, which subsequently is projected along V_I. An introduction to the Fibonacci series and projection from higher dimension can be found in books by Janot (1992) and Senechal (1995).

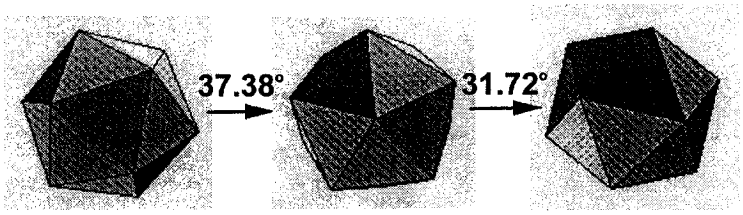

Figure 1.5. An icosahedron viewed along a) threefold axis b) fivefold axis and c) twofold axis. Rotation angles between these orientations are indicated.

transition (Ti-TM) metal alloys; partial lists of alloys reported to contain the i-phase, as listed by Steurer (1990), are presented in Table 1.1 and 1.2. As demonstrated in Fig. 1.5, the locations and symmetries of the TEM diffraction patterns of these alloys agree with the elements of the icosahedral point group, $m\bar{3}5$, showing the expected fivefold, threefold, and twofold rotational symmetries. This icosahedral point group is inconsistent with any crystallographic space group previously known. Hence this structure represents a new type of condensed phase with an extended orientational order but lacks the expected translational symmetry.

The i-phase is unlike the periodic phases whose diffraction patterns along a particular direction have distances between the spots in integer ratios. It has ratios of the power of the golden mean, τ. Along a prominent radial direction the spots can be indexed using two length scales, l and τl, suggesting an incommensurate structure.

Table 1.1. Systems with icosahedral phases. (Steurer 1990)

Alloy systems	References
$Al_{86}Mn_{14}$	Shechtman et al. (1984a)
$Al_{86}Fe_{14}$	Bancel et al. (1985)
$Al_{85}Cr_{15}$	Zhang et al. (1988)
	Inoue et al. (1987b)
Al_4Ru	Anlage et al. (1988)
$Al_{78}Re_{22}$	Bancel and Heiney (1986)
Al_4-V	Chen et al. (1987)
Al-Mo	Chen et al. (1987)
Al-W	Chen et al. (1987)
$Al(Cr_{1-x}Fe_x$	Schurer et al. (1988)
$Al(Mn_{1-x}Fe_x$	Schurer et al. (1988)
$Al_{62}Cr_{19}Si_{19}$	Inoue et al. (1987a)
$Al_{60}Cr_{20}Ge_{20}$	Chen and Inoue (1987)
Al-Cr-Ru	Bancel and Heiney (1986)
Al-Mn-(Cr,Fe)	Janot et al. (1988)
$Al_{73}Mn_{21}Si_6$	Gratias et al. (1988)
$Al_{55}Mn_{20}Si_{25}$	Inoue and Masumoto (1988)
$Al_{75.5}Mn_{17.5}Ru_4Si_3$	Heiney et al. (1986)
$Al_{74}Mn_{17.6}Fe_{2.4}Si_6$	Ma and Stern (1988)
$Al_{75}Mn_{15}Cr_5Si_5$	Nanao et al. (1987)
$Al_{60}Ge_{20}Mn_{20}$	Tsai et al. (1988b)
$Al_{70}Fe_{20}Ta_{10}$	Tsai et al. (1988a)
$Al_{65}Cu_{20}Mn_{15}$	He et al. (1988a)
	Tsai et al. (1988b)
$Al_{65}Cu_{20}Fe_{15}$	Ebalard and Spaepen (1989)
	Tsai et al. (1988b)
$Al_{65}Cu_{20}Cr_{15}$	Tsai et al. (1988c)
$Al_{65}Cu_{20}V_{15}$	Tsai et al. (1988c)
$Al_{65}Cu_{20}Ru_{15}$	Tsai et al. (1988d)
$Al_{65}Cu_{20}Os_{15}$	
Al_6CuLi_3	Saintfort and Dubost (1986)
	Mai et al. (1987)
Al_6CuMg_4	Sastry et al. (1986)
$Al_{51}Cu_{12.5}(Li_xMg_{36.5-x})$	Shen et al. (1988)
Al_6AuLi_3	Chen et al. (1987)

Table 1.1. Systems with icosahedral phases - continued. (Steurer 1990)

Alloy systems	References
$Al_{51}Zn_{17}Li_{32}$	Chen et al. (1987)
$Al_{50}Mg_{35}Ag_{15}$	Mukhopadhyay et al. (1988)
Al-Ni-Nb	Mukhopadhyay et al. (1988)
$(Al,Zn)_{49}Mg_{32}$	Henley and Elser (1986)
$(Al,Zn,Cu)_{49}Mg_{32}$	Mukhopadhyay et al. (1987)
$Ga_{16}Mg_{32}Zn_{52}$	Ohashi and Spaepen (1987)
	Chen and Inoue (1987)
Ti_2Fe	Dong et al. (1986)
	Kelton et al. (1988)
Ti_2Mn	Kelton et al. (1988)
Ti_2Co	Kelton et al. (1988)
Ti-Ni	Zhang et al. (1985)
$Ti_2(Ni,V)$	Zhang et al. (1985)
Nb-Fe	Kuo (1987)
Mn-Ni-Si	Kuo et al. (1986)
$V_{41}Ni_{36}Si_{23}$	Kuo et al. (1987)
$Pd_{58.8}U_{20.6}Si_{20.6}$	Poon et al. (1985)

1.1.1.3. Two Dimensional Quasicrystals: Decagonal. The decagonal phase with its one periodic axis and two non-periodic axes had been discovered, however not recognized as such, prior to the report of the discovery of icosahedral phase. Sastry et al. (1978) reported the discovery of an unknown complex crystalline phase showing anomalous diffraction in a slowly cooled $Al_{60}Mn_{11}Ni_4$ alloy. Shechtman et al. (1984b), discovering the icosahedral phase, also noticed a similar phase in rapidly quenched Al-Mn alloys with annealing. Finally, Chattopadhyay et al. (1985) and Bendersky (1985) identified this phase as a new, 2D quasicrystal, now known as the decagonal phase. Subsequently, many alloys have been reported to exist in decagonal phase.

The prominent zone axes from the decagonal phase are shown in Fig. 1.6. TEM studies along different rotation axes show similarity with the ψ-phase, however there are important differences. Along one direction (A in Fig. 1.6), a tenfold rotational symmetry with quasiperiodic diffraction spots is obtained. Convergent Beam Electron Diffraction (CBED) studies along this tenfold axis show Higher Order Laue Zones (HOLZ) that are absent in patterns taken from the ψ-phase. The ψ-phase rotation studies about axes that are 36° apart produce a different sequence of diffraction patterns indicate that the symmetry is actually a fivefold inversion symmetry. In contrast, rotation by 90° from the tenfold axis in the decagonal phase reveals two different twofold patterns separated by 18° (G and H in Fig. 1.6). The diffraction patterns in these twofold direction reveals periodicity along the tenfold axis and follow a Fibonacci series in the perpendicular direction. This decagonal structure is then quasiperiodic in two dimensions but periodic in the third dimension (Kelton 1993). Some similarity with the ψ-phase can be seen in pattern (J) and (M and I), which show, respectively, a pseudo-fivefold and pseudo-threefold pattern.

1.1.2. Properties of Quasicrystals

Despite the differences, these new phases, quasicrystals, share many common features with conventional crystalline materials. They contain the equivalent of a Bravais lattice with atoms decorating that lattice. The former gives rise to an

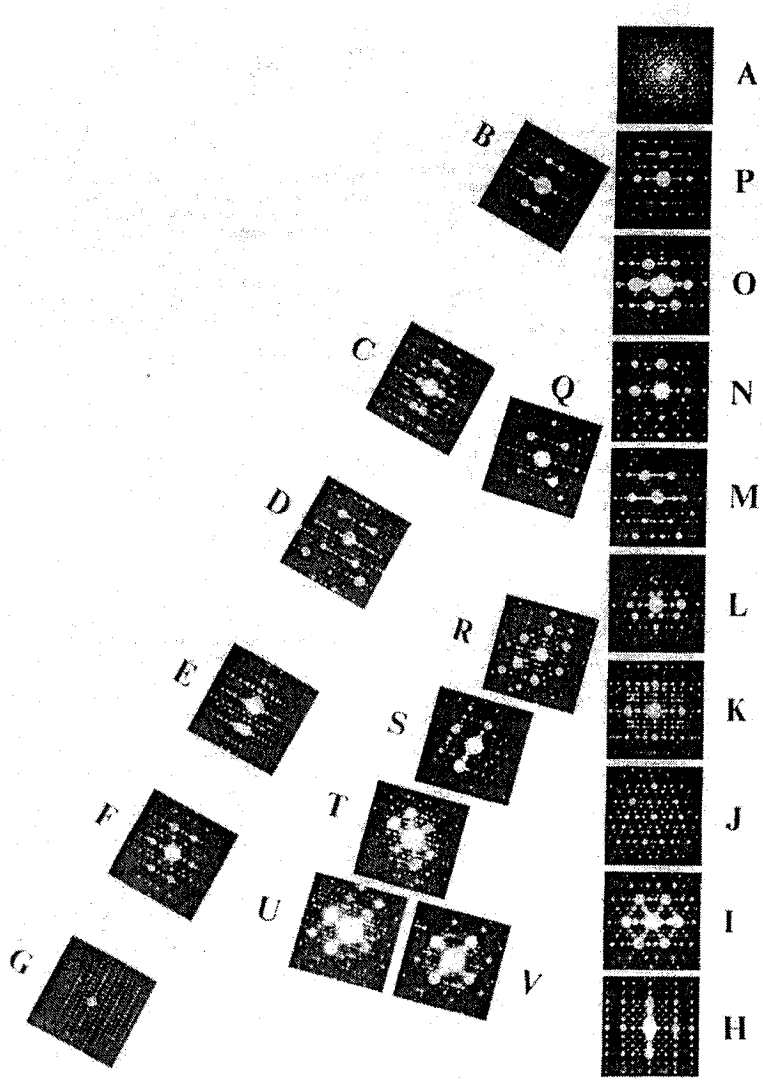

Figure 1.6. Experimentally measured 18° stereographic section of decagonal phase showing SAD patterns for all prominent zone axes, determined from Kikuchi band crossings (Daulton et al. 1991). Further description of these diffraction patterns can be found in Kelton (1993).

Table 1.2. Properties of quasicrystalline materials compared with conventional engineering materials

Materials	Hardness GPa	Fracture Toughness Mpa $m^{1/2}$	Friction Coefficient	Electrical Resistivity $\mu\rho$cm	Thermal Diffusivity $m^2s^1x10^8$
QC Materials	5-10	1	0.05-0.50	700-1000	0.5-1.5
Al Alloys	1-6	20-30	0.5-0.7	3	60-100
Steels	2-8	20-100	0.2-0.8	15-70	15
WC-Cu	13-18	13	0.4-0.8		20-40
Alumina	18-22	5	0.7	10^{20}	10

intrinsic structure factor and the latter a geometric structure factor (Jaric 1986). They contain lattice type defects and they show evidence of chemical ordering.

However, many important differences lead to different and novel behavior. Quasicrystals have new hydrodynamic modes, which are known as phasons. Phasons have no analogue in the ordinary crystals. Additionally, the reciprocal space may be densely filled, and this may lead to exotic electronic properties, since the density of states should contain a dense population of gaps. An extremely high symmetry about specific atomic sites may result in unusual magnetic behavior (Kelton 1993). Quasicrystals also show high hardness and stiffness but low electrical and thermal conductivity, properties that are very different with conventional metallic materials. They also show a very low coefficient of friction (although this is controversial) and low surface energy. Comparisons with some materials are shown in Table 1.3. Research with quasicrystalline materials has also demonstrated many other desirable characteristics such as oxidation and corrosion resistance and unusual optical properties.

1.1.3. Applications of Quasicrystals

The main shortcoming of quasicrystals is their extreme brittleness in bulk form. Fabrication of quasicrystalline components using bulk-forming and machining technologies are not trivial, if not impossible. "This handicap has led to efforts by several groups throughout the worlds - particularly in France, Japan, the United States and Germany - to develop coatings of quasicrystalline materials that could be applied to robust substrates" (Besser and Eisenhammer 1997). The application of quasicrystals as coatings enables the exploitation of their surface properties. They improves the wear resistance of automobile parts and release characteristics of plastic moulding equipment (Besser and Eisenhammer 1997). Since the coatings are 'metallic' and form protective oxides, they can extend the life of components exposed to elevated temperature and oxidizing environments.

While practical uses for the bulk materials remain elusive to date, recent work has shown that coatings of quasicrystals can have spectacular properties. Applications of these materials are not purely in the realm of the potential; they exist already in the realm of the marketplace. High-strength maraging steels, which owe their excellent properties to quasicrystalline precipitate particles, are on the market and are used for surgical needles and instruments and serve as materials for parts in electric razors. Second generation cooking ware utilizing quasicrystalline coatings, shown in Fig.1.7, is on the market benefiting the non-stick properties

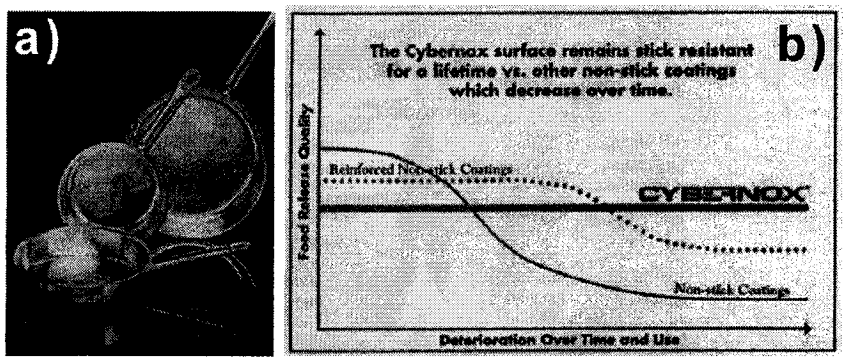

Figure 1.7. a) Cybernox quasicrystalline coated cooking pan b) its performance according to the manufacturer. See Appendix A for references

for food combined with high heat stability and exceptional hardness. This cookware claims superiority over conventional coated cookware and to be impervious to scratching by metal utensils [2].

Dubois (2000) pointed out possible application of quasicrystalline materials in various domains of energy savings, namely thermal insulation, light absorption, power generation and hydrogen storage. Sanchez-Pascual et al. (1999) assessed their application as thermal barriers. Eisenhammer and Lazarov (1994) designed selective quasicrystalline light absorbers by exploiting their optical properties. Cyrot-Lackman et al. (1995) pioneered the idea that certain quasicrystals may be useful for thermopower generation. It has also been shown that titanium-based icosahedral quasicrystals can store large quantities of protons and hence can act as hydrogen-storage media. Other potential applications of the optical properties of quasicrystals are infrared detection (bolometers) and temperature sensors.

[2]however, see Appendix A

A number of potential applications in aircraft engines, in the car industry, in polymer materials and in catalyst are under investigation. A more detailed description on the potential applications of quasicrystals can be found in a paper by Dubois (2000).

1.2. Quasicrystalline Coatings

There are many known routes to synthesize quasicrystalline phases. The first method, employed by Shetchman, is rapid cooling. There are also single-grain quasicrystal synthesis methods that are very useful in creating large single-grain where quasicrystal properties can be measured relatively easily. However, in this section, only methods that are known to synthesize quasicrystalline phases in the form of coatings will be discussed.

Thermal-spray and Physical Vapor Deposition (PVD) techniques share similar steps in forming the coatings: 1) creation of the deposition species, 2) transportation of the species to the substrate, and 3) the formation of the coating on the substrate (Besser and Eisenhammer 1997). The major difference between the two methods is that in the former the deposited species are large molten droplets and in the latter atoms, ions or very small clusters.

Plasma spray has been widely used to synthesize quasicrystalline films. Nevertheless it has its own problems due to porosity and the need for surface finishing. A plasma sprayed coating is a composite material, comprising not only of the deposited materials but also pores, cracks and oxides. It is essential that the coating

process itself as well as the final steps of polishing the surface preserve the appealing properties of the quasicrystal. In some cases, polishing to remove surface roughness induces phase transformations (Dubois 2000).

1.2.1. Plasma Spray

The thick coating route follows basically a three-step process (Dubois et al. 1994b): (i) gas atomization of the liquid alloy, (ii) plasma spraying of this powder to obtain a thick coating on a substrate and (iii) mechanical polishing to get rid of the substantial roughness of the as-deposited coating. In the final step, it is important to reduce the roughness of the surface to the mandatory specification for most applications, e.g. low friction and low adhesion. Mechanical polishing is usually carried out to give a nice surface finish, however due to quasicrystal brittleness and the possibility of phase transition upon mechanical grinding, this process is not trivial.

A few primary problems have been identified in manufacturing Al-Cu-Fe quasicrystalline coatings by thermal spray. The primary one is reduced aluminium content in the deposited coatings compared to the original composition in the starting powders. A practical solution is to increase the aluminium content, but to acquire a desired final composition, a fine control of the composition is very crucial. A High Velocity Oxygen Fuel (HVOF) technique is an alternative to reduce the aluminium vaporization due to its lower flame temperature. Another problem

is related to phase formation in the coating. With a good control of composition, the solidification path, which is quite complex, may prohibit the formation of the ψ phase, resulting in mixture of metastable crystalline phase (for example β and λ - see section 1.3.1) along with the quasicrystalline phase. These coatings may be annealed to yield a single-phase quasicrystalline structure, but this post-deposition process is not very practical for most applications. An alternate possibility is to preheat the substrates.

Even with the broad range of materials that have been found to form quasicrystalline phases, it is difficult - using typical methods - to deposit a coating that has the desired stoichiometry and quasicrystalline phase structure.

1.2.2. Physical Vapor Deposition

The more suitable techniques rely upon physical vapor deposition and are now routinely used for the production of a large variety of thin films (Dubois 2000). Pulsed laser deposition (Sonsky et al. 1997), electron beam deposition (Yoshioka et al. 1995; Eisenhammer and Trampert 1997) and thermal vapor deposition (Mukhopadhyay and Weatherly 2001) are other techniques that have been used to produce quasicrystalline thin films. However, a standard industrial method to produce high quality thin film is magnetron sputtering. This method yields dense materials, is relatively cheap and can be adapted to coat complicated shapes.

One fundamental question in the synthesis of quasicrystalline coating by PVD is the phase formation mechanism. In their paper, Besser and Eisenhammer (1997) summarized a few different hypotheses regarding the growth mechanism. The mechanism also differs depending on the route the phase is formed. We will quote some of the mechanisms summarized in their paper in this section and later will devote much more on this topic, specifically on sputtered coatings, in Chapter 5.

"It has been argued that quasicrystals are formed during the plasma spray since the atomic arrangements in the melt and in the quasicrystalline phase are similar and include small icosahedral clusters (Nelson and Halperin 1985). During quenching this atomic arrangement in the melts and in the quasicrystalline phase is obtained even in alloys that form thermodynamically metastable quasicrystalline phases. However the coating in PVD is deposited atom by atom, and therefore other mechanisms are necessary for the formation of the quasicrystalline phase. In contrast to quenching, thermodynamically stable quasicrystals can be formed by solid-state diffusion at high temperatures. This leads to the question of whether diffusion is the driving mechanism in thin-film preparation.

In 1985, stacks of elemental layers of Al and Mn were deposited (Knapp and Follstaedt 1985), which precluded the direct formation of quasicrystals in the as-deposited coating. The quasicrystals phase was subsequently formed by electron-beam mixing with 400 keV Xe ions. Later, Al-Mn quasicrystal films were obtained by simply heating stacks of Al/Mn layers at 250-425°C (Follstaedt and Knapp

1986). Thus it was shown that the thermodynamically metastable phase of icosahedral Al-Mn can be formed by solid-state diffusion from an atomic arrangement that does not exhibit a local icosahedral structure (Follstaedt and Knapp 1986), in contrast to the situation during quenching from the melt where the stable crystalline phase of Al-Mn is only obtained by annealing at higher temperatures.

In 1987, Al-Mn thin films were produced by sputtering a prealloyed Al-Mn target (Kreider et al. 1987). In this case, the atoms arrive on the substrate in the correct stoichiometry and formation mechanisms other than solid-state diffusion might occur. However at low substrate temperature (e.g., -100°C to 50°C), the films appeared to be amorphous. The quasicrystalline phase was obtained only at substrate temperatures between 225°C and 400°C, which are comparable to the temperatures at which diffusion is sufficient to produce the quasicrystal state from elemental layers. Later it is argued that the amorphous films produced by sputtering at lower substrate temperatures are not truly amorphous but rather consist of extremely small (2 nm diameter) quasicrystalline grains (Chen and Spaepen 1988). These early results show that large-grained quasicrystals were formed solely by solid-state diffusion and no direct formation mechanism was found." (Besser and Eisenhammer 1997)

1.3. Quasicrystal Systems

The two systems that were taken as the subject of this research were icosahedral Al-Cu-Fe and decagonal Al-Cu-Fe-Cr alloy systems.

Table 1.3. Composition of crystalline phases in Al-Cu-Fe system (Grushko et al. 1996)

Phase	Al	Cu	Fe	
λ	74	5	21	Extends from $Al_{13}Fe_4$ up to 6 at. % Cu
τ	54	42	4	Metastable, appears in a wide range inside I-ω-θ-η
β	53	33	14	Extends from AlFe up to 40 at. % Cu
η	49.0	50.5	0.5	
θ	67.8	31.8	0.4	
ω	69	21	10	

Table 1.4. Structure of crystalline phases in Al-Cu-Fe system (Grushko et al. 1996; Quiquandon et al. 1996; Black 1955)

Phase	Alloy	Crystal structure	a Å	b Å	c Å	β
λ	$Al_{13}Fe_4$	monoclinic	15.489	8.0831	12.476	107.72°
β	Al(Fe,Cu)	cubic	2.94			
θ	Al_2Cu	tetragonal	6.6063		4.4872	
ω	Al_7Cu_2Fe	tetragonal	6.34		14.87	

1.3.1. Al-Cu-Fe System

The Al-Cu-Fe system was first studied by Tsai (Tsai et al. 1987) because of its low friction. Of the more than 100 different quasicrystalline materials known to date, materials based around Al-Cu-Fe are attractive, and have already been used for non-stick coating applications. The phase diagram of Al-Cu-Fe compounds is very complicated, and a brief explanation of some of the structures involved is relevant.

The phase diagram, microstructure and phase transformations in Al-Cu-Fe bulk quasicrystals have been widely studied (Grushko et al. 1996; Quiquandon et al. 1996; Gayle 1992; Gratias et al. 1993). The isothermal section at 700°C of the Al-Cu-Fe phase diagram near the icosahedral phase is shown in Fig.1.8.

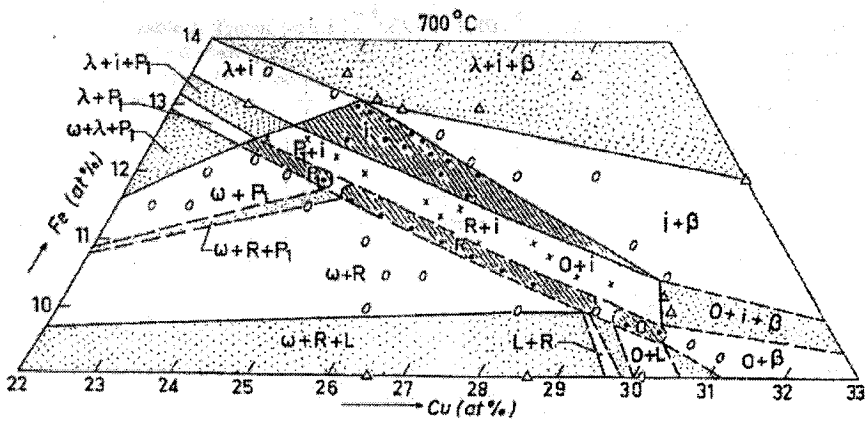

Figure 1.8. An isothermal at 700°C of the Al-Cu-Fe phase diagram showing the domains of the perfect icosahedral phase and its approximants: P1 (pentagonal with a periodicity of 52.31 Å); R(rhombohedral); and O (orthorhombic) phases. The symbols have the following meanings; Δ: three-phase domain; $\circ$: two-phase domain; filled circle: one-phase domain; x: at least two-phase domain, but the differences of the concentration and structure of the phases are so small that the determination of the tie-lines is not possible. Broken lines indicate an approximate boundary of a phase domain (a precise determination is impossible owing to the small difference in concentration). Inside the icosahedral domain there is a region around $Al_{62}Cu_{25.5}Fe_{12.5}$ where the perfect icosahedral phase remains unchanged on annealing at lower temperature. The characteristics of such other crystalline phases as β, λ and ω can be found in (Saadi et al. 1996; Faudot 1993) and are described in Tables 1.4 and 1.5. (Quiquandon et al. 1996)

At 700°C three main single-phase domains are present corresponding to approximants. They are listed below. (i) A pentagonal approximant P1 with point group $\bar{5}$m, around the composition $Al_{63.6}Cu_{24.5}Fe_{11.9}$, first identified by Bancel (1993). This phase is a 1D periodic structure along the fivefold axis. The 1D lattice parameter is equal 52.31 Å. (ii) A rhombohedral approximant R with space group

$R\bar{3}m$, extending from $Al_{63.4}Cu_{25}Fe_{11.6}$ to $Al_{61.6}Cu_{28}Fe_{10.4}$, first identified by Audier and Guyot (1990) in a $Al_{63.5}Cu_{24}Fe_{12.5}$ sample. This phase is a 3D periodic structure, in which the unit cell is a rhombohedron with an angle equal to 32.14 Å. (iii) An orthorhombic approximant O with space group Immm, around the composition $Al_{60.3}Cu_{30}Fe_{9.7}$. This phase is a 3D periodic structure with a unit cell with a=32.16 Å, b=116.34 Å, c=19.85 Å.

All of these approximants become icosahedral (imperfect) at high temperature; the transformation occurs between 715°C and 740°C, depending on the composition. They transform to the rhombohedral state below about 680°C. The transformations ψ to approximants (P1, R, Q) to R are thermodynamically reversible. However, the kinetics is very sluggish when the initial state is not the as-quenched state. Defects introduced by the quench process increase the transformation rate.

1.3.2. Al-Cu-Fe-Cr System

The Al-Cu-Fe-Cr system had never been studied by metallurgists before the discovery of quasicrystals (Dubois et al. 1994b). The interest in this system can be traced back to the discovery of the stable Al-Cu-Fe quasicrystals by Tsai et al. (1987, 1988d). By introducing chromium into the Al-Cu-Fe system, it is possible not only to search for new quasicrystals or the related crystalline phases, but also to improve the performance of the quasicrystalline materials. In the first paper about the Al-Cu-Fe-Cr phases (Dong and Dubois 1991), it was shown that the Cr

element destabilizes the icosahedral phase and that it favors the formation of the decagonal quasicrystals, and its close approximants.

A remarkable resemblance between the Al-Cu-Fe-Cr and the Al-Cu-Co structures were shown by Dong and Dubois (1993) using HREM (High Resolution Electron Microscopy). The Al-Cu-Co system is well known for the existense of the stable decagonal phase (He et al. 1988b). The decagonal phase and its approximants can be constructed with some polygonals units by connecting the atomic clusters with ten-fold symmetry as observed in HREM images. The differences between these two systems is that in the Al-Cu-Co system, the edge length of the units are τ times larger that the ones in Al-Cu-Fe-Cr system.

Dubois and his coworker were the first to investigate the tribological properties of coatings, starting with the Al-Cu-Fe system (Dubois et al. 1991, 1993, 1994a), and then extending to the Al-Cu-Fe-Cr system. Their attention focused on the preparation of non-stick cookware. The Al-rich corner of the phase diagram of the Al-Cu-Fe-Cr system was explored for promising quasicrystals coating materials (Dong and Dubois 1991; Dong et al. 1992). A metastable icosahedral phase was found in rapidly quenched samples, which transforms into the approximants of the decagonal phase upon annealing. The decagonal phase was formed within a certain cooling rate limit. If the cooling rate was too high, the icosahedral phase formed while slow solidification led to formation of the crystalline approximants.

In the Al-Cu-Fe-Cr system, there are five polymorphous approximants that have been observed [3]. All of them, having large unit cells, belong to orthorhombic and monoclinic systems (Li et al. 1995). Additionally, they also form micro-crystalline structures with pseudo 10-fold symmetry. These phases cover a larger composition field in the phase diagram compared to the Al-Cu-Fe icosahedral phase and its approximants.

[3]Recently, another new approximant which belong to hexagonal system is reported (Li et al. 2002; Widjaja and Marks 2002)

CHAPTER 2

Experimental Techniques and Procedures

The research utilized SPEAR (Sample Preparation Evaluation Analysis and Reaction system) (Collazo-Davila et al. 1995), an in-situ system which allows sample manipulation, including transfer, under ultra high vacuum (UHV). The system includes a magnetron sputtering chamber for thin film growth, a transmission electron microscope (UHV H9000), surface characterization tools (i.e. X-ray Photoelectron Spectroscopy (XPS), Auger Electron Spectroscopy (AES), Schottky Field Emission Electron Gun (SE)) and a gas cell for oxidation studies. The system is shown in Figs. 2.1. and 2.2. Substrate preparation techniques, both for bulk and TEM substrates, will also be described in this chapter. Techniques for thin film deposition and characterization procedures will also be described.

2.1. SPEAR

2.1.1. SINBAD

Depositions were carried out in a magnetron sputtering chamber named SINBAD. SINBAD is a specially designed system for the in-situ investigation of thin solid films. Initially, it was a Molecular Beam Epitaxy (MBE) chamber on the SPEAR system which had two effusion cells configured for growth of gallium arsenide.

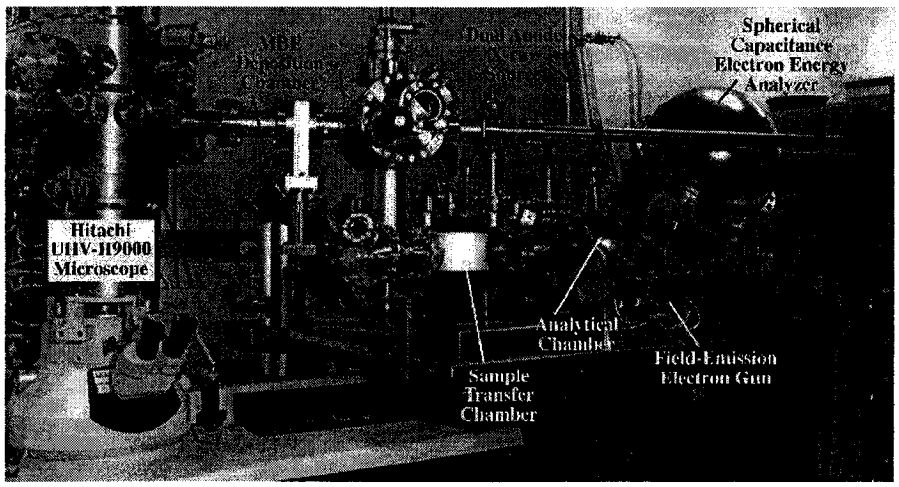

Figure 2.1. Side view of SPEAR and Hitachi UHV-9000 TEM

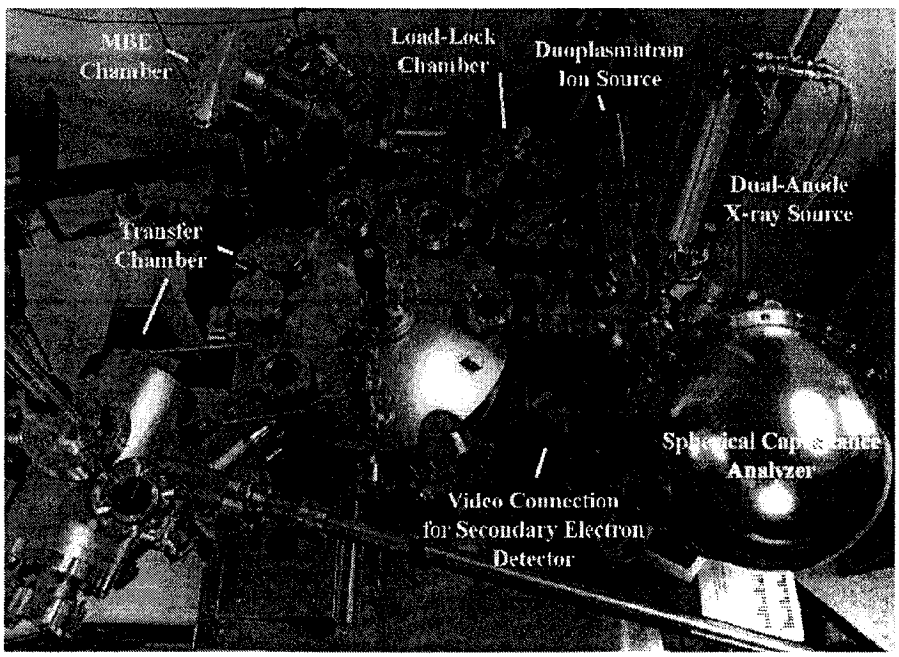

Figure 2.2. Top view of SPEAR

This MBE unit was then redesigned for deposition of boron nitride films (Bengu et al. 1998) and nanotubes (Bengu and Marks 2001) using ion beam-assisted deposition. The most recent adaptation replaces the deposition system with a magnetron sputtering system. The new unit, SINBAD, is pumped by a 280 l/s turbomolecular pump (Varian Vacuum, Lexington, MA) and a 220 l/s ion pump (Physical Electronics, Eden Prairie, MN), with a base pressure in the low 10^{-10} Torr. Just like the SPEAR system, SINBAD is designed to handle and deposit onto thin 3 mm TEM ready samples. The sample stage employed the same heating mechanism present in the analytical chamber which allowed for resistive heating and biasing of the sample.

2.1.2. Analytical Chamber

In analytical chamber, an X-ray Source producing Al or Mg K-alpha x-rays, with a maximum power output of 400 watts, is used with a Spherical Capacitance Analyzer (SCA) for acquiring XPS data. The SCA analyzes the energy of the incoming electrons and is able to acquire XPS and AES spectra. This allows analysis of elements present in the surface and the quantification of surface composition. It also has sufficient resolution to detect binding energy shifts and hence characterizes the chemical states of the elements. For example, in the case of oxidation, it can be used to study oxidized elements and surface segregation.

The role of the analytical chamber is to prepare and also to characterize surfaces chemically. Samples, if necessary, can be cleaned through a combination of sequential ion milling and annealing. Ion milling is accomplished using a duoplasmatron ion source with a microbeam ion gun column (Physical Electronic). The gun has a variable gas source and can produce oxygen, argon or xenon ions with a minimum probe size of less than 5 μm. The maximum accelerating voltage is 10 kV and is operable down to a minimum voltage of 240 V. Combined with a Channeltron (channel electron multiplier) detector and a video imaging system, the ion-miling process can be controlled precisely and observed in real time. This is done by the acquisition of ion-induced secondary electrons to form images during the milling.

There are two different methods available for annealing in the analytical chamber. The first one is a resistive heating method. It is done by passing a DC (Direct Current) through the sample and the sample holder. This method can resistively heat the molybdenum ring to a temperature of about 1000°C, however the poor thermal contact between the sample and the ring will limit the actual temperature of the sample. The second heating method is through the use of an electron gun (Kimball Physics Inc.). Electrons with energy of 1-10 keV are aimed at the surface of the samples enabling heating up to 2000°C. While this method seems ideal, care must be taken with samples that are vulnerable to electron beam damage. This

method, however, cannot be used to directly anneal oxide substrates due to the loss of oxygen under electron beam irradiation.

2.2. Substrate Preparation

Substrates, in general, were prepared in the form of 3 mm diameter discs. A slight modification has been made to allowed samples of up to 1x2 cm as a substrate to be introduced into SPEAR and SINBAD. Initial deposition was made on thick discs for SEM and EDX study. Structural studies were conducted on electron transparent samples. Various substrates were used in the experiments: MgO [100], Al_2O_3 [0001], Si [100] and NaCl [100].

2.2.1. TEM Sample Preparations

Substrates were prepared using standard TEM sample preparation techniques. Magnesium Oxide (MgO) (001) substrates were prepared by: cutting to 3 mm disc using an ultrasonic disc-cutter; mechanical thinning with 600 and 1000 grit SiC (Silicon Carbide) paper; mechanical dimpling; chemical etching (50% phosphoric acid at 85°C) to perforation followed by Ar^+ ion milling to remove the residual contaminants from etching. Subsequently the substrates were annealed in oxygen at 1000°C for 2-3 hours to allow recovery and recrystallization from defects introduced during preparation (Perry and Merrill 1997). The heat treatment also leads to formation of flat atomic steps. After insertion into the UHV chamber, samples were evaluated using XPS and TEM to ensure surface cleanliness and to document

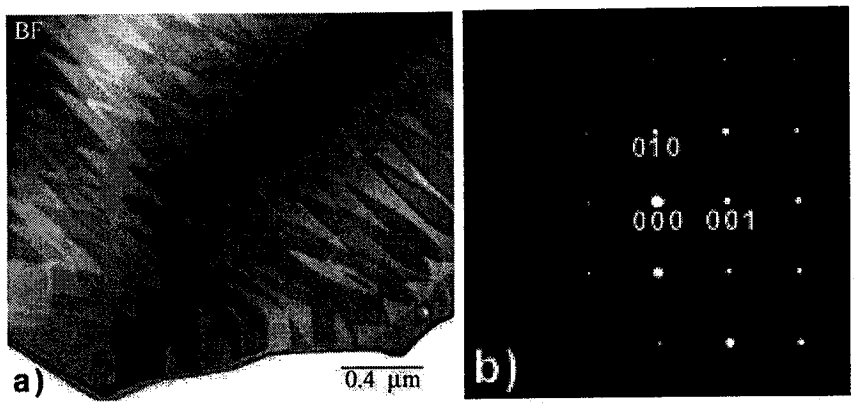

Figure 2.3. a. TEM bright field image of MgO substrate showing terraces and atomic steps. b. Diffraction pattern of MgO along the [100] zone axis

the substrate surface morphology prior to deposition. XPS studies show a clean MgO surface and TEM studies reveal the presence of step bunches separated by 100-200 nm wide terraces. The morphology and diffraction pattern of clean MgO (100) are shown in Fig. 2.3; Fig. 2.4 shows the XPS spectrum indicating a clean surface.

Aluminum oxide (Al_2O_3 sapphire) (0001) substrates were prepared using similar TEM sample preparation techniques: cutting to 3 mm disc; thinning; mechanical dimpling; followed by Ar^+ ion milling to perforation. Subsequently the substrates were annealed in air at 1400°C for 2-4 hours to allow recovery and recrystallization from defects introduced during preparation (Kim and Hsu 1991; Susnitzky and Carter 1992). This annealing treatment leads to a 1x1 diffraction pattern as shown in Fig. 2.5.

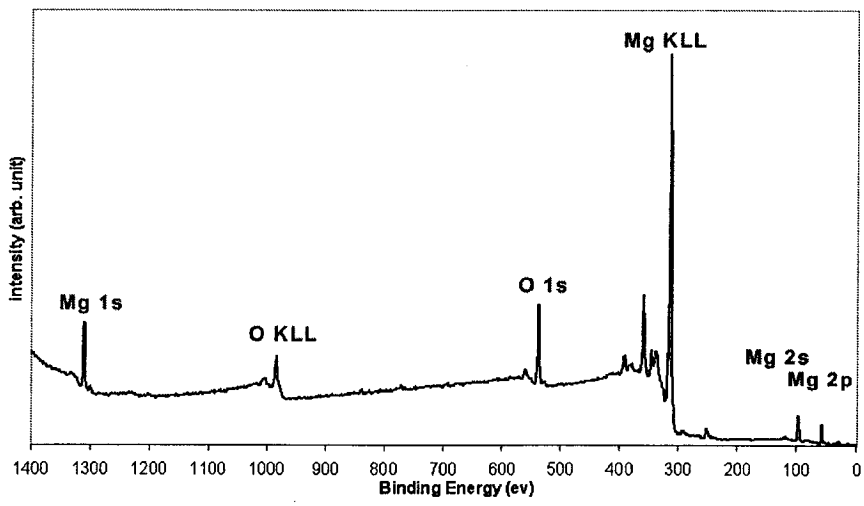

Figure 2.4. XPS spectrum of a clean surface

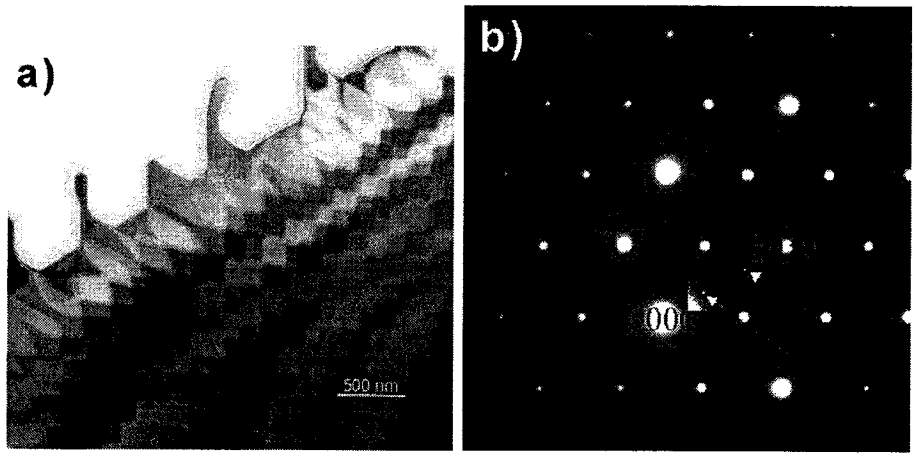

Figure 2.5. a. TEM bright field image of Al_2O_3 substrate showing terraces and atomic steps. b. Diffraction pattern of Al_2O_3 along the [0001] zone axis showing 1x1 termination. Intensity and contrast at and near $(10\bar{1}0)$ and $(20\bar{2}0)$ spots are modified to aid the visualization

2.2.2. Bulk Substrate

Silicon substrates were polished using 600 grit SiC paper. For 3 mm disc dimension, a rotary cutter with SiC solution were used to cut the disc. Si [100] substrates

were used as bulk substrates for the following experiments: deposition rate measurement, composition measurement by EDX and SEM imaging and analysis of thick films.

NaCl (Sodium Chloride) substrates were cleaved with razor blades along the (100) planes. To accommodate the samples into the Mo (Molybdenum) rings, the NaCl samples were cleaved to fit into the rings. The sodium chloride substrates were subsequently removed, after thin film deposition, by dissolving in water to acquire free-standing thin films. These thin films were then suspended on Mo, Ni or Cu hole-grids and studied using TEM.

To obtain multiple TEM samples of free-standing film from a single deposition run, sample handling was modified to accommodate larger samples. NaCl substrates of the size 5 mm x 20 mm were put on top of two cylindrical stubs with the same dimension as the Mo rings. These stubs sit on the position of Mo rings in the introduction module to provide stability to the NaCl crystal during sample transfer. Another stub/ring was put on top of the crystal, this is the holder for the gripper during deposition. The three rings were attached to the NaCl crystal by carbon tape. This carbon tape is UHV compatible, retains its stickiness even after a load lock bake, and is easily removed from the crystal after deposition. A schematic of the sample construction is shown in Fig 2.6.

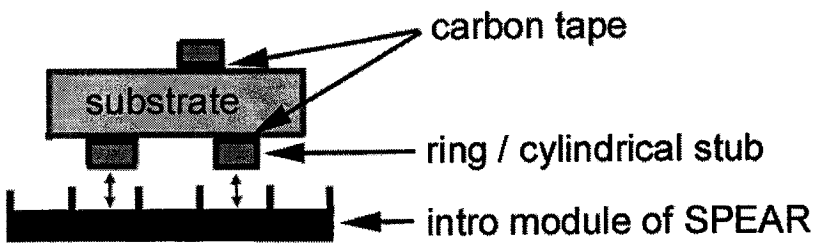

Figure 2.6. A schematic of the holder construction to accommodate larger sample in the SPEAR intro module

2.2.3. In-situ Preparation

For single grain quasicrystal substrates for metal film deposition experiment, in-situ sample preparation is required. Due to the nature of Al-Cu-Fe alloys, thin oxide layers exist on both surfaces of the samples. To create a truly quasiperiodic surface, the oxide layer needs to be removed prior to metal deposition. The surface is prepared in-situ using iterative argon ion milling and direct electron beam annealing. The annealing is necessary to recover the aluminum composition on the surface; aluminum is preferential sputtered and leads to the presence of a cubic structure on the surface. The annealing was carried within a temperature range of 500-600°C for about one hour. The chemical state of the surface is monitored using XPS; Fig.2.7. shows the XPS spectra before and after sputtering. Once the contamination levels were at or near the detection limit of the instrument, the sample surface is considered clean and the next step can be conducted.

For TEM samples, after cycles of sputtering and annealing, the samples were inserted into microscope and characterized to ensure that the sample is still usable

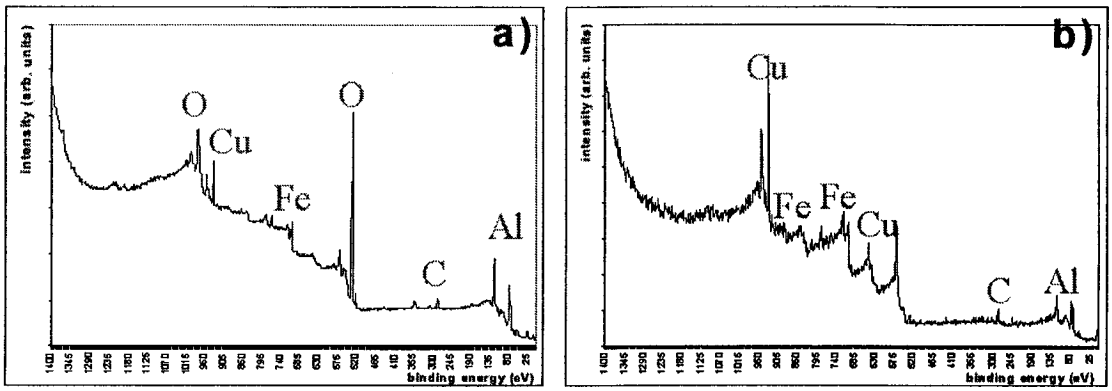

Figure 2.7. XPS spectra of the substrate prior to (a) and after (b) sputtering to remove surface oxide

and the surface structure is quasiperiodic. Fig.2.8. shows the diffraction pattern of the substrate prior and after the annealing treatment. Annealing may also lead to thickening of the samples; in this case further sputtering is required if the sample if too thick.

2.3. Thin Film Growth

Depositions were done in a magnetron sputtering chamber with a base pressure of 10^{-10} Torr. Typical deposition parameters were: pressure 2-3 x 10^{-3} Torr Argon (99.998% purity), 100-300 W and no substrate bias. Deposition rate was determined by depositing a thick coating unto a flat substrate. Part of the substrate was covered by titania powders (suspended in organic solvent) to prevent deposition in the masked area. After deposition, the mask (titania powders) was removed and a needle profilometer was used to measured the film thickness, deduced from the height difference of deposited and masked area. The deposition rate at room

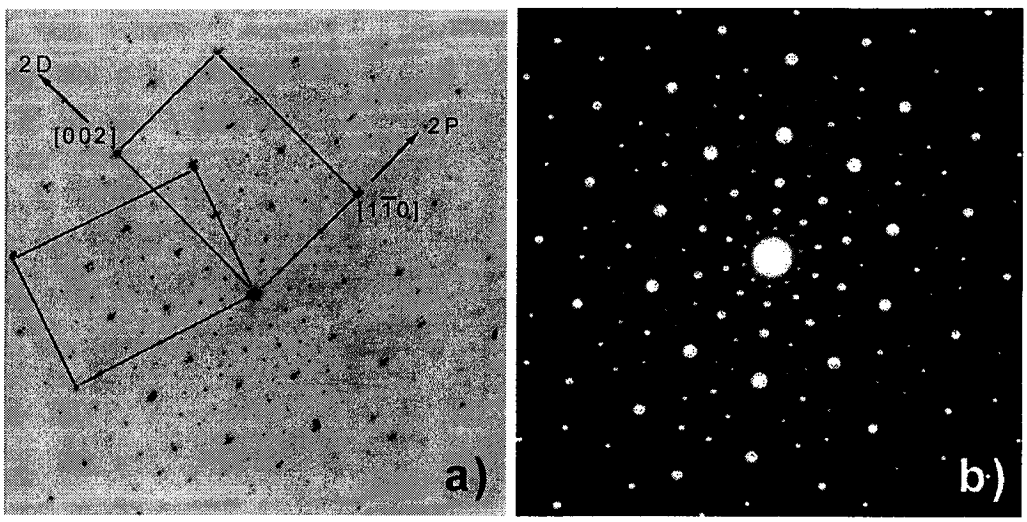

Figure 2.8. TEM diffraction patterns of substrate prior to (a) and after (b) annealing treatment. Diffraction patterns of a cubic structure resulting from deficiency of aluminum on the surface appear as extra spots in (a)

temperature was determined to be approximately 13 nm/min with the following deposition parameters: pressure 2.7 x 10^{-3} Torr Ar, 150 W and no substrate bias.

The sample manipulation stage was used to heat the substrate and thus anneal the thin film. The substrate temperature was measured with a close-focus infrared pyrometer calibrated to the sample emissivity.

The targets were, in general, manufactured in two different ways: vacuum arc melting to create a metal alloy and the powder metallurgy of pure elements. There are advantages and disadvantages to these two different methods. While films from powder metallurgy targets have relatively more homogeneous composition throughout the deposition, they have a higher content of oxygen, compared to films produced using vacuum-arc-melted targets. The oxygen content results from

oxidized powders prior to compacting and sintering process in powder metallurgy; it becomes more significant due to the high content of aluminum, which is readily oxidized at ambient. Targets from vacuum arc-melting have lower contamination level of oxygen but have a problem with homogeneity. The composition of films varies as a function of deposition time due to the inhomogeneity of the composition through the target depth. This is a result of the inability to create a single phase target. A single phase target, already in the quasicrystalline phase, is not preferred due to its low heat and electrical conductivity. These can be overcome using radio-frequency sputtering, however the brittleness of the target can lead to target spalling or cracking.

2.4. Transmission Electron Microscopes

Transmission electron microscopy (TEM) is a standard method of determining structural details ranging from the micron level to the atomic scale, critical information for this research. While High Resolution Electron Microscopy (HREM) and Transmission Electron Diffraction (TED) are staples for characterization of quasicrystals (Hiraga 1991), they are not the only ones. Other more classical microscopy techniques such as simple bright field and dark field are useful.

2.4.1. Hitachi UHV H-9000

The microscope, a modified version of the Hitachi H-9000 High Resolution Transmission Electron Microscope (TEM), has remained largely unchanged since it was

first developed (Marks et al. 1988; Bonevich and Marks 1992). The pumping system of this microscope has been modified from the original configuration to achieve a UHV operating pressure of less than $1x10^{-10}$ Torr. Care has been taken not to preserve the capabilities of the TEM and to retain a point-to-point resolution of 0.2 nm.

The Hitachi UHV-H9000 TEM [1] is equipped with a Gatan Parallel Electron Energy Loss Spectroscopy (EELS) and a Charge Coupled Device (CCD) Camera, both interfaced to computers. The older CCD camera (for TV) was recently replaced with a newer one with a capability to acquire digitally a 14-bit image as well as perform a real time fast fourier transform. EELS can provide both local chemical information and electronic structure information. Classical microscopy techniques such as simple bright field and dark field are useful for this research. High Resolution Electron Microscopy can be performed with resolution of better than 0.18 nm. This TEM was used in all the in-situ studies of the thin films.

2.4.2. Hitachi H-8100

The Hitachi H-8100 TEM [2] is a 200 kV thermionic emission (tungsten (W) hairpin filament) microscope with a large specimen tilt (+ 45°) pole piece with a PGT

[1]The details of this system can be found at: http://www.numis.nwu.edu/internet/uhvhrem.html

[2]The details of this system can be found at: http://www.nuance.northwestern.edu/epic/tem.htm

X-Ray detector and analysis system for Energy Dispersive X-ray Spectroscopy (EDXS). This TEM was used in ex-situ studies of the thin films.

2.4.3. Hitachi HF-2000

The Hitachi HF-2000 [3] is a TEM with a high brightness cold Field Emission Gun (cFEG) operated at 200 kV. It has a Bright Field / Annular Dark Field (BF/ADF) Scanning Transmission Electron Microscope (STEM) detectors with simultaneous Emispec PC acquisition system for STEM, EDS and EELS detectors for automated line scans and maps. This TEM has a smaller probe and higher brightness than the H8100 to allow better resolution in chemical composition determination via EDS.

2.4.4. JEM 3000F

The JEOL JEM 3000F [4] is a 300 kV field emission TEM at Brookhaven National Lab with a point resolution <0.165 nm. This TEM is equipped with a CCD camera to capture the images digitally.

---

[3]The details of this system can be found at: http://www.nuance.northwestern.edu/epic/tem.htm

[4]The details of this system can be found at: http://www.bnl.gov/tem/htmls/TEM.html

2.5. Other Characterization Techniques

2.5.1. Scanning Electron Microscope

The Hitachi S-3500 [5] is a Scanning Eelectron Microscope (SEM) with a W hairpin filament. Vacuum conditions can be varied from standard vacuum pressures (10^{-4} Pa) to 270 Pa inside the specimen chamber. It has a magnification range from 25x to 300,000x and a PGT Energy Dispersive X-Ray analyzer with digital pulse processing, capable of light element analysis (down to Boron), X-ray linescans and maps and digital image capture (up to 4k x 4k) with feature analysis.

2.5.2. Atomic Emission Spectroscopy

Inductively Coupled Plasma - Atomic Emission Spectroscopy (ICP-AES) stands for optical emission spectrometry with inductively coupled plasma. Argon gas flowing through a radio frequency field forms a plasma where it is kept in a state of partial ionisation. This allows it to reach very high temperatures of up to approximately 10,000 °C.

The ICP-AES technique exploits the fact that excited electrons emit energy at a given wavelength as they return to their ground state. Each chemical element emits energy at wavelengths specific to its chemical character. The intensity of the energy emitted at a specific wavelength is proportional to the concentration of that element in the sample. Therefore, by analyzing the wavelengths and their

[5]The details of this sytem can be found at: http://www.nuance.northwestern.edu/epic/sem.htm

intensities, quantification of the elemental composition with respect to a reference standard can be acquired.

The sample for ICP-AES needs to be prepared as solution. This solution is introduced into the plasma as a fine droplet aerosol. The light emitted are separated into different wavelengths and captured by light-sensitive detectors. This technique allows simultaneous analysis of multiple elements (up to forty elements). It is able to detect most metalic elements in concentration down to the ppb (part per billion) level.

Samples were prepared in a particle-free liquid. A Thermo Jarrell Ash Atomscan Model 25 Sequential ICP Spectrometer was used [6]. It is equipped with vacuum optics covering the spectral range from 160 to 850 nm. The specifications of the instrument are: Wavelength range: 160-850 nm, Resolution: 0.008 nm at 160-335 nm, 0.018 nm at 335-670 nm, 0.040 nm at 670-850 nm, sample size: 5 mL and detection limits: ppb range. A standardization curve was generated using Intensity versus Concentration values. For most elements the response is linear up to a concentration of around 70 ppm (μg/ml). For this range, only a blank and a high standard are needed to standardized the instrument. When making samples and standards the following guidelines were followed. Concentration of elements of interest stays below 70 ppm (μg/ml) with the best range 1-40 ppm. The high standard's concentration is higher but close to the expected concentration of the

[6]The details of this system can be found at
http://pyrite.chem.northwestern.edu/analyticalserviceslab/ICP/instruments.htm

element in the sample. A matrix of the standards are matched to the samples and acid concentration stays below 5% in the final dilutions of sample and standard.

2.5.3. X-ray Photoelectron Spectroscopy

Surface analysis by XPS is conducted by irradiating a solid in high vacuum with monoenergetic x-rays and analyzing the emitted electrons by their energy. The x-rays interacts with the elements in the surface causing electrons to be emitted via the photoelectric effect. Each element has a unique spectrum. Chemical elements can be deduced by identifying the peak positions and their chemical states can be determined from peak positions and shift. Quantification data can be obtained from integrating the peak area.

In addition to photoelectrons, Auger electrons are also emitted due to relaxation of the excited ion after photoemission. The Auger electron possesses a kinetic energy equal to the difference between the energy of the initial ion and the doubly charged final ion. Its energy is independent of the mode of the initial ionization, hence independent of the x-rays energy.

Despite the deeper penetration length of photon (x-rays), since the electrons mean free path in solids is very small, XPS is a surface-sensitive technique. Only electrons originate within tens of angstroms below the surface can leave without energy loss; these are the most useful ones. The electrons that undergo inelastic scattering will appear as background.

The emitted electrons have measured kinetic energies given by:

$$KE = h\nu - BE - \phi_s, \tag{2.1}$$

where hν is the energy of the photon, BE is the binding energy of the atomic orbital from which the electron originates, and ϕ_s is the spectrometer work function.

In XPS studies, it is often important to determine the relative compositions of the various elements in the sample. A peak area tehcnique in quantification is typically more accurate than the peak height method. The assumption in the basic quantification calculation is that the sample is homogenous; for a non-homogenous sample, e.g. a sample with an oxide layer on the surface, multiple data acquisations at different electron exit angles are required.

We follow the following equations in quantification of composition as described by Moulder et al. (1992). For a homogenous sample, the number of photoelectrons per second in a specific spectra peak is given by:

$$I = nf\sigma\theta y\lambda AT, \tag{2.2}$$

where n is the number of atoms of the element per cm^3 of the sample, f is the x-ray flux in photons/cm^2, σ is the photoelectric cross-section for the atomic orbital of interest in cm^2, θ is an angular efficiency factor for the instrumental arrangement based on the angle between the photon path and detected electron, y is the efficiency in the photoelectric process for formation of photoelectrons of the normal

photoelectron energy, λ is the mean free path of the photoelectrons in the sample, A is the area of the sample from which photoelectrons are detected, and T is the detection efficiency for electrons emitted from the sample. We can define an atomic sensitivity factor, S, as

$$S = f\sigma\theta y\lambda AT. \tag{2.3}$$

If we consider a strong line from each of the two elements, then:

$$\frac{n1}{n2} = \frac{I_1/S_1}{I_2/S_2} \tag{2.4}$$

This expression may be used for all homogenous samples if the ratio S_1/S_2 is matrix-independent for all materials. It is certainly true that such quantities as σ and λ vary somewhat from material to material, but the ratio of each of the two quantities σ_1/σ_2 and λ_1/λ_2 remains nearly constant. Thus, for any spectrometer, it is possible to develop a set of relative values of S for all of the elements.

A general expression for determining the atom fraction of any constituent in a sample, C_x, can be written as:

$$C_x = \frac{n_x}{\sum n_i} = \frac{I_x/S_x}{\sum I_i/S_i} \tag{2.5}$$

XPS was used to measure the composition of as-deposited and oxidized thin films as well as to evaluate the surface contaminations of the substrates. Quantification was done using peak area values estimated with FitXPS Version 2.0 [7]. Peaks chosen for integration and their atomic sensitivity factors (S) are based upon empirical peak area value corrected for the transmission function of our XPS system (Wagner et al. 1981).

2.5.4. Energy Dispersive X-ray Spectroscopy

While in XPS, X-rays are used to induced electrons from the samples and then the emitted electrons are analyzed to characterized the samples, in EDXS, electrons are the probe and X-rays are the output. When an electron beam strikes the surface of a sample, it causes X-rays to be emitted from the material. The energy of the X-rays emitted depends on the material under examination.

The relative metallic composition of the as-deposited films was measured by ex-situ EDS in a Hitachi S-3500 Scanning Electron Microscope (SEM). The compositions of decagonal and hexagonal grains were determined from EDS in a Hitachi HF-2000 TEM. All EDS measurements were calibrated using standard samples whose compositions were determined by ICP-AES.

[7]The newer version of this program, FitXPS, can be downloaded from:
http://www.sljus.lu.se/download/fitxps212.zip

CHAPTER 3

Quasicrystalline Thin Films: Growth and Microstructure

In this chapter, the growth and microstructure of quasicrystalline thin films will be discussed. The effect of growth and post-growth parameters, such as temperature, composition, heat treatment, for two different quasicrystalline systems, Al-Cu-Fe-Cr and Al-Cu-Fe will be presented. The emphasis of the work is to study and control the structure of the films. Later, in chapter 5, we will discuss more on the fundamentals of growing quasicrystalline thin films.

3.1. Al-Cu-Fe-Cr Quasicrystalline Films

3.1.1. Room Temperature Growth and Annealing Treatment

Thin films of approximately 25 nm thickness were grown on MgO (001) at room temperature and an even coverage of film on the substrate was observed. In addition to MgO diffraction spots, Selected Area Diffraction (SAD) shows diffuse patterns characteristic of an amorphous structure (Fig. 3.1a). In-situ High Resolution Electron Microscopy (HREM) of the film extending out of the edge of MgO (Fig. 3.1b) shows a featureless image. The power spectrum of the HREM image (Fig. 3.1c) confirms the absence of crystalline order in the film. Therefore,

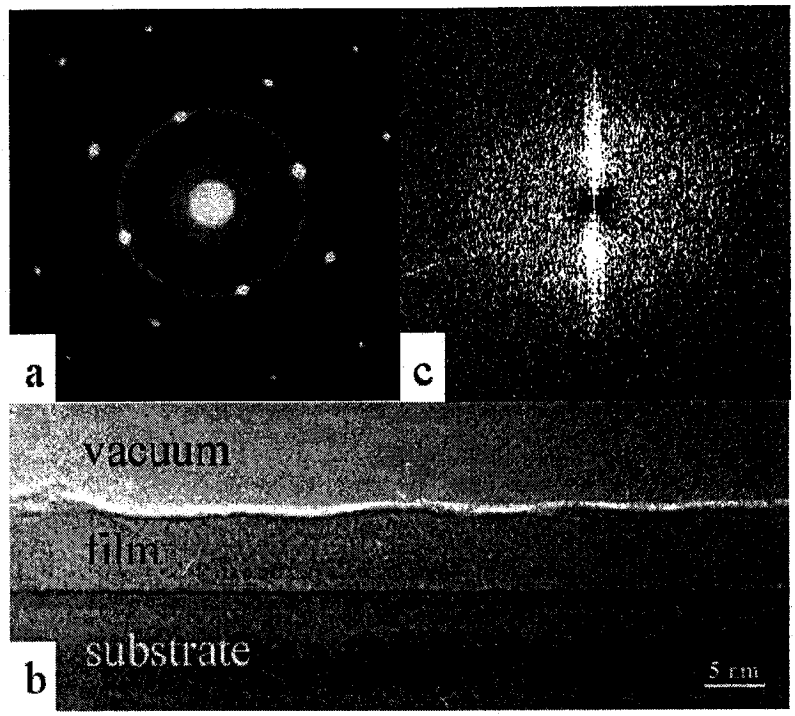

Figure 3.1. Room temperature growth on MgO (001) a) Diffraction pattern b) HREM image c) Power spectrum of (b). In a) there is some 'ring-like' character, indicating partial order (e.g. first and second nearest neighbours) in the initial material.

it can be concluded that growth at room temperature results in a thin film with an amorphous structure.

This amorphous phase in the initial sample is metastable; after a short UHV annealing (~4 minutes) at 310°C, the film transforms into a mixture of quasicrystalline and crystalline grains. Diffraction patterns from the decagonal phase (tenfold axis) and its hexagonal approximant ([110] zone axis) on the MgO substrate are shown in Figs. 3.2. Further annealing experiments showed coarsening behavior (Fig. 3.3a). Moire fringes that were sparse and hard to discern in the annealed

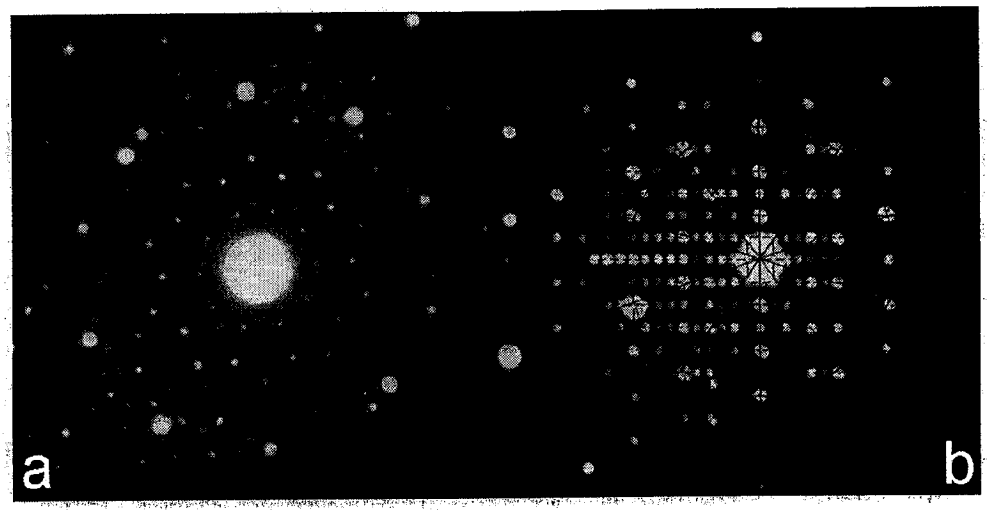

Figure 3.2. Diffraction pattern of quasicrystalline phases in annealed film a) SAD pattern of decagonal phase along ten-fold axis b) Micro-probe diffraction pattern of hexagonal approximant along the [110] zone axis, marked are unit cell and pseudo ten-fold rotation.

sample become clearly visible after further annealing for four minutes at 360°C (Fig. 3.1b). The fringes in the annealed image show large overlapping grains.

For thicker films (130-390 nm), room temperature growth shows some level of crystallinity (Fig. 3.4a) which can be attributed to substrate heating during deposition. Upon atom bombardment, the substrate temperature increases resulting in higher adatom mobility leading to the formation of crystalline phases. The diffraction patterns from these thicker films grown at room temperature are similar to those from films grown on heated substrates (Fig. 3.4b), albeit with a difference in the grain sizes. These nanocrystalline phases may be similar to those observed in other studies of as-deposited films using XRD (Daniels et al. 2000).

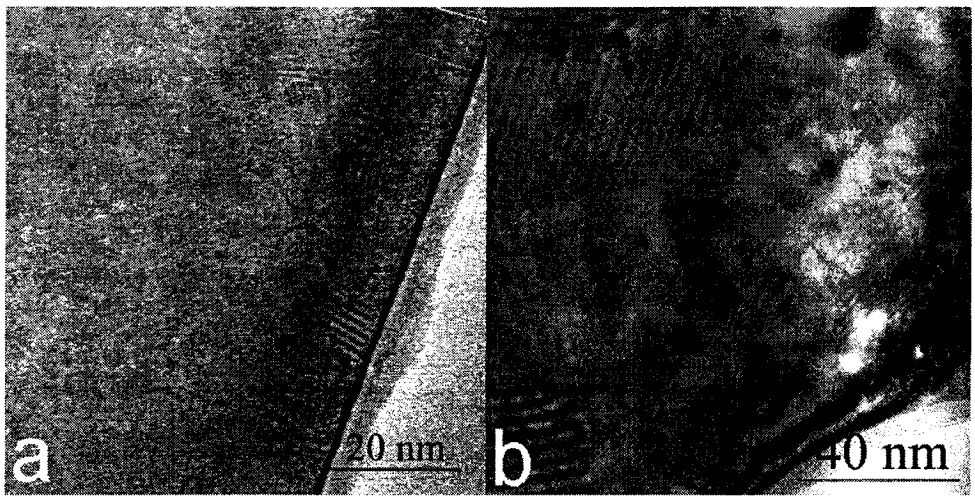

Figure 3.3. Bright field images of annealed film showing grain growth a) annealed at 310°C for 4 minutes b) further annealing at 360°C for 4 minutes.

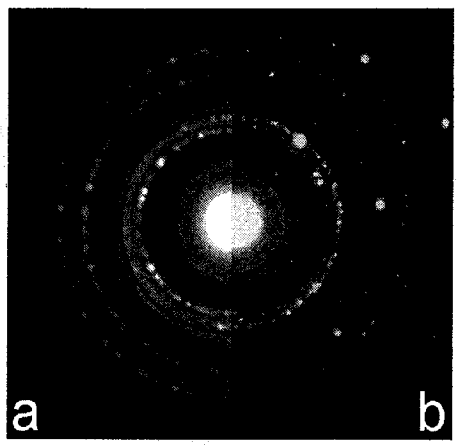

Figure 3.4. Comparison of diffraction patterns. a) Composite diffraction pattern with different exposure times from as-deposited film on salt, grown at room temperature, film thickness ~390 nm. b) Diffraction pattern from film deposited at 310°C on MgO, film thickness ~60 nm.

3.1.2. High Temperature Growth and Annealing Treatment

Growth at higher temperature (~350°C) on rough MgO (001) substrate exhibits a turtle shell-like pattern with large plateaus surrounded by channels (see Fig. 3.5), characteristic of island growth. XPS studies (Fig. 3.6.) of this film show a very noticeable Mg peak which can be attributed to the spaces between the plateaus formed by the islands – the Mg peak would otherwise be undetectable by XPS for this film thickness as evident from room temperature growth with similar coverage (Fig.3.7). Growth at this temperature results in a crystalline film (Fig. 3.4b.) which transforms into a mixture of quasicrystalline and crystalline phases upon subsequent annealing. High temperature growth on atomically flat Al_2O_3 and MgO substrates also follows similar trends and the films preserve the step features of the substrate. Fig.3.8. shows the high temperature growth on Al_2O_3 with smaller islands near the steps due to higher nucleation rate.

3.1.3. Chemical Composition of Quasicrystalline Phase

Chemical compositions of the samples measured by in-situ XPS and ex-situ EDX are compiled in Table. 3.1. The composition of the decagonal and hexagonal phases are close to one another, which explains the coexistence of both phases in most of the deposited films. Fig. 3.9. shows the EDX spectra of the phases, comparing two grains of each phase, normalized with respect to the intensity of aluminum. Because the initial compositions of the film differs from the compositions of the

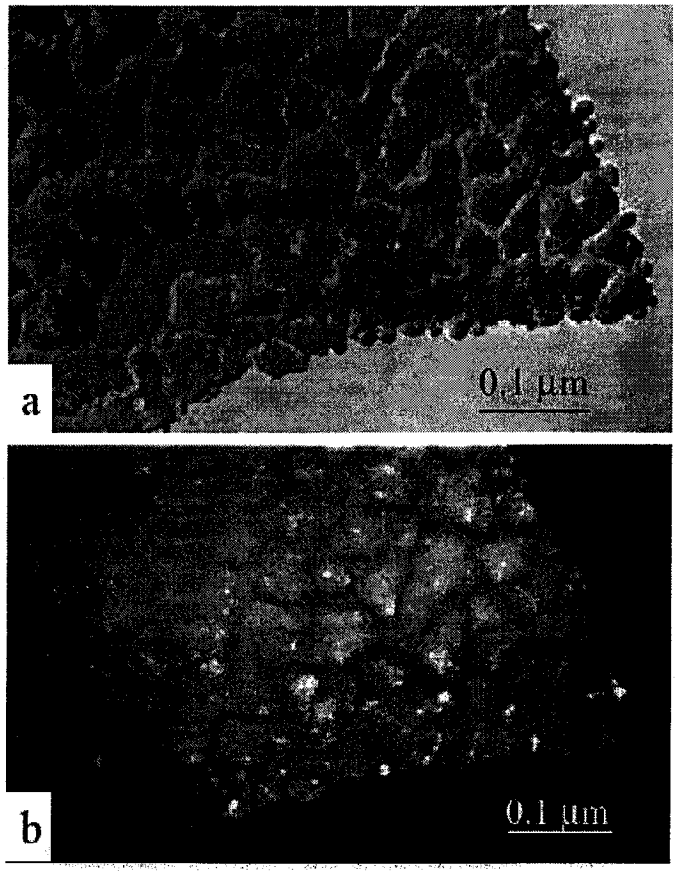

Figure 3.5. a) Bright field and b) dark field images of deposition on MgO at 310°C showing island growth, film thickness ~25 nm.

quasicrystalline phases, secondary unwanted phases also coexist in the films. These phases will be discussed in section 3.1.6.

The oxygen content at the surface is less than 5% and that of the film (determined by depth profiling) is approximately 1%. Keeping the sample at 10^{-6} Torr for one day results in increase of both the oxygen (about 40%) and aluminum content of the surface.

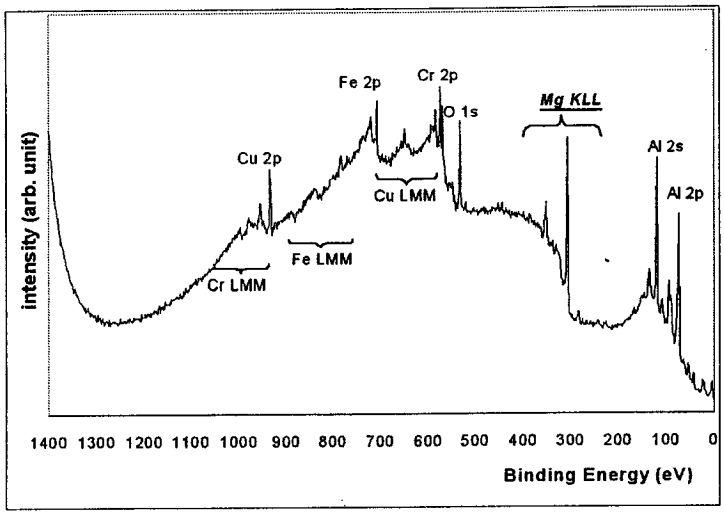

Figure 3.6. XPS spectrum from deposition on MgO at 310°C, film thickness ~25 nm.

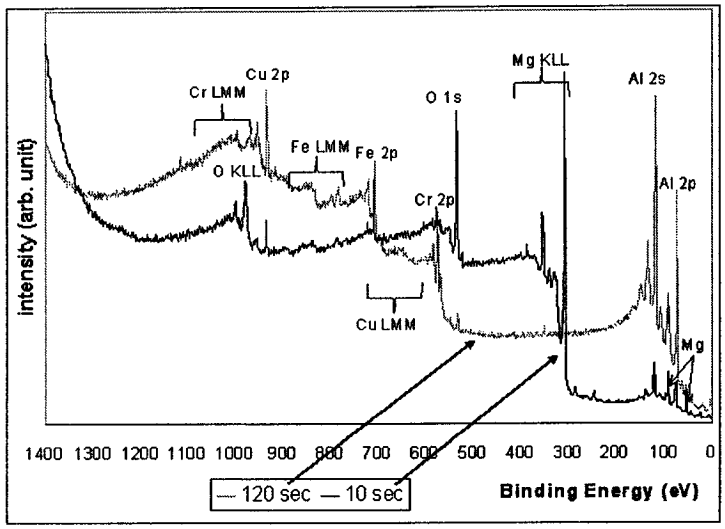

Figure 3.7. XPS spectra of Al-Cu-Fe-Cr thin film deposited at room temperature showing even coverage and no sign of islanding. The 10 sec and 120 sec deposition time correspond to films thicknesses of ~2 nm and ~25 nm respectively.

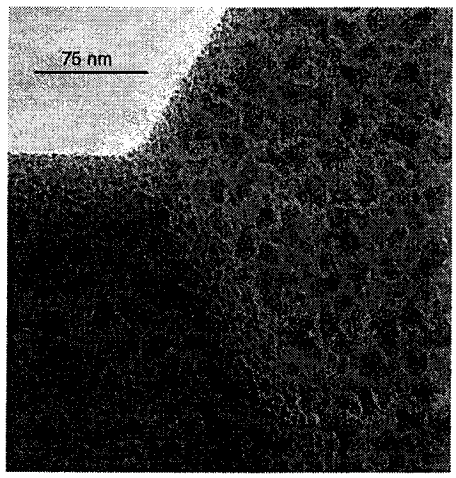

Figure 3.8. Bright field image of high temperature growth on flat Al_2O_3 substrate showing island mode. Smaller islands are observed near the steps and edges of the substrates.

Table 3.1. Chemical composition of the quasicrystalline thin films

Sample	Average Composition				Technique
	Al	Cu	Fe	Cr	
As-deposited films	86.3±4.4	3.9±0.7	5.4±0.4	4.4±0.5	in-situ XPS
As-deposited films	82.5±4.3	4.0±0.5	7.9±0.7	5.5±0.3	ex-situ EDX
Decagonal phase	78.3±4.5	7.6±1.4	7.5±1.9	6.6±1.0	ex-situ EDX
Hexagonal phase	76.1±4.3	10.8±1.3	7.3±0.4	5.8±0.3	ex-situ EDX

3.1.4. Effect of Bias

Thin films were grown on Si substrate at room temperature for the study of the effect of bias on surface roughness. One sample was grown without bias and the other with negative bias of -100 V. Both films were grown for the duration of 15 minutes. A growth of 15 minutes at room temperature with no bias at 150 W is equivalent to 13.8 nm/min, as deduced from Fig. 3.10.

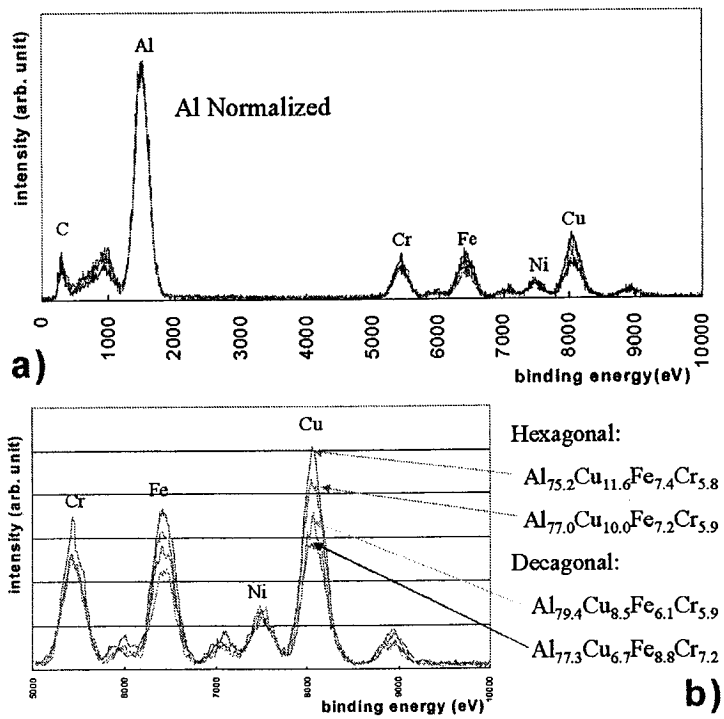

Figure 3.9. EDX spectra a) and details b) of the Al-Cu-Fe-Cr decagonal and hexagonal phases. The spectra are normalized with respect to Al intensity. Only small differences in composition exist between the two phases

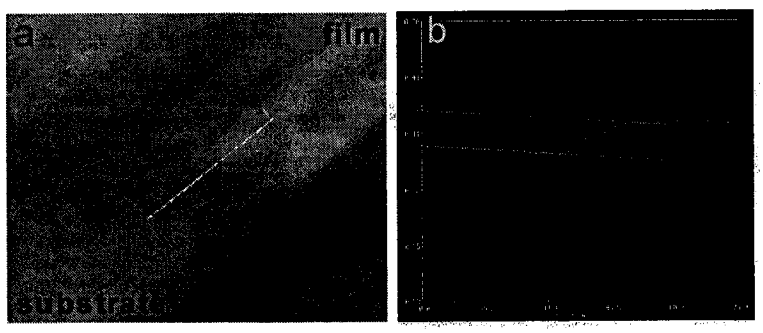

Figure 3.10. White-light interferometer image of film deposited at room temperature with no bias on silicon substrate. Part of the substrate was covered during deposition. a) Image with line scan from substrate to film b) the height at different points along the line.

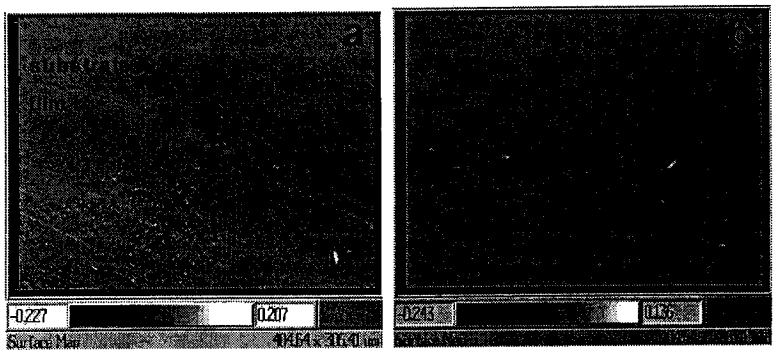

Figure 3.11. White-light interferometer image showing difference in roughness of a) unbiased sample showing part of the substrate which was covered during deposition and b) biased sample.

The roughness of the surface depends on the initial substrate roughness. The prepared substrates have r.m.s. (root mean square) roughness of about 27 nm. Film deposited without bias at room temperature will deposit uniformly and will reduce the initial roughness, however due to its thickness of about 200 nm, roughness due to the substrate is still dominant as shown in Fig. 3.11. This film is also less dense compared to the one deposited with bias. The biased sample had a r.m.s. roughness of about 4 nm compared to 11.7$\pm$3.1 nm for the unbiased. Application of bias improves the roughness as well as the density of the film.

3.1.5. Quasicrystalline Phases

We analyzed the films after heat treatments and found they consisted of a decagonal phase and its approximants (mainly hexagonal), an icosahedral phase and its approximants, and other crystalline phases. The hexagonal approximant is a new approximant to the Al-Cu-Fe-Cr decagonal phase with lattice parameters of

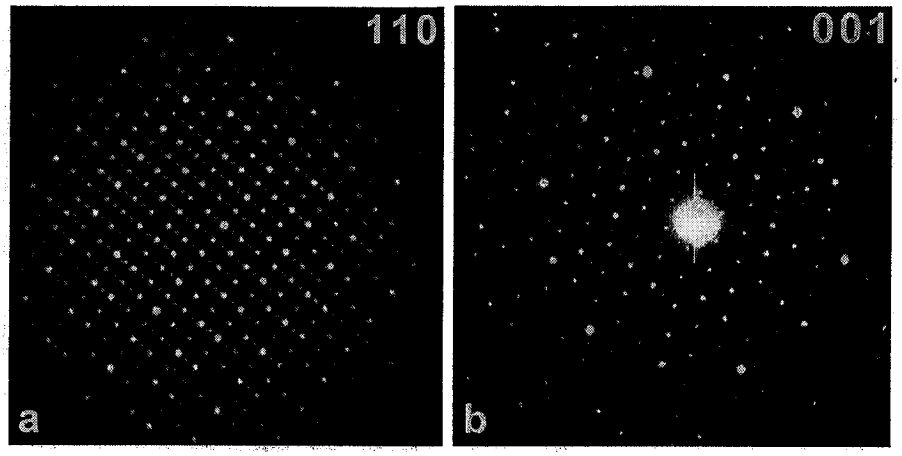

Figure 3.12. Diffraction pattern of the hexagonal approximant of decagonal Al-Cu-Fe-Cr phase showing a) [110] zone axis and b) [001] zone axis.

a=2.23 nm and c=1.25 nm (Widjaja and Marks 2002); [110] is the pseudo tenfold axis, where the lattice parameters were calculated using the MgO substrate as a calibrant (Fig. 3.2b). This confirms the previous report of the hexagonal phase as a new crystalline approximant of the Al-Cu-Fe-Cr decagonal phase (Li et al. 2002) in addition to the known orthorhombic and monoclinic approximant phases (Li et al. 1995). Shown in Fig. 3.12. are the diffraction patterns of the hexagonal phase along [110] and [001] zone axis.

3.1.6. Phase Segregation

For samples with annealing temperatures ranging from 300°C to 550°C, we observed a transformation from amorphous phases to a mixture of quasicrystalline and crystalline phases and grain growth. Higher annealing temperatures and

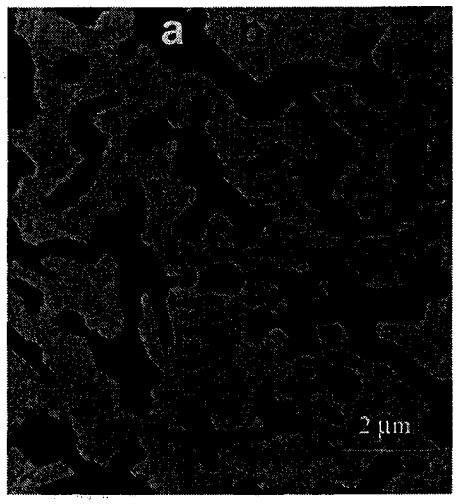

Figure 3.13. Bright field image showing thick quasicrystalline grains (a) after annealing at 575°C for 3 hours. Crystalline regions (b) surrounding these grains are very thin compared to the quasicrystalline regions.

longer annealing times resulted in larger grains. However at temperatures above 575°C, diffusion is highly enhanced. This results in thick quasicrystalline grains (Fig. 3.13.) and also leads to massive surface roughening. The regions surrounding these phases are crystalline and are very thin compared to the quasicrystalline grains.

The average composition of the thin regions is $Al_{38.9\pm3.6}Cu_{4.7\pm0.6}O_{56.4\pm4.1}$ as measured by EDX. The Cu signal observed is from the supporting grid and hence the composition of the crystalline regions is $Al_{41}O_{59}$ - fully oxidized aluminum film. This can be explained as follows: enhanced diffusion leads to the rapid growth of quasicrystalline phases resulting in the expulsion of excess elements

(mainly aluminum) to the surrounding matrix. These get oxidized upon subsequent exposure to air.

To study the phase segregation further, thin films of 300-400 nm thick were deposited on sodium chloride at room temperature. The films were annealed in an Ar flowing furnace at 400°C for 5 hours, removed from the substrate and supported by a holey C film on a Ni grid. The sample was further analyzed using a HF-2000 TEM in STEM mode to study the composition homogeneity across the film. Fig. 3.14. shows an area where a pure aluminium grain is observed (marked with a circle). An EDX line scan was carried out (marked with a line on the image) for 11 points with a step of 32 nm. The composition profiles of Cr-Fe-Cu and Al across the line scan are shown in Fig. 3.15. This result confirms the existence of aluminum grain in the film.

In addition to majority decagonal and hexagonal phases as discussed above, different minority phases exist. Depending on the importance of a specific physical property, these phases may be very crucial in determining the performance.

Growth on a 510°C heated substrate (with UHV post-annealing at the same temperature), as shown in Fig. 3.16, results in a similar phase segregation. Aluminum islands of the size 100-200 nm are observed. The SEM image along with EDX composition data reveals a little bit of the complexity. At least four different regions can be identified. Aluminium islands (region 1), similar to the aluminum

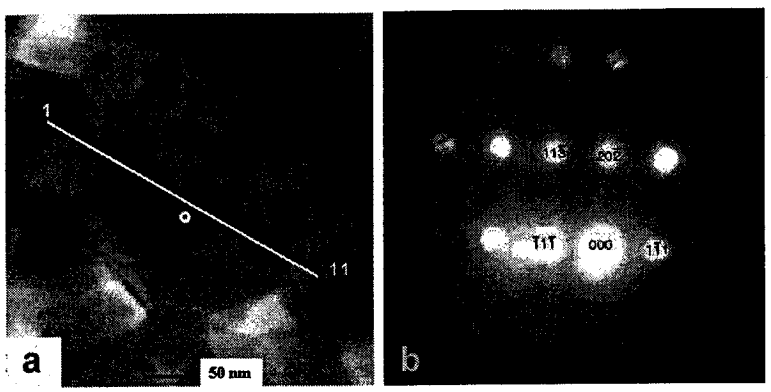

Figure 3.14. Segregation in Al-Cu-Fe-Cr systems upon annealing: a) grain of pure aluminum phase b) diffraction pattern of aluminum grain showing zone axis [121].

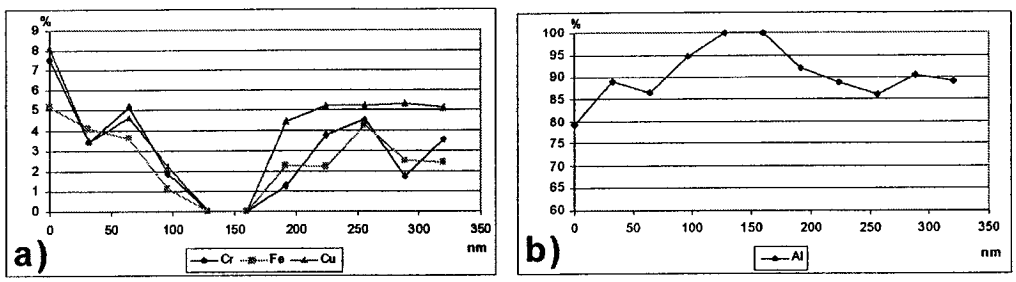

Figure 3.15. EDX scan for the corresponding line scan in Fig. 3.14 for a) Cu, Fe and Cr, and b) Al.

grains observed in Fig. 3.14., are surrounded by copper-rich aluminum alloys (region 3). Smaller islands of chromium-rich aluminium alloys are also observed while most of the 'flatter' areas (region 4), which are the majority, have a more homogenous composition. This film can not be straightforwardly compared to the rest of the films discussed in this chapter because it has a higher aluminum content in the initial film due to use of a different target, however, it serves the purpose to ilustrate the importance of composition in engineering the final structure.

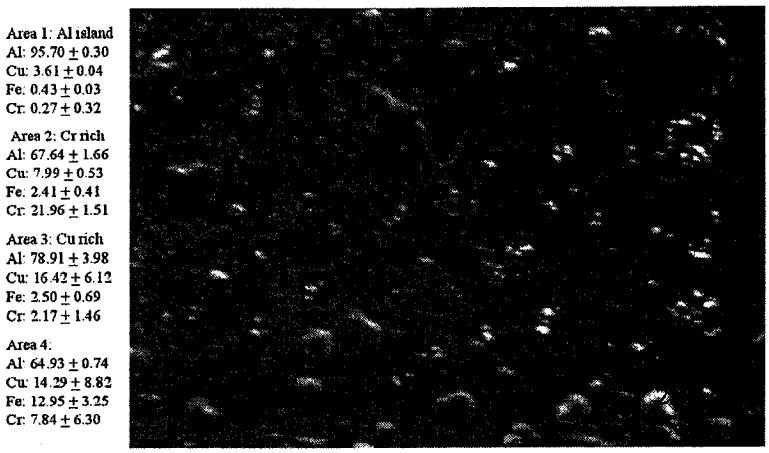

Figure 3.16. SEM image showing phase segregation for growth and post-growth annealing at 510°C.

3.2. Al-Cu-Fe Quasicrystalline Films

3.2.1. Experimental Details

Thin films of Al-Cu-Fe were grown on cleaved sodium chloride substrates in a magnetron sputtering chamber with a base pressure of $3x10^{-8}$ Torr. Depositions were carried out at 2.8 mTorr Argon (99.998% purity), 150 W and at room temperature without a substrate bias. The target was a metal alloy made through vacuum arc melting. After the deposition process, the samples were cleaved into two parts. One part was kept in the as-deposited state while the other sample was annealed in a furnace (at atmospheric pressure) with a continuous flow of Argon at 400°C for 4 hours. The annealed sample was then cut into two sections, and one was annealed further at 500°C in air for an additional 4 hours.

The sodium chloride substrates were subsequently removed by dissolving in water to acquire free-standing thin films of thickness approximately 150 to 200 nm. These thin films were then suspended on Mo hole-grids and studied using a Hitachi H-8100 TEM. The relative metallic compositions were determined from Energy Dispersive X-ray (EDX) spectroscopy, calibrated using single crystal icosahedral $Al_{63}Cu_{25}Fe_{12}$ as the standard. To detect phase transformations, Differential Scanning Calorimetric (DSC) studies were carried out from room temperature to 600°C at a heating rate of 5°C/min

3.2.2. As-deposited sample

Figure 3.17. shows TEM bright field images of films in the as-deposited condition and after the aforementioned annealing treatments. The as-deposited sample (Fig. 3.17a.) shows a nanocrystalline structure with a grain size < 10 nm. This structure was attributed to a combination of a rapid quenching effect and a small increase of the substrate temperature due to atom bombardment during deposition. The sample annealed at 400°C (Fig. 3.17b.) showed mostly a continuous film while the sample treated at 500°C (Fig. 3.17c.) exhibited some level of discontinuity across the thin film.

While there are few reports that claim the structure of the room-temperature as-deposited samples to be amorphous (Ding et al. 1997; Yoshioka et al. 1995), this is almost certainly strictly correct only when the substrate is cooled (e.g. to liquid

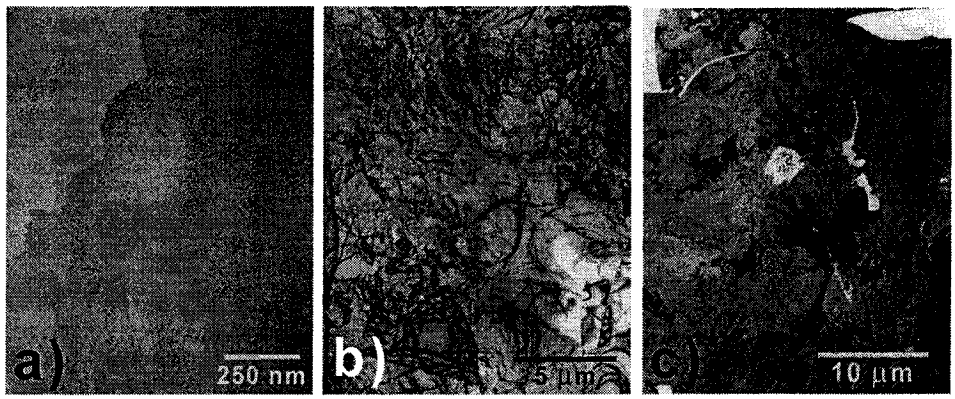

Figure 3.17. TEM bright field images of Al-Cu-Fe thin films in: a) the as-deposited condition; b) the sample annealed at 400°C in Ar; and c) the sample annealed at 500°C in air.

nitrogen (Chien and Lu 1992) or liquid helium (Roth et al. 1999) temperatures) or when substrate heating due to atomic bombardment can be prevented (e.g. the growth of very thin films (Widjaja and Marks 2002)). Production of amorphous films requires very high deposition rates and low substrate temperature; the latter immobilizes or freezes adatoms on the substrate where they impinge and prevents them from diffusing and seeking out equilibrium lattice sites (Ohring 1992). Due to the small grain sizes, nano-scale crystalline phases are generally indistinguishable from amorphous phase in XRD studies; however they are easily observable in TEM imaging.

3.2.3. Crystalline phases

The sample annealed at 400°C in Ar was composed of crystalline grains with an average grain size of a few microns, as shown in Fig. 3.18. Note that the average composition of the film in the sample annealed at 400°C in Ar was $Al_{64\pm3}Cu_{23\pm2}Fe_{13\pm1}$. Upon annealing at 400°C, the film formed large grains of intermetallic phases, demonstrating conventional grain growth driven by the reduction of grain boundary energy. No phase transformation to the quasicrystalline phase was observed. This finding was confirmed by DSC, which showed an exothermic peak at 440±15°C.

The structure of the intermetallics is the CsCl cubic β-phase, Al(Fe, Cu) with a lattice parameter of 0.294 nm. A diffraction pattern along the <212> zone axis is shown in Fig. 3.18c. This cubic structure is similar to the β-phase in the bulk phase diagram (Gratias et al. 1993) that extends over a large range of composition. A similar structure also appeared on the surface of a single grain icosahedral Al-Cu-Fe alloy upon ion bombardment (Qin et al. 1995; Yang et al. 1996; Shen et al. 1998); this was attributed to the preferential sputtering of aluminum from the surface.

The crystalline cubic β-phase in the 400°C annealed sample is a metastable phase at this composition and temperature, however there may be other metastable crystalline phases. In addition to the micron sized cubic β-phase grains, smaller grains of sizes less than 50 nm appear in the form of precipitates or islands at the

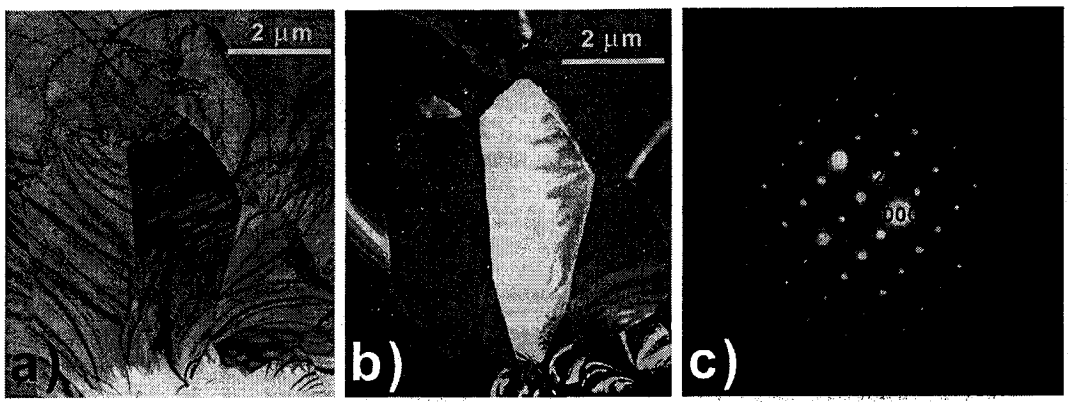

Figure 3.18. Observations made in thin film annealed at 400°C in Ar: a) TEM bright field image; b) TEM dark field image; and c) the electron diffraction pattern showing [212] zone axis of cubic crystalline β-phase.

surface, while larger grains of about 100-200 nm were found at grain boundaries, as shown in Fig 3.19a.

In addition to the majority cubic β-phase, Chien and Lu (Chien and Lu 1992) reported the existence of a second phase in their sample upon annealing at 450°C based on their XRD results, but were uncertain whether the second phase was cubic β-crystals with small grain sizes or amorphous. It needs to be noted that their film was deposited at liquid nitrogen temperature to try and produce an initial amorphous phase. However it is unlikely that the original amorphous phase will remain after the annealing treatment.

The secondary phases in our sample are crystalline with small grains that appear as precipitates and islands - in the matrices, on the surface and at grain boundaries. Fig.3.19a. is a TEM bright field image of a grain showing needle

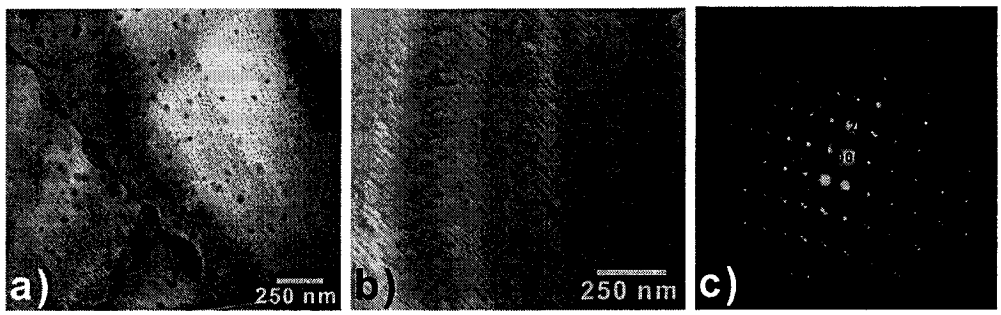

Figure 3.19. a-b) TEM bright field images of films annealed at 400°C in Ar showing small precipitates on larger cubic β-grains and larger precipitates at the grain boundaries; c) diffraction pattern of (a) near [213] zone axis of cubic crystalline β-phase.

precipitates along with islands; this image is equivalent to tilting the grain in Fig.3.19b. Combining these two images, it appears that these precipitates assume the shape of platelets and are highly textured within the matrix.

The β-phase in the bulk phase diagram has the composition of $Al_{50}Fe_{50-x}Cu_x$ (extends from AlFe up to 40% atomic percentage Cu) (Gayle 1992). Although the average composition of the grains, $Al_{64\pm3}Cu_{23\pm2}Fe_{13\pm1}$, is closer to the ω-phase (tetragonal Al_7Cu_2Fe with a = 0.634 nm and c = 1.487 nm), the larger grained crystalline phase is the cubic β-phase. Nevertheless, the true composition of the β-phase in the films may be less than the average composition due to contributions from the secondary phases. It is likely that the secondary phases are the θ-phase (tetragonal Al_2Cu with a = 0.6063 nm and c = 0.4872 nm) and/or the ω-phase. Both the θ- and ω- phases are richer in aluminum than the β-phase, allowing for a reduction of the aluminum content in the matrix, hence, gives more stability to the β-phase. The θ-phase can be incorporated into the β-phase matrix

coherently with relatively small strains, $e_x=e_y=(|2a_\beta-a_\theta|)/2a_\beta=3.1\%$ and $e_z=(|5a_\beta-3c_\theta|)/5a_\beta=1.2\%$. High-resolution electron microscopy is required to confirm this hypothesis. Fig. 3.19.e. shows the diffraction pattern along [213] zone axis of image in Fig. 3.19.a.; strong spots correspond to the matrix (β-phase) spots and weaker spots to the secondary phases. It is evident that the secondary phases are highly textured from the nonexistence of ring patterns.

3.2.4. Quasicrystalline phases

For the sample that was further annealed in air at 500 °C after annealing at 400 °C in Ar, the average composition of the film was $(Al_{65\pm3}Cu_{22\pm2}Fe_{13\pm1})_{84}O_{16}$. The high oxygen content was attributed to a surface oxide since the thickness of the film was only about 150-200 nm. Upon annealing at higher temperature, the intermetallic grains transformed into icosahedral ψ-grains. This film structure showed a large amount of the ψ-phase with grain sizes on the order of microns, similar to the grain sizes of the crystalline cubic β-phase. Figure 3.20. shows a bright field image of an icosahedral grain oriented along a 5-fold axis and the diffraction patterns of icosahedral grains from different zone axes.

In some cases regions which had the external shape that would be expected of a grain, but only contained fragments, were observed as shown in Fig. 3.21.a. We interpret this as a sacrificial grain, which decomposed during the phase transformations on annealing at the higher temperature.

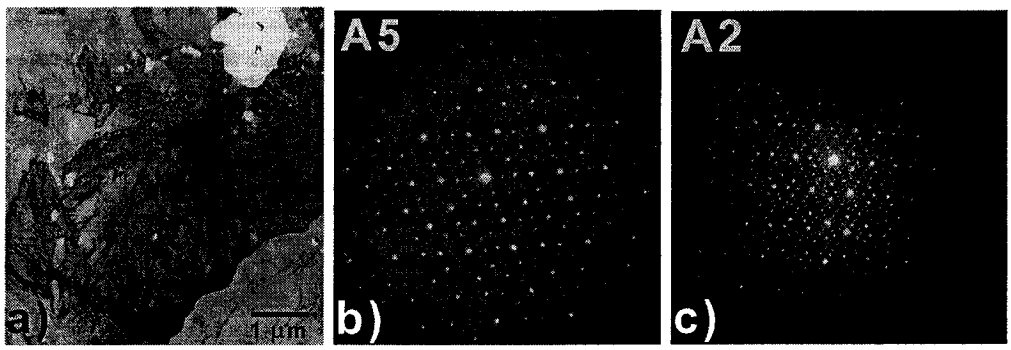

Figure 3.20. a) Bright field image of an icosahedral grain oriented along a zone axis; b) Electron diffraction pattern of icosahedral phase showing 5-fold symmetry; c) Electron diffraction pattern of icosahedral phase showing 2-fold symmetry.

Three main features were identified in these regions, namely a mixture of phases of composition $(Al_{78\pm4}Cu_{3\pm1}Fe_{19\pm2})_{75\pm4}O_{25\pm4}$ that was located within the region (Fig. 3.21.b-c.); an amorphous alumina residue $(Al_{97\pm1}Fe_{3\pm1})_{42\pm2}O_{58\pm2}$ (Fig. 3.21.d-e.); and an icosahedral grain adjoining the region (Fig. 3.21.f-g.).

The existence of the sacrificial grains is attributed to the composition fluctuation from the perfect icosahedral composition. These grains allow others to transform into ψ-phase. It appears that elements diffuse into neighboring grains without significant migration of grain boundaries. Elements near the boundary of the sacrificial grain diffused into other grains to form the ψ-phases (Fig. 3.21.f.) leaving fragments in the center of the grain. Areas where the elements diffused out from the grains (Fig. 3.21.d.) were identified as the oxide layer.

The fragments in the center of the grain, with the average composition of $Al_{78\pm4}Cu_{3\pm1}Fe_{19\pm2}$ (excluding the oxygen), have the composition of the λ-phase.

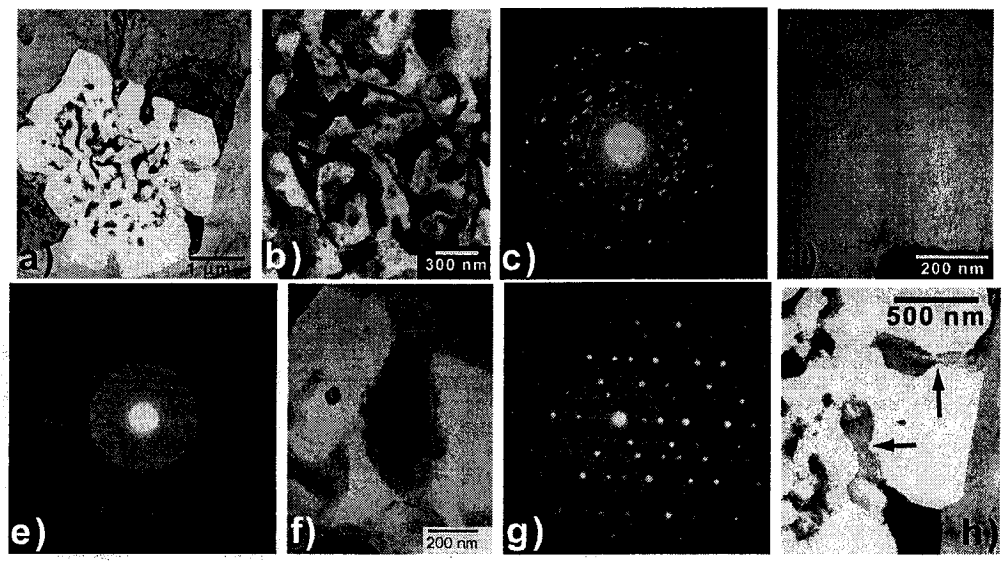

Figure 3.21. a) Image of sacrificial grain due to phase transformation into quasicrystalline phases. The three main features associated with the transformation are shown in (b-h); b) TEM image of a mixture of phases remaining in the region; c) the corresponding diffraction pattern of phases in (b); d) TEM image showing the amorphous alumina residue; e) the corresponding diffraction pattern of the amorphous alumina residue; f) TEM image of an icosahedral grain adjoining the sacrificial grain; g) the corresponding diffraction pattern of the icosahedral grain. h) formation of λ-phase fragments.

Most spots in the diffraction pattern in Fig. 3.21.c. can be indexed as the λ-phase, the rest is due to minor secondary phases. The λ-phase is the monoclinic $Al_{13}Fe_4$-phase (with a = 1.5489 nm, b = 0.80831 nm, c = 1.2476 nm, and β = 107.72° (Black 1955)), which extends up to 6% atomic percentage of Cu. Similar to the crystalline β-phase that creates secondary phases (θ- and ω-phases) in 400°C annealed samples, the ψ-phase expels the excess aluminum element in the form of λ-phase. The mechanism of the λ-phase expulsion can be inferred from

Fig. 3.21.h. Excess elements segregate to the grain boundaries with the sacrificial grains creating finger-like shapes. The finger-like shape becomes a fragment due to curvature reduction diffusion (shown by the arrows in Fig. 3.21.h.) and coalesces with others to form the mixtures of fragments observed in Fig. 3.21.b. These fragments become interconnected by further diffusion.

We hypothesize that mass transfer by diffusion of the elements to the neighboring grains is higher than what can be accomodated by lateral grain growth. This leads to a rapid growth along the third dimension, resulting in films with high roughness. Bonasso et al. (2002) reported observation of clusters with size of 500-1000 nm wide upon annealing Al-Cu-Fe film of 150 nm thickness. This effect has also been observed in a similar growth of 150 nm Al-Cu-Fe-Cr quasicrystalline thin films where the average roughness was more than 50 nm after phase transformation (Widjaja and Marks 2002). The roughening phenomenon is prominent in thin films where the grain size is comparable to or larger than the film thickness.

In a sputter deposition of Al-Cu-Fe film on a heated substrate at 460°C, Eisenhammer and Trampert (1997) reported that for a coverage equal to 3.5 nm the Al-Cu-Fe icosahedral phase grows as isolated nano-particle with a mean diameter of about 15 nm and projected layer thickness amounted to 13-14 nm. Therefore, the high-temperature as-deposited Al-Cu-Fe film in their experiment is discontinuous, similar to our annealed sample at 500 °C. Our previous study on Al-Cu-Fe-Cr decagonal thin films shows similar behavior upon annealing at 575°C (Widjaja and

Marks 2002), where the decagonal and the hexagonal approximant coexist with other crystalline phases exhibiting a turtle shell-like pattern with large plateaus surrounded by channels.

In addition to diffusion, the interface and surface energies of the phases also play an important role in microstructural evolution. The lower surface energy of icosahedral phase compared to the crystalline phases results in a preference to grow as islands. A more accurate theory of the cubic-icosahedral phase transformation, in relationship with morphology and microstructural evolution, requires in-situ heating TEM studies where nucleation and phase growth can be observed directly. Nevertheless, we believe our proposed microstructural evolution in β-ψ -phase transformation, as summarized in Fig. 3.22, based on our observation to be substantial even though the mechanism is not directly observed.

Furthermore, Figs. 3.18.a. and 3.20.a. show that both crystalline and quasicrystalline grains have comparable sizes - on the order of microns. By implementing a two-stage annealing process, the size of the icosahedral grains can be controlled indirectly with a lower temperature anneal prior to phase transformation.

3.2.5. Oxide Layer

The oxidized regions of the film, which from EDX were identified to be almost pure aluminum oxide, were fairly stable at this annealing temperature. This oxide

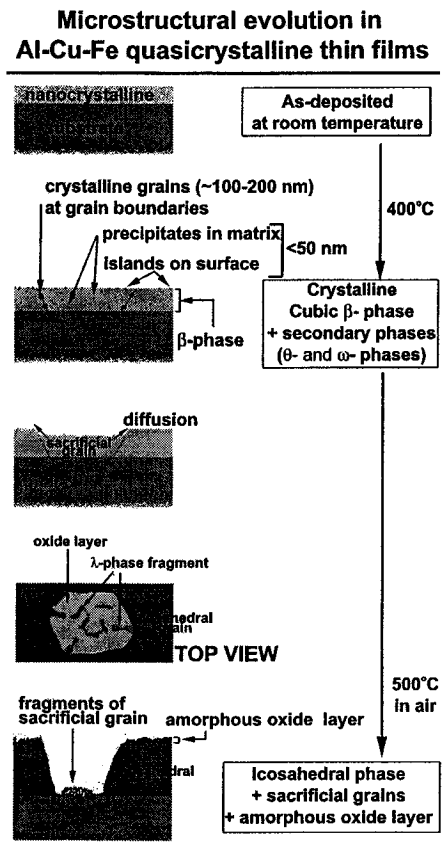

Figure 3.22. Schematic of microstructural evolution in Al-Cu-Fe quasicrystalline thin films.

layer residue was similar to the oxide layer elsewhere on the film, due to oxidation at high temperature (Fig. 3.23a), and was amorphous (Fig. 3.23b). This was also observed in Al-Cu-Fe-Cr thin films where annealing at 575°C resulted in a thin residue of aluminum oxide (Widjaja and Marks 2002). It was observed that this oxide layer delaminated easily, indicating poor adhesion to the quasicrystalline film (Fig. 3.23c).

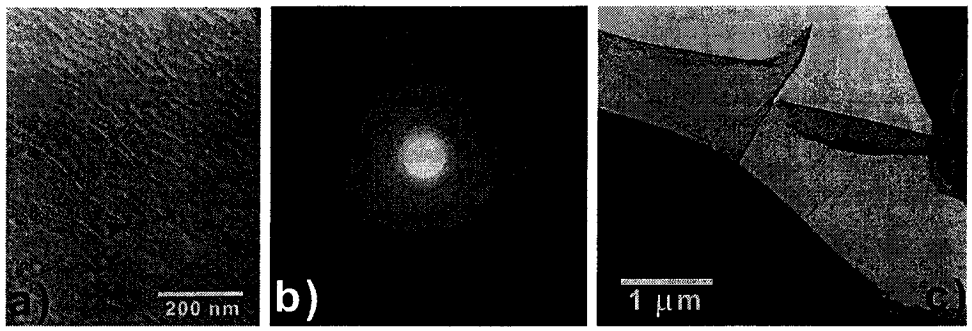

Figure 3.23. a) TEM image of the oxide layer of the film showing an amorphous structure; b) diffraction pattern of the oxide layer; c) delamination of the oxide layer from the quasicrystalline film.

CHAPTER 4

Quasicrystallline Thin Films: Epitaxial and Interface

Shortly after the discovery of quasicrystals, it was established that the structure of icosahedral Al-Mn undergoes a phase transition when exposed to irradiation of energetic particles (Urban et al. 1985). Bombardment with Ar^+ ions at room temperature transforms the quasicrystalline surface into a crystalline cubic structure due to preferential sputtering of the Al atoms from the surface.

The resultant crystalline structure has a specific orientation relationship with respect to the quasicrystalline substrate. Similar behavior has been observed in other quasicrystal systems such as decagonal $Al_{70}Ni_{15}Co_{15}$ (Zurkirch et al. 1998; Qin et al. 1995), icosahedral $Al_{65}Cu_{20}Fe_{15}$ (Yang et al. 1996; Shen et al. 1998), decagonal $Al_{70}Cu_{15}Co_{15}$ (Zhang and Geng 1992; Zhang and Urban 1989) and decagonal $Al_{75}Ni_{10}Fe_{15}$ (Zhuang et al. 1993). Many studies have been devoted to determining the orientational relationship between the quasicrystal and crystal phases by means of Transmission Electron Microscopy (TEM) (Qin et al. 1995; Yang et al. 1996; Zhang and Geng 1992; Zhang and Urban 1989), Low Energy Electron Diffraction (LEED) (Shen et al. 1998), Secondary Electron Imaging (SEI) (Zurkirch et al. 1998) and Reflection High-Energy Electron Diffraction (RHEED) (Shimoda et al. 2000b, 2001, 2002).

Of some interest from an application viewpoint is the question of whether or not one can grow these quasicrystalline films epitaxialy. Previous studies on phase transformation on single grain quasicrystals due to ion sputtering, partially listed above, have shown that the crystalline layers formed on the surfaces have certain orientations with respect to the single crystals. This support the idea that there is an interface configuration where certain angular orientation will result in lower energy. The epitaxy in this case may be governed by local rearrangement of atoms in a relatively small scale due to kinetic energy from ion bombardment. The possibility to nucleate and grow epitaxy quasicrystalline thin films is a different question and crucial to be answered.

One would expect some anisotropy of properties could be exploited in thin film applications. Surface properties, for example friction, will depend on in-plane orientation of the rubbing surfaces and the direction of sliding (Gyalog and Thomas 1995; Ko and Gellman 2000). An epitaxy quasicrystalline film with a specific out-of-plane orientation will perform differently depending on the existence of in-plane orientation preferences. A random in-plane orientation will effectively result in an isotropic surface where one might still expect a low frictional value independent of direction. This will also dictate the adhesion between the substrate and the film. On the other hand, a strong preference for one in-plane orientation will result in surface anisotropy.

4.1. Epitaxial Quasicrystalline Thin Films

There is already one paper (Li et al. 1997), which used post-annealing of magnetron deposited films on sapphire substrates at 600°C, and x-ray diffraction as a test for orientation. This paper explains the epitaxy on the basis of flat surfaces of the decagonal planes which will allow minimal interface energy; however it neglects the preference for an in-plane orietation.

Excepting this work, research in this area had been limited to establishing the relationship between quasicrystal single crystals to their crystalline approximants induced by ion sputtering (Zhang and Geng 1992; Zhuang et al. 1993; Shen et al. 1998) and quasicrystal precipitates to their crystalline matrixes due to ion implantation (Zhang et al. 1997). These may impose restrictions on the geometric orientation because the phases appear as a result of local rearrangement or displacement of atoms due to energetic particles.

More recently, there had been studies on the geometric relationship between crystalline thin films on quasicrystal substrates by physical vapor deposition. Shimoda et al. (2000b) attempted to grow Au thin film ($\sim$ 0.19 nm) on decagonal Al-Ni-Co and reported the orientation of the alloyed $AuAl_2$ layer with respect to the substrates. Bolliger et al. (2001) reported epitactic growth of aluminum film ($<$ 8 nm) on the fivefold-symmetric surface of icosahedral Al-Pd-Mn, however the stability was limited to 50°C due to diffusion of Al into the sample.

The majority of these works, as shown in Fig. 4.1., however, explain the observed orientation of the structures from a stereographic projection through a description of the rotation axis alignment. While this is a valid approach for describing the orientation, this method offers no insight into the fundamental mechanism behind the preferred orientation. Three existing papers (Shimoda et al. 2000b; Zurkirch et al. 1998; Bolliger et al. 1998) described their findings via an atomic model of the two dimensional interface between the quasicrystal and crystal phases that is obtained by superimposing the surface structures, as shown in Figs. 4.2. and 4.3. The validity of these atomic models relies heavily on a real space structural model for the quasicrystal system, which may not be readily available or, in some cases, may not be correct. Furthermore, their models fall short of the long range fitting for the superimposed structure since the misfit dislocations and interface relaxations are ignored.

Shen et al. (1998) explained the orientation relationship between different surfaces of icosahedral Al-Cu-Fe and its cubic phase via a structural model of cubic close packed and icosahedral packed clusters, as shown in Fig. 4.4. This approach allows only one single orientation for any given system; this is in contrast to observations where multiple orientations were observed, even for the same surfaces, for example the Al-Ni-Co 2D surface (Qin et al. 1995). It should be noted that all of the methods employed to date do not take into account the role of the interfacial energy. Thus, there is a need to develop an improved model that will enhance the

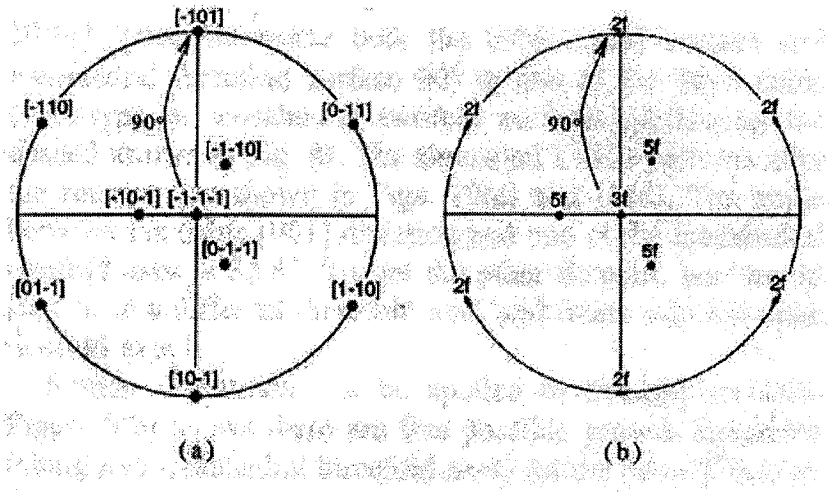

Figure 4.1. Stereographic projection of a) cubic along [111] and b) icosahedral along 3-fold zone axis showing similarity and alignment of rotation axis (Shen et al. 1998)

fundamental understanding of quasicrystal-crystal epitaxy. In none of the work to date has there been any attempt to explain the observed orientational relationship. In addition, it is not clear in any of the prior work if true thermodynamic equilibrium of the quasicrystal-substrate interface has been achieved.

4.1.1. Experimental Details

Thin films were deposited in a magnetron sputtering chamber with a base pressure of 5 x 10^{-10} Torr. Deposition were carried out at 2.8 x 10^{-3} Torr Argon (99.998 purity), 150 W and no substrate bias. The average compositions of the films were $Al_{86.3\pm4.4}Cu_{3.9\pm0.7}Fe_{5.4\pm0.4}Cr_{4.4\pm0.5}$ and $Al_{82.5\pm4.3}Cu_{4.0\pm0.5}Fe_{7.9\pm0.7}Cr_{5.5\pm0.3}$ as

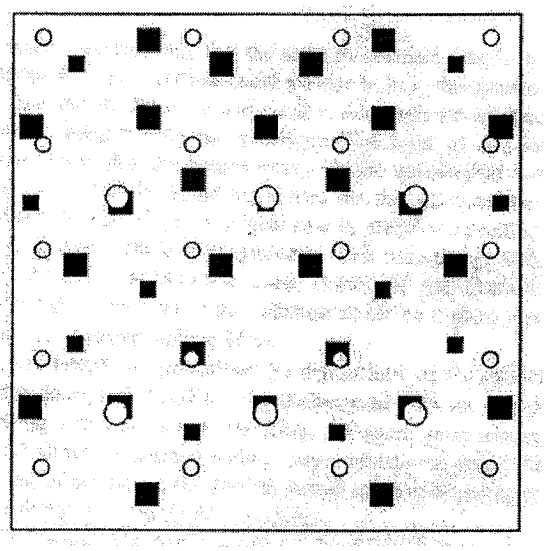

Figure 4.2. Superimposition of $Al_{72}Ni_{12}Co_{16}$ quasicrystal and $AuAl_2$ crystal surfaces. (Shimoda et al. 2000b)

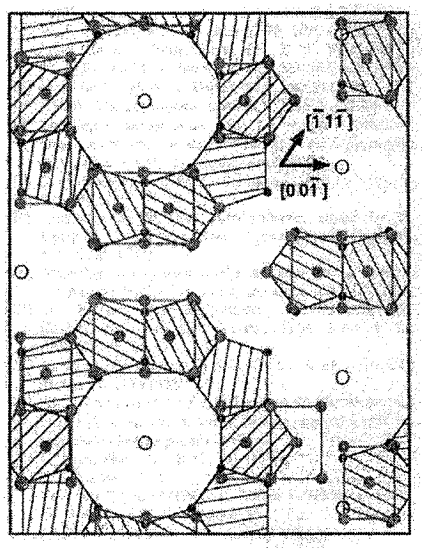

Figure 4.3. Superimposition of $Al_{70}Pd_{20}Mn_{10}$ quasicrystal and Al crystal surfaces. (Bolliger et al. 1998)

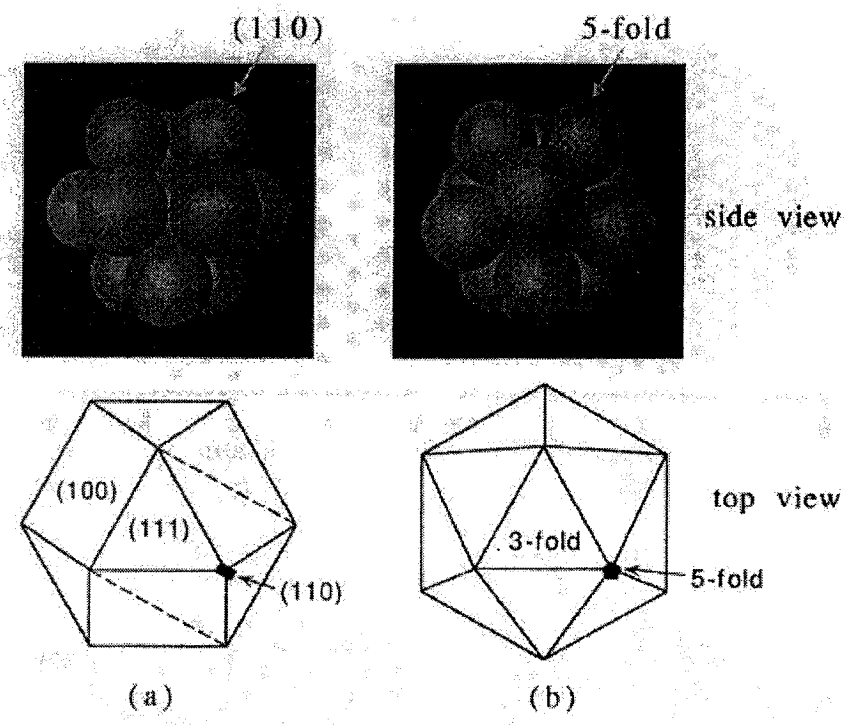

Figure 4.4. Structural model comparing a) ICP (Icosahedral Close-Packed) and b) CCP (Cubic Close-Packed) clusters. (Shen et al. 1998)

measured by in-situ XPS and ex-situ EDX (Energy Dispersive Spectroscopy) respectively (calibrated via Atomic Emission Spectroscopy). Measurements by EDX of the composition of single grains of the decagonal phase gave a composition of $Al_{78.3\pm4.5}Cu_{7.6\pm1.4}Fe_{7.5\pm1.9}Cr_{6.6\pm1.0}$. As a consequence, the overall film was not phase pure, but this is not relevant for the results described herein.

The samples were taken out from the UHV chamber and put in a flowing Ar tube furnace for annealing. The annealing treatment proceeded in two steps: preheating at 575°C for 22 hours and subsequent heating at 800°C for 2 hours. The samples were then brought to room temperature with a cooling rate of less than 4°C per minute. Studies on thin films annealed at 300-400°C did not show any specific orientations between the decagonal films and the atomically flat crystalline substrates (Widjaja and Marks 2002). The preheating temperature was chosen to allow grains reorientation because at this temperature solid diffusion is enhanced (Widjaja and Marks 2002). Additional heating at 800°C was intended to equilibrate the samples as observed in multilayer post annealing of Al-Cu-Co decagonal material (Li et al. 1997). The annealed samples were studied using a Hitachi H-8100 TEM.

Samples for diffraction intensity measurement were deposited on sodium chloride crystals at room temperature and annealed in flowing Ar to form the decagonal phase. The substrates were removed by dissolving in water to acquire free standing thin films. These were then suspended on holey-carbon films in Ni grids and studied using a JEM-3000 TEM. Diffraction patterns were recorded digitally using Digital Micrograph 3.00 and were processed using Semper software; the diffraction intensity were measured using a cross correlation method (Xu et al. 1994).

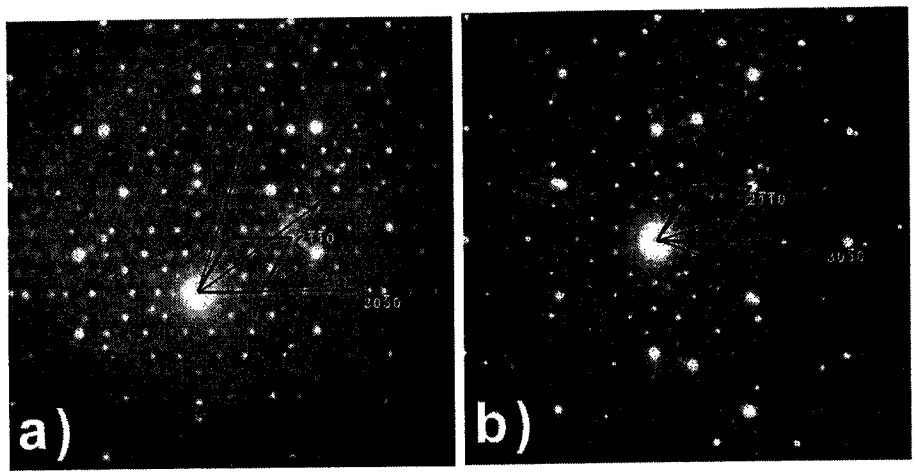

Figure 4.5. Superimposed diffraction patterns from decagonal quasicrystals on sapphire substrate showing $A_{10}||[0001]_{Al_2O_3}$: a) $A_{2P}||[10\bar{1}0]_{Al_2O_3}$ and b) $A_{2D}||[10\bar{1}0]_{Al_2O_3}$. The two unique orientations are related with six degree rotation of the decagonal phase along the ten-fold axis with respect to the crystalline substrate. (Widjaja and Marks 2003a)

4.1.2. Results

Selected Area Diffraction patterns on the annealed samples as shown in Fig. 4.5. correspond to a decagonal diffraction pattern superimposed on the substrate diffraction pattern. The decagonal phases in the thin films have the ten-fold axis oriented parallel to the substrate surface normal, $A_{10}||[0001]_{Al_2O_3}$.

Diffraction pattern of the decagonal phase along the ten-fold direction and the sapphire substrate show tenfold symmetry (equivalent to 36° rotation) and three fold symmetry (equivalent to 120° rotation). Therefore the unique orientation of both diffraction patterns is limited to 12° of rotation. Only two unique relative

orientations were observed, $A_{2D}|||[10\ \bar{1}\ 0]_{Al_2O_3}$ and $A_{2P}|||[10\bar{1}0]_{Al_2O_3}$, where A_{2D} and A_{2P} represent the two types of the two-fold axes in decagonal phase.

4.1.3. Analysis

A common approach for describing the observed two unique orientations is symmetry and alignment of rotation axis (Zhang and Geng 1992; Zhang and Urban 1989; Shen et al. 1998; Bolliger et al. 2001). In the configuration observed in Fig. 4.5., there are common symmetry element - mirror planes - which is the subgroup common to both structures, and alignment of the 2-fold decagonal with 2-fold of the sapphire.

However, while this is a viable way of describing the orientation relationship, it does not answer the fundamental question - the energetics. Interface energies between two crystalline materials are relatively well understood, and there are three commonly used models: the coincident site lattice model (Grimmer 1984, 1989; Wolf and Yip 1992; Sutton and Balluffi 1995), coincidence of reciprocal lattice planes (CRLP) (Fletcher and Adamson 1966; Ikuhara and Pirouz 1996; Stemmer et al. 1996) and the d-spacing concept (Wolf and Yip 1992; Sutton 1992; Sutton and Balluffi 1995). Of these the original CRLP model can be applied to quasicrystals, with one important extension that appears to have been omitted to date in the literature.

Our initial simple model results in a total energy of form:

$$E \approx E_o - \left\{ \sum_{\kappa} \frac{I(\mathbf{q})}{\kappa} \right\}, \tag{4.1}$$

where κ is the magnitude of the vector joining two diffraction spots from the bicrystal and I($\mathbf{q}$) is the intensity of the diffraction spots for the wavevector $\mathbf{q}$. The derivation for this equation and a more rigorous development will be further discussed in section 4.2.

A schematic reciprocal lattice is shown in Fig. 4.6. We included the diffraction spots of alumina (corundum structure) which are forbidden in the bulk but allowed at a surface or interface. Since E $\sim$ -1/κ, the spots with small κs dominate the energy term. Therefore, only the set of spots that are closest to $(10\bar{1}0)$ and $(1\bar{2}10)$, set A for the (11100) spots and set B corresponding to the (12210) reflections, needed to be considered in the calculation. Reciprocal spacings of $(10\bar{1}0)$ and $(1\bar{2}10)$ of Al_2O_3, (11100) and (12210) of the decagonal were calculated and measured to be 2.4243 nm^{-1}, 4.199 nm^{-1}, 2.5399$\pm$0.0219 nm^{-1} and 4.1068$\pm$0.0319 nm^{-1}. The measured intensity ratio I_A/I_B was 2.7$\pm$0.6.

Starting with the configuration where A_{2P} is aligned with $[10\bar{1}0]$, and using this as the rotational origin of 0°, the summation of -I($\mathbf{q}$)/κ for the spots from different sets,

$$E \approx -\left\{ \sum_{\kappa_A} \frac{I(\mathbf{q_A})}{\kappa_A} + \sum_{\kappa_B} \frac{I(\mathbf{q_B})}{\kappa_B} \right\} \tag{4.2}$$

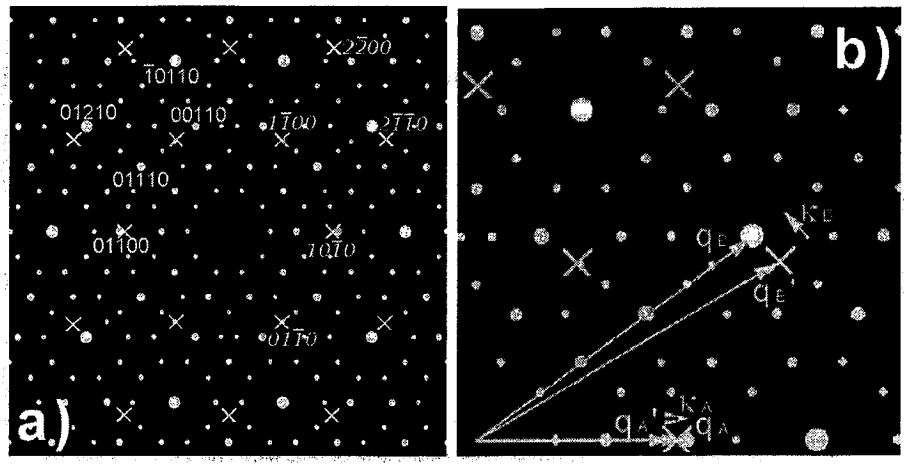

Figure 4.6. Schematic reciprocal lattice planes of decagonal quasicrystal and alumina crystal: a) filled circles and *X*s mark decagonal and alumina diffraction spots respectively; b) decagonal ($\mathbf{q}_A$ and $\mathbf{q}_B$) and alumina ($\mathbf{q'}_A$ and $\mathbf{q'}_B$) vectors in reciprocal lattice and their corresponding $\boldsymbol{\kappa}$ vectors ($\boldsymbol{\kappa_A}$ and $\boldsymbol{\kappa_B}$).

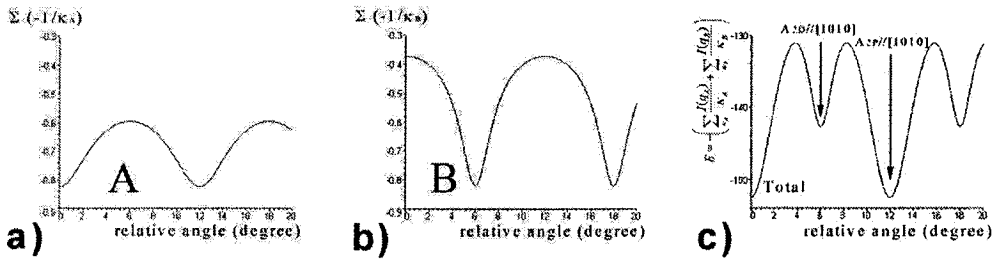

Figure 4.7. Energy calculation: a) E=-1/κ_A for set A; b) E=-1/κ_B for set B; and c) total energy; showing two minima corresponding to $A_{2P}|||[10\bar{1}0]_{Al_2O_3}$ and $A_{2D}|||[10\bar{1}0]_{Al_2O_3}$. The graph shows the 12° rotation periodicity.

is plotted in Fig. 4.7.

There are energy minima, at 0° ($A_{2P}|||[10\bar{1}0]_{Al_2O_3}$) and 6° ($A_{2P}|||[1\bar{2}10]_{Al_2O_3}$). These minima are equivalent to $A_{2D}|||[10\bar{1}0]_{Al_2O_3}$ and $A_{2P}|||[10\bar{1}0]_{Al_2O_3}$, which are the observed orientations.

4.2. Interface Model for Quasicrystal-Crystal

A very simplistic view of the epitaxial growth places importance upon the principle that the coherent overgrowth of crystal material Y on crystal X is likely to occur if some undistorted crystal plane of Y can be laid down on top of the exposed face of X, in such a way that a large fraction of the Y atoms can be made to coincide with the sites of X atoms. It can be further understood that the greater the number of coincidences per unit area, the lower the energy of the resulting interface will be. This basic principle is the backbone of the coincidence-site-lattice (CSL) theory which was first investigated by Friedel (1926) and later explored by Ranganathan (1966) and applied to cubic lattices by Grimmer (1974a, b); Grimmer et al. (1974); Grimmer (1976).

The CSL concept was implicitly incorporated in the approach superimposition of real space atomic models employed by Shimoda et al. (2000b); Zurkirch et al. (1998); Bolliger et al. (1998). Unfortunately their approach lacks theoretical mathematical expressions that include the interfacial energy. In earlier work by Warrington et al. (1997), a CSL theory was applied to investigate grain boundaries in icosahedral quasicrystals. The CSL method employed is a N-dimensional CSL (Fortes 1983) due to the quasi-periodic nature of quasicrystals. The focus of this work was to determine the quasicrystal rotations in order to classify disorientation and to find the degeneracy of different values of the coincidence index. However, such an N-dimensional approach does not offer the potential to

solve the problems associated with the interfacial energy in the systems; hence a three-dimensional (3D) structural description needs to supplement the hyper-crystal description. (Mandal and Lele 2000)

4.2.1. Coincidence Reciprocal Lattice Planes Model for Quasicrystals

Given that the nature of the system is quasi-periodic, the three-dimensional (3D) reciprocal space of quasicrystals can be mathematically described through a projection from a periodic higher dimension. In addition to that, the reciprocal space can also be directly deduced from electron diffraction patterns. The 3D approach in a CRLP model for a quasicrystal-crystal interface enables the calculation of the interfacial energy in a similar approach to a crystal-crystal epitaxy. We employ this reciprocal space approach to explain the experimentally observed orientation preference.

The improved CRLP model is based on the crystal-crystal epitaxy model previously developed by Fletcher (1964) that will be shown also to be applicable to quasicrystal-crystal epitaxy. The original CRLP model by Fletcher and Lodge (1975) was exploited as the starting point, as described in the following paragraphs.

The potential energy $V_\circ$ of a **Y** atom at position **r** outside a plane face of a **X** crystal with atomic positions **R**, $V_\circ(\mathbf{r})$, can be written in terms of its Fourier components $V_\circ(\mathbf{k})$ as:

$$V_\circ(\mathbf{r}) = \frac{N}{8\pi^3} \int V_\circ(\mathbf{k}) exp(i\mathbf{k}.\mathbf{r}) d\mathbf{k}, \tag{4.3}$$

$$V_o(\mathbf{k}) = \frac{1}{N}\sum_{R}^{-} v(\mathbf{k}) exp(-i\mathbf{k}.\mathbf{R}), \tag{4.4}$$

where N is the (infinite) number of atoms in the crystal and $v(\mathbf{k})$, the Fourier transform of the atomic potential $v(\mathbf{r})$, is given by

$$v(\mathbf{k}) = \int v(\mathbf{r}) exp(-i\mathbf{k}.\mathbf{r}) d\mathbf{r}. \tag{4.5}$$

Assuming the crystals to be undistorted, the total interaction energy between two crystals, E_o^T, can be expressed through the summation of $V_o(\mathbf{r})$ over all the atomic position $\mathbf{R}'$ of the Y crystal, resulting in:

$$\begin{aligned} E_o^T &= \sum_{R'}^{+} V_o(\mathbf{R}') \\ &= \frac{1}{8\pi^3}\sum_{R'}^{+}\sum_{R}^{-} \int v(\mathbf{k}) exp[i\mathbf{k}.(\mathbf{R}' - \mathbf{R})] d\mathbf{k}, \end{aligned} \tag{4.6}$$

where the plus and minus signs on the summations indicate that it extends only over the upper and lower half-space, respectively.

The equation to describe the interfacial energy per unit area, E_o, can then be simplified to:

$$\begin{aligned} E_o = \quad & \frac{1}{2\pi AA'} \delta_{\mathbf{k}_s,\mathbf{q}_s} \delta_{\mathbf{k}_s,\mathbf{q}'_s} exp(i\mathbf{k}_s.\mathbf{B}_s) \\ & \times \sum_{R'_3}^{+}\sum_{R_3}^{-} \int v(\mathbf{k}) exp[ik_3.(R'_3 - R_3 + B_3)] dk_3, \end{aligned} \tag{4.7}$$

with a sum over all surface reciprocal lattice vectors for each crystal $\mathbf{q}_s$ and $\mathbf{q}'_s$, where A and A′ are areas of the surface unit cells, $\mathbf{B}$ is the relative translation of the two lattices, the subscript 3 represents the component of a vector normal to the interface, $\mathbf{R}$ and $\mathbf{R}'$ have been redefined such that each is measured from an origin fixed on a lattice point of its respective crystal, $\mathbf{R}_s$ and $\mathbf{R}'_s$ are the associated surface lattice vectors and $\mathbf{k}_s$ is the component of $\mathbf{k}$ parallel to the surface.

We will now allow elastic displacement of atoms near the interface with a displacement of:

$$F(\mathbf{R}) = -\sum_{\kappa}{}^{+} 2[D_\kappa sin(\boldsymbol{\kappa}.\mathbf{R}) + C_\kappa cos(\boldsymbol{\kappa}.\mathbf{R})] - C_\circ, \tag{4.8}$$

where $\boldsymbol{\kappa}$ is a vector corresponding to allowed distortion components. Thus, the interfacial energy described in equation (4.6) becomes:

$$E_\circ^T = \frac{1}{8\pi^3}\sum_{R'}{}^{+}\sum_{R}{}^{-}\int v(\mathbf{k})exp[i\mathbf{k}.(\mathbf{R}' + \mathbf{F}' - \mathbf{R} - \mathbf{F})]d\mathbf{k}, \tag{4.9}$$

Repeating the same procedure applied to Eq. (4.6) to result in Eq. (4.7), Eq (4.9) can be transformed for a simple basis into:

$$
\begin{aligned}
E_o = \quad & \frac{1}{2\pi AA'} \sum_{k_s} V_o(\mathbf{k}_s, B_3) exp(i\mathbf{k}_s.\mathbf{B}_s) \\
& \left\{ \prod_{\kappa} J_0(2\mathbf{k}.\mathbf{D}_\kappa) J_0(2\mathbf{k}.\mathbf{C}_\kappa) \right\} \times \left\{ \prod_{\kappa} J_0(2\mathbf{k}.\mathbf{D}'_\kappa) J_0(2\mathbf{k}.\mathbf{C}'_\kappa) \right\} \\
& \times \{ \delta_{k_s,q_s} \delta_{k_s,q'_s} + \sum_{n=1}^{\infty} \sum_{\kappa}{}^{+} \left[\frac{J_n(2\mathbf{k_s}.\mathbf{D}_\kappa)}{J_0(2\mathbf{k_s}.\mathbf{D}_\kappa)} + i^n \frac{J_n(2\mathbf{k_s}.\mathbf{C}_\kappa)}{J_0(2\mathbf{k_s}.\mathbf{C}_\kappa)} \right] \delta_{q_s+n\kappa,q'_s} \delta_{k_s,q'_s} \\
(4.10) \qquad & + \sum_{n=1}^{\infty} \sum_{\kappa}{}^{+} \left[\frac{J_n(2\mathbf{k_s}.\mathbf{D}'_\kappa)}{J_0(2\mathbf{k_s}.\mathbf{D}'_\kappa)} + i^n \frac{J_n(2\mathbf{k_s}.\mathbf{C}'_\kappa)}{J_0(2\mathbf{k_s}.\mathbf{C}'_\kappa)} \right] \delta_{q_s+n\kappa,q'_s} \delta_{k_s,q_s} + \ldots \}
\end{aligned}
$$

In Fletcher's original derivation, only a simple basis for the unit cell was employed, and the delta functions arose via a sum over all atoms in the interface, i.e.

$$
(4.11) \qquad \sum_{R} exp(i\mathbf{k}.\mathbf{R}) = N\delta_{k,q}
$$

for N atoms. This is not correct in general, and the equation has to be modified by replacing everywhere $\delta_{k_s,q_s}\delta_{k_s,q'_s}$ by $\mathrm{U}(\mathbf{q})\mathrm{U}(\mathbf{q}') \times \delta_{k_s,q_s}\delta_{k_s,q'_s}$, where

$$
(4.12) \qquad U(\mathbf{q}) = \sum_{R} exp(i\mathbf{q}.\mathbf{R})
$$

with a sum over the basis of the unit cell. This term, Eq (4.12), which by analogy to crystallographic direct methods where it also arises, is referred to as a Unitary Structure Factor (Giacovazzo 1998).

From Eq. (4.10) (after expanding the Bessel functions and keeping first-order terms only) and (4.12), an energy minimization with respect to $\mathbf{D_k}$ and $\mathbf{B}$ results in an approximate total energy of the form:

$$E \approx E_0 - t\sum_{\kappa} \frac{[U(\mathbf{q})v(\mathbf{q})]^2}{\kappa} \tag{4.13}$$

where E_0 is the coincidence part of the boundary energy, t is a constant, κ is the vector joining two diffraction spots from the bicrystal and $v(\mathbf{q})$ is the atomic interaction potential. The constant t, which depends on many parameters such as shear modulus, bulk modulus and Poisson's ratio, is important to calculate an expected value for the total energy; however the value of this constant is not meaningful in our consideration since only relative values are important, hence t was chosen arbitrary to give a convenient energy scale. A more complete solution can be obtained by equating the tractions across the interface; we will only use this first-order approximation here.

An accurate interaction potential is unknown at the present time for the quasicrystal crystal interface; nevertheless we will use a model potential for exploratory calculations introduced by Fletcher (1967) which has the form:

$$v(\mathbf{q}) = H\left(\frac{a+b}{a}\right)^3 \{exp\,[2.5q(a+b) - 4] + 1\}^{-1}, \tag{4.14}$$

where H is a scale constant, a and b are atomic radii of crystals X and Y, respectively. In this model, only interactions with atoms lying in neighboring planes

Table 4.1. Expected value for atomic radii and alpha. The values are calculated based on a weighted average of the individual atomic radius (The values for atomic radius are calculated values using self-consistent-field functions [(Clementi and L.Raimondi 1963; Clementi et al. 1967)])

Quasicrystal Compound	Atomic Radius (Å)	Crystal Compound	Atomic Radius (Å)	α
$Al_{65}Cu_{20}Fe_{15}$	1.291	$Al_{50}Cu_xFe_{1-x}$	1.339	6.574
$Al_{70}Ni_{15}Co_{15}$	1.278	$Al_{50}Ni_xCo_{1-x}$	1.343	6.550
$Al_{65}Cu_{20}Co_{15}$	1.226	$Al_{50}Cu_xCo_{1-x}$	1.330	6.390
$Al_{70}Ni_{15}Co_{15}$	1.278	$AuAl_2$	1.367	6.610
$Al_{70}Ni_{15}Co_{15}$	1.278	$PtAl_2$	1.377	6.635

parallel to the interface are considered; in addition this potential has a repulsive core which is not so hard. The Fourier transform $v(\mathbf{q})$ and the direct potential $v(\mathbf{r})$ used are shown in Fig. 4.8. for the case a = b. The model potential in Eq. (4.14) can be further simplified into:

$$v(\mathbf{q}) = \{exp\,[\alpha q - 4] + 1\}^{-1} \tag{4.15}$$

where α is equal to 2.5 (a + b); the values of α are tabulated in table 4.1 for all cases in our computations.

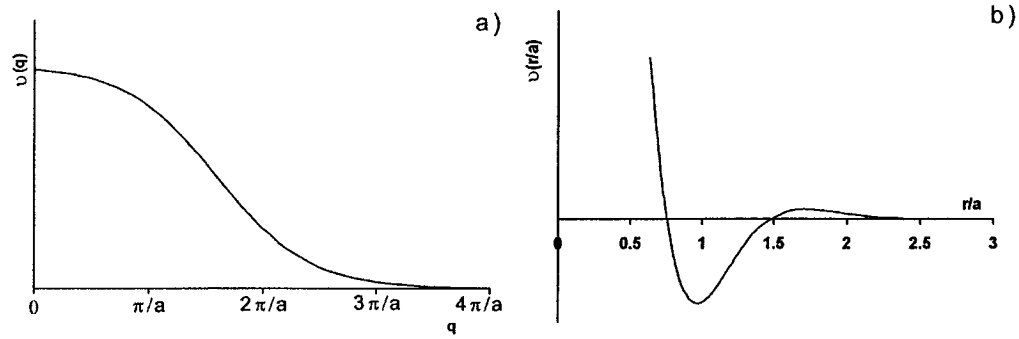

Figure 4.8. a) Fourier transform of the interaction potential model used in this calculation and given in Eq.4.14, drawn for b=a. b) The interaction potential in real space. (Widjaja and Marks 2003b)

4.2.2. Calculation for Quasicrystal-Crystal Epitaxy

The majority of the previous work on quasicrystal-crystal epitaxial systems has been devoted to the epitaxial relationship between crystalline structures on single-grain quasicrystal resulting from ion bombardment processing. Thermodynamically, the stability of the aforementioned systems is uncertain since the ion bombardment process is commonly conducted at room temperature. Nevertheless, even with limited thermal energy available to allow atomic movement to achieve a thermodynamically stable interface, the kinetic energy introduced by ion fluxes may supply the required energy. The abundance of literature data on ion bombarded surfaces is advantageous for analysis, even though these systems do not make ideal case studies.

Recently, studies on the epitaxial relationships between crystalline thin films on quasicrystal substrates via physical vapor deposition have been reported. Shimoda

et al. attempted to grow Au thin films on decagonal Al-Ni-Co and reported the orientation of the alloyed $AuAl_2$ layer with respect to the substrates.(Shimoda et al. 2000b, 2001) Similar observation was later reported for $PtAl_2$. (Shimoda et al. 2002) Widjaja and Marks presented evidence of epitaxial Al-Cu-Fe-Cr decagonal thin films on atomically flat Al_2O_3 [0001] surface.(Widjaja and Marks 2003a) It appears that these are the only reports on thermodynamically stable epitaxial relationships in crystal-quasicrystal systems where the interface relationship is well described. (Bolliger et al. 2001; Franke et al. 2002; Li et al. 1997) [1]

Computations were carried out on various ion-bombarded surfaces for three quasicrystal systems: the icosahedral Al-Cu-Fe system and the decagonal Al-Ni-Co and Al-Cu-Co systems. Calculations were also performed for quasicrystal-crystal thin film epitaxy for the following systems: $AuAl_2$ and $PtAl_2$ thin films on a 10-fold surface of decagonal Al-Ni-Co and decagonal Al-Cu-Fe-Cr thin film on corundum Al_2O_3 [0001]. A complete comparison of the observed and simulated results is tabulated in table 4.2. Table 4.3. summarizes the corresponding calculated results and position of the peaks relative to a set of references.

[1]Bolliger et al. (2001) reported epitactic textures of fcc Al on icosahedral Al-Pd-Mn quasicrystal. However, this paper does not report the interface relationship between the fcc Al and the 5-fold surface of icosahedral Al-Pd-Mn; instead it reports the alignment of [111] axes of fcc Al with one of five threefold-symmetry axes of the substrate quasicrystal at 37.37° away from the surface normal. Franke et al. (2002) reported a quasicrystalline epitaxial single element (antimony and bismuth) monolayer on icosahedral Al-Pd-Mn and decagonal Al-Ni-Co quasicrystal surfaces. Li et al. (1997) reported growth of epitaxial Al-Cu-Co decagonal on alumina substrates using X-ray diffraction but was unable to study the geometric orientations at the interface.

Table 4.2. Orientation relationship in crystal-quasicrystal epitaxy. 'Primary?' indicates if the observed alignment appears as the primary peak (global minimum). 'Fit?' indicates whether the calculation matches the experimentally observed configuration. 1) Yang et al. (1996), 2) Wang et al. (1993), 3) Qin et al. (1995), 4) Zurkirch et al. (1998), 5) Zhang and Urban (1989), 6) Shimoda et al. (2000b), 7) Shimoda et al. (2001), 8) Shimoda et al. (2002) and 9) Widjaja and Marks (2003a).

No	Quasicrystal system	Parallel Axis QC‖Crystal	In-plane alignment Observed	Ref.	Calculated	Primary?	Fit?
1	Al-Cu-Fe	$5f_{ic}\|\|[110]_{CsCl}$	$2P\|\|[1\bar{1}0]$ - $2D\|\|[001]$	[1]	$2P\|\|[1\bar{1}0]$ - $2D\|\|[001]$	No	Yes
2	Al-Cu-Fe	$5f_{ic}\|\|[113]_{CsCl}$	$2P\|\|[1\bar{1}0]$	[1]	$2P\|\|[\bar{1}\bar{2}1]$	Yes	Yes
3	Al-Cu-Fe	$2f_{ic}\|\|[111]_{CsCl}$	$2f\|\|[1\bar{2}1]$	[2]	$5f\|\|[1\bar{1}0]$	Yes	Yes
4	Al-Cu-Fe	$3f_{ic}\|\|[111]_{CsCl}$	$3f\|\|[1\bar{1}0]$	[2]	$3f\|\|[1\bar{1}0]$	Yes	Yes
5	Al-Ni-Co	$10f_{dec}\|\|[110]_{CsCl}$	$2P\|\|[001]$ - $2D\|\|[1\bar{1}0]$	[3, 4]	$2P\|\|[001]$ - $2D\|\|[1\bar{1}0]$	Yes	Yes
6	Al-Ni-Co	$2D_{dec}\|\|[110]_{CsCl}$	$10f\|\|[1\bar{1}0]$ - $2P\|\|[001]$	[3]	$10f\|\|[1\bar{1}0]$ - $2P\|\|[001]$	Yes	Yes
7	Al-Ni-Co	$2D_{dec}\|\|[111]_{CsCl}$	$10f\|\|[1\bar{1}0]$	[3]	$2P\|\|[\bar{2}\bar{1}3]$	Yes	No
			$10f\|\|[1\bar{1}0]$	[3]	$10f\|\|[1\bar{1}0]$	No	Yes
8	Al-Ni-Co	$D_{dec}\|\|[100]_{CsCl}$	$2f\|\|[001]$	[3]	$2f\|\|[001]$	Yes	Yes
9	Al-Cu-Co	$10f_{dec}\|\|[110]_{CsCl}$	$2P\|\|[1\bar{1}0]$ - $2D\|\|[001]$	[5]	$2P\|\|[1\bar{1}0]$ - $2D\|\|[001]$	Yes	Yes
10	Al-Cu-Co	$2P_{dec}\|\|[110]_{CsCl}$	$10f\|\|[1\bar{1}0]$ - $2D\|\|[001]$	[5]	$10f\|\|[1\bar{1}0]$ - $2D\|\|[001]$	Yes	Yes
11	Al-Ni-Co	$10f_{dec}\|\|[110]_{AuAl_2}$	$2D\|\|[001]$ - $2D\|\|[\bar{1}12]$	[6, 7]	$2D\|\|[\bar{1}12]$	No	Yes
12	Al-Ni-Co	$10f_{dec}\|\|[110]_{PtAl_2}$	$2D\|\|[001]$ - $2D\|\|[\bar{1}12]$	[8]	$2D\|\|[\bar{1}12]$	No	Yes
13	Al-Cu-Fe-Cr	$10f_{dec}\|\|[0001]_{Al_2O_3}$	$2P\|\|[10\bar{1}0]$	[9]	$2P\|\|[10\bar{1}0]$	Yes	Yes
14	Al-Cu-Fe-Cr	$10f_{dec}\|\|[0001]_{Al_2O_3}$	$2D\|\|[10\bar{1}0]$	[9]	$2D\|\|[10\bar{1}0]$	No	Yes

Table 4.3. Peak positions and reference in calculated configurations. 'P' or 'S' indicates if the observed peak appears as primary or secondary peak, respectively. '*' denotes ambiguity of the peak in the experimental data. Dash symbol, '-', indicates no special alignment or no significant secondary peak.

No	Quasicrystal system	Parallel Axis QC‖Crystal	Ref. 0°	primary angle	primary align.	secondary angle	secondary align	Obs.
1	Al-Cu-Fe	$5f_{ic}\|\|[110]_{CsCl}$	$2D\|\|[1\bar{1}0]$	$\pm 9.45°$	-	$+18°$	$2P\|\|[1\bar{1}0]$	S
2	Al-Cu-Fe	$5f_{ic}\|\|[113]_{CsCl}$	$2D\|\|[1\bar{1}0]$	$18°\pm 1.2°$	$2P\|\|[\bar{1}\bar{2}1]$	$0°$	$2D\|\|[1\bar{1}0]$	P*
3	Al-Cu-Fe	$2f_{ic}\|\|[111]_{CsCl}$	$2f\|\|[1\bar{2}1]$	$\pm 1.7°$	$5f\|\|[1\bar{1}0]$	-	-	P*
4	Al-Cu-Fe	$3f_{ic}\|\|[111]_{CsCl}$	$3f\|\|[1\bar{1}0]$	$0°$	$3f\|\|[1\bar{1}0]$	-	-	P
5	Al-Ni-Co	$10f_{dec}\|\|[110]_{CsCl}$	$2P\|\|[001]$	$0°$	$2P\|\|[001]$	-	-	P
6	Al-Ni-Co	$2D_{dec}\|\|[110]_{CsCl}$	$10f\|\|[1\bar{1}0]$	$0°$	$10f\|\|[1\bar{1}0]$	-	-	P
7	Al-Ni-Co	$2D_{dec}\|\|[111]_{CsCl}$	$10f\|\|[1\bar{1}0]$	$\pm 19.1°$	$2P\|\|[\bar{2}\bar{1}3]$	$0°$	$10f\|\|[1\bar{1}0]$	S
8	Al-Ni-Co	$D_{dec}\|\|[100]_{CsCl}$	$2f\|\|[001]$	$0°$	$2f\|\|[001]$	-	-	P
9	Al-Cu-Co	$10f_{dec}\|\|[110]_{CsCl}$	$2P\|\|[1\bar{1}0]$	$0°$	$2P\|\|[1\bar{1}0]$	-	-	P
10	Al-Cu-Co	$2P_{dec}\|\|[110]_{CsCl}$	$10f\|\|[1\bar{1}0]$	$0°$	$10f\|\|[1\bar{1}0]$	-	-	P
11	Al-Ni-Co	$10f_{dec}\|\|[110]_{AuAl_2}$	$2D\|\|[001]$	-	-	$\pm 0.7°$	$2D\|\|[\bar{1}12]$	S*
12	Al-Ni-Co	$10f_{dec}\|\|[110]_{PtAl_2}$	$2D\|\|[001]$	-	-	$\pm 0.7°$	$2D\|\|[\bar{1}12]$	S*
13	Al-Cu-Fe-Cr	$10f_{dec}\|\|[0001]_{Al_2O_3}$	$2P\|\|[10\bar{1}0]$	$0°$	$2P\|\|[10\bar{1}0]$	$\pm 18°$	$2D\|\|[10\bar{1}0]$	P&S

Quasicrystal reciprocal lattice points and structure factors were simulated using the QUAREF program (Weber 2000, see appendix B for details); the 3D reciprocal space quasi-lattices were generated by a projection method from a higher dimension hyper-cube. Lattice parameters for the hyper-cube and the corresponding space group are given in table 4.4. along with the crystalline structure data.

Calculations of U(**q**) for quasicrystals were simplified by incorporating only the intrinsic structure factor which is independent of the specific decoration of the lattice due to the complexity of real decorated lattices. Unlike crystalline materials, diffraction patterns of quasicrystals generally cannot be decomposed into the intrinsic structure factor and geometric structure factor (Jaric 1986). The former is attributed to the quasi-lattice, while the latter is due to the decoration.

The values of atomic radii for the crystalline and quasicrystalline structures considered in the atomic potential calculation were taken to be the expected values of the systems:

$$\hat{a} = \sum_i x_i a_i \tag{4.16}$$

where x_i and a_i are the atomic percentage and radius for element i, respectively, in the compound. Table 4.1. contains the calculated values of the expected atomic radii for all systems in this simulation and the corresponding α values.

Table 4.4. Structure and (quasi)lattice data input for calculations. 1) Dai and Wang (1990), 2) Shen et al. (1998), 3) Steurer and Kuo (1990), 4), Zurkirch et al. (1998), 5) Shimoda et al. (2001), 6) Shimoda et al. (2002), 7) Steurer et al. (1993), 8) Zhang and Geng (1992), 9) Yamamoto and Hiraga (2000), 10), Weber and Yamamoto (1998), 11) Widjaja and Marks (2003a).

No	Quasicrystal						Crystal			
	system	structure	symmetry	a (A)	c (A)	Ref.	structure	a (A)	c(A)	Ref
1	Al-Cu-Fe	icosahedral	F-3-5	8.966		[1]	CsCl	2.942		[2]
2	Al-Ni-Co	decagonal	P10.5/mm	3.3931	4.807	[3]	CsCl	2.8		[4]
							$AuAl_2$	5.998		[5]
							$PtAl_2$	5.922		[6]
3	Al-Cu-Co	decagonal	P10.5/mm	3.368	4.4148	[7]	CsCl	2.9		[8]
4	Al-Pd-Mn	icosahedral	m-3-5	9.123		[9]				
	Al-Pd-Mn	decagonal	P10.5/mmc	2.820	12.06	[10]				
5	Al-Cu-Fe-Cr	decagonal	[measured experimentally]			[11]	Al_2O_3	4.763	13.003	[11]

Better average values of the atomic radius can be calculated from the density of the alloys ρ :

$$\frac{4}{3}\pi(R_{WS})^3 = \frac{1}{\rho}, \tag{4.17}$$

where R_{WS} is the average Wigner-Seitz radius. Comparison of the average atomic radius values calculated from concentration weighted atomic radii (Clementi and L.Raimondi 1963; Clementi et al. 1967), concentration weighted of the Wigner-Seitz radius for each element (Andersen et al. 1985) and density calculation for these alloys (from Eq. 4.17), $Al_{72.6}Ni_{10.5}Co_{16.9}$, $Al_{72}Ni_{20}Co_8$ and $Al_{70}Pd_{21}Mn_9$, is tabulated in Table 4.5. Due to the lack of comprehensive data of density measurements for the quasicrystal and crystal systems, the atomic radius values for the α values are taken from concentration-weighted atomic radii, Eq. 4.16. These values deviate about five percent from the values derived from the density measurement, however the contribution to the final result, Eq. 4.13, due to this deviation is negligible.

In the calculation, the reciprocal lattice planes for the two crystals were reciprocal surface unit cells. For periodic crystals, reciprocal surface unit cells were constructed under the following simplifications: (1) The surface unit cell was determined based on bulk truncation without any reconstruction. (2) All elements were considered to behave similarly for surfaces containing more than one element. Note that the reciprocal surface unit cells may be denser than those normally observed

Table 4.5. Comparison of calculated average atomic radii (in Å) from concentration-weighted atomic radii, concentration weighted Wigner-Seitz (WS) radii, and bulk density measurements. References for the values of density used in the radius calculations are given. Wignes-Seitz radius values are taken from Andersen et al. (1985)

Alloys	Eq. 4.16.	WS	Eq. 4.17.
$Al_{72.6}Ni_{10.5}Co_{16.9}$[(Khoukaz et al. 2000)]	1.270	1.288	1.337
$Al_{72}Ni_{20}Co_8$[(Steinhardt et al. 1998)]	1.269	1.370	1.204
$Al_{70}Pd_{21}Mn_9$[(Zumkley and Nakajima 2000)]	1.326	1.372	1.209

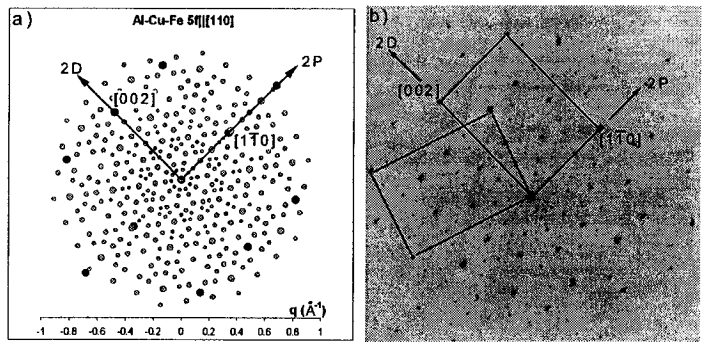

Figure 4.9. Comparison between (a) simulated and (b) experimentally observed configurations in ion-sputtered 5-fold surface of Al-Cu-Fe quasicrystals. Gray and black spots represent the quasicrystal and crystal spots, respectively.

in bulk electron diffraction patterns. The reciprocal unit cells included in the calculations are limited to magnitudes less than 1 $Å^{-1}$; $\mathbf{q}$ vectors with larger values are considered negligible due to the exponential decaying nature of the interaction potential as shown in Eq.4.15. Since nature of surface interface structures in quasicrystalline systems is unknown, the surface reciprocal lattices were constructed

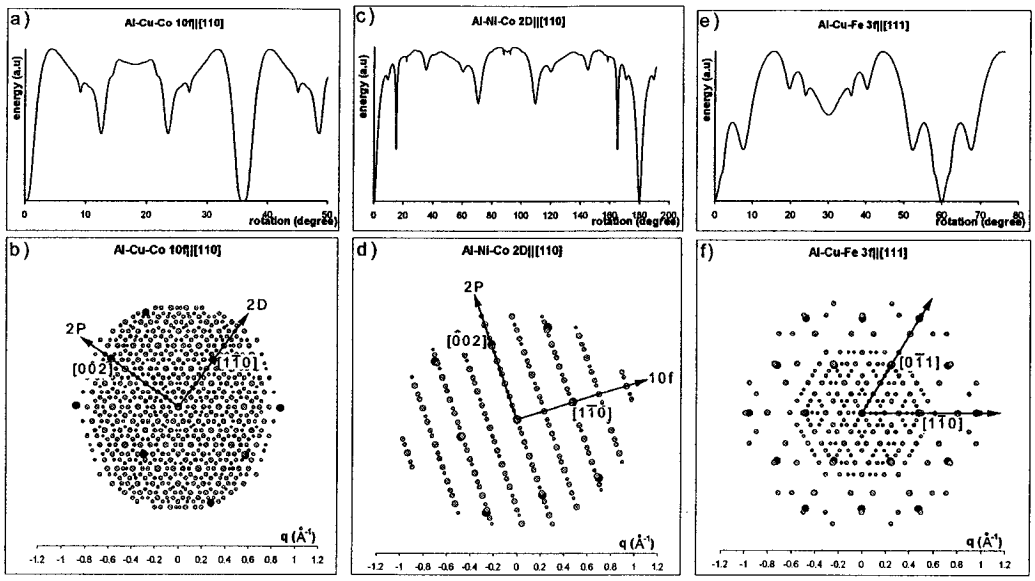

Figure 4.10. Interfacial energy calculation and its corresponding structure, respectively, at 0° rotation (which is the minimum) for (a) and (b) Al-Cu-Co $10f_{dec}\|[110]_{CsCl}$, (c) and (d) Al-Ni-Co $2D_{dec}\|[110]_{CsCl}$ and, (e) and (f) Al-Cu-Fe $3f_{ic}\|[111]_{CsCl}$; crystal-quasicrystal epitaxy is due to ion bombardments. Gray and black spots represent the quasicrystal and crystal spots, respectively.

based on bulk structures; many experiments have confirmed the quasi-periodic nature of the surface. (Shen et al. 2000; Cai et al. 2001; Shimoda et al. 2000a)[2]

4.2.3. Results and Discussion

In most cases, calculations showed perfect fits between simulated and observed configurations; exceptions will be discussed further in this section. Figures 4.9

[2]While most reports confirmed a similar quasiperiodic surface phase as in the bulk, Naumovic et al. (2001) and Bolliger et al. (1999) reported a formation of a stable decagonal quasicrystalline Al-Pd-Mn surface layer on a Al-Pd-Mn icosahedral single crystal by sputtering and annealing.

(a-b) show a comparison between the calculated and experimentally observed configuration for the ion-sputtered Al-Cu-Fe single-grain quasicrystal 5-fold surface. In these plots, surface spots have been eliminated to assist in the visual comparison, however these spots were taken into consideration during the calculations. Experimental observations in other systems can be easily compared to simulated results; references are given in table 4.2. Numerical data for peak positions, types and references are given in table 4.3. Results for the interfacial energy calculation and the corresponding structure for three different cases are plotted in Fig. 4.10 (a)-(f) as examples. The configurations shown in Fig. 4.10 match the experimental observation perfectly; surface spots are also removed to ease visual comparison. In all figures, unless otherwise noted: (1) surface spots are removed, (2) the sizes of the spots correspond to the intensities however are not to be scaled, and (3) the gray and black spots represent, respectively, the quasicrystal and crystal spots.

We will look further into the case of ion sputtered Al-Ni-Co decagonal 2-fold surface as an example. For this surface, two different out-of-plane alignments have been observed, that is 2D axis of the decagonal phase parallel to <110> direction ($2D_{dec}||[110]_{CsCl}$) and parallel to <111> direction ($2D_{dec}||[111]_{CsCl}$) of the CsCl crystalline phase. Henceforth, the notation V||[hkl] will be used to indicate alignment of the V rotation axis of the quasicrystal phase with <hkl> direction of the crystalline phase and the notations 2D-2P, 5f, 10f and 3f will refer to the two

two-fold axes rotated relatively to each other by 18°, the five-fold axis, the ten-fold axis and the three-fold axis of the quasicrystals, respectively.

In the 2D||[110] case, the in-plane alignment of 10f||[1$\bar{1}$0]-2P||[001] is observed and it fits the calculated structure. However, the calculated structure for 2D||[111] is 2P||[$\bar{2}\bar{1}$3] while experimental observation is 2P||[$\bar{1}\bar{1}$2] (equivalent to 10f||[1$\bar{1}$0]). This observed configuration, differs from the calculated one, however, appears in the calculation as second minima, with the primary minima position at $\pm$ 19.1° rotation from them. Figures 4.11 (a-b) illustrate the calculated structures at both minima; surface reciprocal spots were plotted. Configuration in Fig. 4.11b. 10f||[1$\bar{1}$0], which fits the observed data, has a higher number of near plane- coincidence, however Fig. 4.11a. with configuration 2P||[$\bar{2}\bar{1}$3] resulted in much lower energy due to a very small κ value from closer coincidence in one plane. Analysis on the energy graph Fig. 4.11c. shows a very sharp peak for the configuration described by Fig. 4.11a. [Full Width Half Maximum (FWHM) less than 0.05°] while a wide peak for Fig. 4.11b. [FWHM >14°] is evident. This energy profile allows the system to achieve 10f||[1$\bar{1}$0] alignment relatively easily since only small fluctuation is needed to move the system to this minimum. The simulated configuration in Fig. 4.11d. is the case observed in ref [(Qin et al. 1995)]; here, surface spots have been removed and bulk spots are indexed.

Two cases of CsCl structure on icosahedral Al-Cu-Fe, [113] on 5-fold and [111] on 2-fold surfaces were investigated and gave results which differ by less than

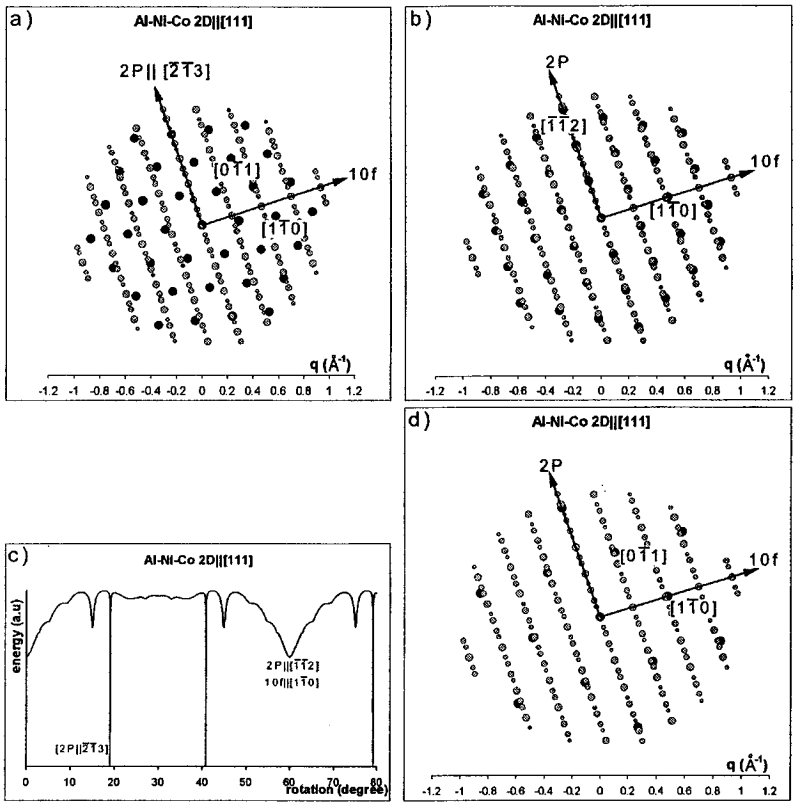

Figure 4.11. Comparison of two simulated configurations at two different minima for Al-Ni-Co 2D||[111]. a) Configuration at the lowest energy at 19.1° and b) at the other minimum at 0°; c) interfacial energy calculation; and d) experimentally observed configuration. Directions for 2-fold axis for quasicrystals are given and diffraction spots for the crystal are indexed. Gray and black spots represent the quasicrystal and crystal spots, respectively.

2 degrees rotation. This difference may be real, but can also be attributed to mistakes in experimental observation due to small angle differences between the orientations. The angle between $[1\bar{1}0]$ and $[\bar{1}\bar{2}1]$ in CsCl structure is 73.2° and the angle between two 2P axis is 72°; while the angle between $[1\bar{1}0]$ and $[1\bar{2}1]$ in CsCl is 30° and 2-fold and 5-fold axis is 31.7° . In the literature, observations usually

reported these configurations, both for 2P||[$\bar{1}\bar{2}1$]-2P||[$1\bar{1}0$] and 5f||[$1\bar{1}0$]-2f||[$1\bar{2}1$], to be similar due to their small angle differences. It is ambiguous whether both or only one configuration was observed.

Similarly, for the case in which the [110] CsCl structure on 5-fold icosahedral Al-Cu-Fe is observed, the orientation appears as secondary peak (local minimum) instead of the primary minimum in accordance with most of the calculations. Calculations limiting contributing **q**s in reciprocal space up to 0.6 Å^{-1} resulted in the observed orientation as the lowest energy. For thin film growth of Au and Al on Al-Ni-Co substrates, calculations showed a similar trend to the case of [110] on the 5-fold surface; only by limiting the contributing **q** values to 0.6 Å^{-1}, the simulation matched the experimental data.

This discrepancy can also be attributed to the simplistic nature of the interaction potential form. A more sophisticated and correct model is required to be able to understand the interaction across the interface, and hence be able to predict (and explain) the observed experimental data to a higher accuracy. However, with this simple model we show that we are able to explain the majority of experimentally observed in-plane relationships reported in the literature. In addition to that, there is no justification that the observed orientations should be the global minima of the interfacial energy.

Observations of multiple in-plane alignments for the same out-of-plane alignment have been reported by Widjaja et al. for Al-Cu-Fe-Cr decagonal thin films on

atomically flat Al_2O_3 substrates (see section 4.1.2) (Widjaja and Marks 2003a). A similar energy calculation showed existence of two unique minima corresponding to two unique in-plane alignments. Each of these configurations has been independently observed experimentally on the same sample.

Using the similar idea for crystal-crystal epitaxy that we extend to include quasicrystal-crystal epitaxy, we can now move and apply the same approach for quasicrystal-quasicrystal epitaxy. From Eq. 4.13, the energy actually appears to have an infinite negative value as we approach the coincidence-boundary configuration $\kappa = 0$, but the real situation is that the coincidence boundary of any order represents a cusped minimum in the energy. The depth of this minimum depends on the strength of the potential component brought into coincidence. Nevertheless, without the exact knowledge of the potential form and necessity to calculate the value of interface energy, we can predict similar behavior in quasicrystal-quasicrystal epitaxy. The only existing report is Al-Pd-Mn quasicrystals (Menguy et al. 1993; Sun and Hiraga 1993). Menguy et al. (1993) reported phason-phonon-assisted epitaxy at icosahedral-decagonal interfaces in Al-Pd-Mn quasicrystals. The closeness of their structure has been used as a basis to explain their oriented 5-fold/10-fold axis. In this case the lattice planes match very well, as shown in the superimposed simulated 2D reciprocal space patterns for the 5-fold and 10-fold directions in Fig. 4.12.

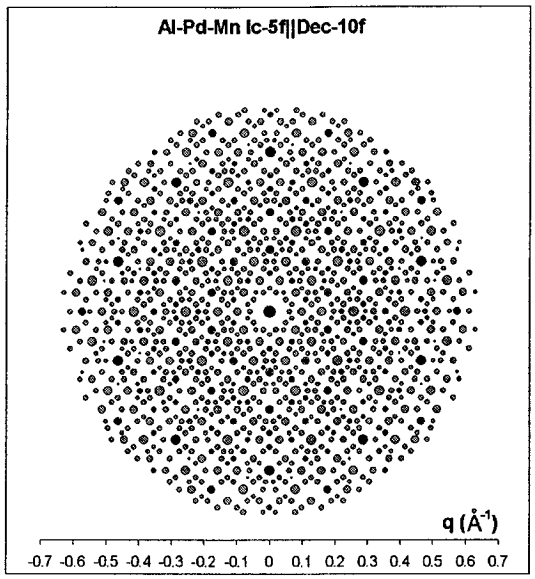

Figure 4.12. Simulated configuration for Al-Pd-Mn icosahedral-decagonal epitaxy. Gray and black spots represent the decagonal and icosahedral spots, respectively.

The results reported herein indicate that quasicrystalline materials can have specific orientational relationships in interfaces to crystals, and that these obey very similar rules to those that govern crystalline interfaces. In real space it is hard to model this (except via some large approximant to the quasicrystal), but the first-order approach is viable and should be completely general in reciprocal space. Equation 4.13). shows that with appropriate simplification we can find the most probable orientation relationship between a quasicrystal-crystal structure, which is the configuration with a small $\boldsymbol{\kappa}$ vector, a large interaction potential $v(\mathbf{q})$ and a large unitary structure factor $\mathrm{U}(\mathbf{q})$. The $\mathrm{U}(\mathbf{q})$ term that should be included will weight the analysis towards orientations with more atoms aligned, and may

be important in general although often the $1/\kappa$ term will dominate. Only small $\mathbf{q}$s are dominant and need to be considered due to exponential decay of interaction potential $v(\mathbf{q})$. By simple calculation one can find relatively easily the most stable configuration. However, as shown in some cases in our computations, the most stable configuration is not always the experimentally observed configuration. This can be explained by an analysis of the kinetics.

Due to the difference in $\mathbf{q}$ vectors of quasicrystals and crystals, which is the $\boldsymbol{\kappa}$ vector, dislocations are created to accommodate the strain. Unlike the observations of dislocations in quasicrystal phases, only a few papers have reported the study of interfacial dislocation in quasicrystal-crystal epitaxy (Zhang and Geng 1992; Zhang and Li 1990; Zhuang et al. 1993). Zhuang et al. (1993) reported the observation of misfit dislocations between the B2 surface layer and decagonal $Al_{75}Ni_{10}Fe_{15}$ that are parallel but less regularly spaced. They observed two types of spacing with a distance ratio of the golden mean of $(1+\sqrt{5})/2$, which were attributed to quasi-periodic nature of the misfit strain field of the decagonal phase. Nevertheless, more work need to be done to relate the strain due to $\boldsymbol{\kappa}$ and the observed dislocation density in crystal-quasicrystal epitaxy.

4.2.4. Conclusion

We have a developed coincidence reciprocal lattice plane model to calculate the interfacial energy for quasicrystal-crystal epitaxy based on Fletcher's original work.

This simple model is able to explain and predict most of the experimentally observed relative orientations for epitaxy as reported in literature. This model relies on the coincidences of the reciprocal lattice planes to calculate the boundaries energy; the higher density of coincidence results in lower energy between the two systems.

Some difficulties to fit the simulated and observed configurations may arise from the kinetics of system, resulting in a metastable configuration. Nevertheless, all experimental configurations appear as local minima in the energy calculations. The nature of the currently unknown interaction potential model requires further development; nonetheless, the combination of exponential form for the potential model and q-space cutoff appears to work very well for all tested cases. As knowledge and understanding of surface structures of quasicrystals improve, a better model for the surface reciprocal lattices can be constructed.

We show that with this simple approach epitaxial relationships between crystals and quasicrystals can be established relatively accurately.

CHAPTER 5

Growing Quasicrystalline Thin Films

This chapter will discuss and summarize some of the fundamentals of growing quasicrystalline thin films. Specifically two issues will be dealt with, i.e. compositional and structural control and evaluation in growing quasicrystalline thin films. Additionally, a discussion on the growth mechanism will be presented including a short review of growth mechanism via different routes of thin film growth.

5.1. Control and Evaluation of Thin Films Composition

It has been shown in earlier chapters that it is very important to control the film composition to produce a high quality quasicrystalline phase. The icosahedral system, Al-Cu-Fe is more intolerant in the composition field where one can acquire a single phase region, while it appears that for Al-Cu-Fe-Cr system, the composition field for decagonal phase it larger. Regardless, it is crucial to be able to control the final composition of the system.

In a system like ours, with a single-target magnetron sputtering, it is very difficult to control the composition since there are not many adjustable parameters. The final composition will vary only by small amounts by adjusting the bias voltage, substrate temperature, etc - these parameters however will also change other

properties of the film, hence they are not freely adjustable to control composition. Therefore, the target initial composition needs to be designed as precisely as possible to achieve the correct final composition.

Due to the compositional issue, it is best to avoid growing quasicrystalline films by a single-target magnetron sputtering. Powder metallurgy to produce the targets will result in a better homogeneity of composition, given the particle sizes are small enough, however, the incorporation of the unwanted oxygen is almost impossible to avoid due to the presence of aluminum. Alloys as targets can be prepared from the pure elements (Al, Cu, Fe and Cr) by induction melting in an inert crucible under an inert atmosphere. A major difficulty for this preparation is that at high temperature there exists a peritectic transformation that will induce a macrosegregation during the cooling process, which leads eventually to large inhomogeneities of composition in the ingot (Quiquandon et al. 1996). This segregation will result in inhomogeneity in composition during deposition. This is particularly crucial when depositing very thin films.

To prevent segregation, the alloys need to be remelted and rapidly quenched under an inert atmosphere. This will produce a mostly quasicrystalline phase target. However, the thermal and electrical conductivity of the target is so poor that many other precautions need to be taken. A radio-frequency (RF) magnetron system will help to prevent target charging, although issues like target cracking due to its inherent brittleness need further precautions. In addition to that, the

single phase target complicates the process itself by the requirement of a very good target manufacture.

A more feasible route to have a good control of composition is through a multi-target sputtering system. For example, to deposit Al-Cu-Fe quasicrystalline thin films, one uses three sputtering guns, each equipped with a pure metallic target. High purity metallic targets are rather easy to acquire. Composition variation can be controlled by designing the shutter time, target power, distance, etc. Sample rotation is a neccessity to homogenize the film composition. However, even with the ability to control the composition rather accurately, it is not trivial to achieve the single phase region for icosahedral Al-Cu-Fe system (Symko 2002).

The ability to control the initial composition accurately needs to be complemented by the ability to measure the composition accurately. Analytical methods such as EDX, XPS and WDX are common in determining the compositions of the film but the error and uncertainty in the measurements is beyond the compositional tolerance to acquire the single phase region. Additionally, many of such methods require an assumption that the composition is homogenous across the analyzed areas. While it is relatively easy to measure the composition with these methods, calibrations with standards, for example single grain quasicrystal, are extremely important. A more accurate method, however, for example AES or AAS is required to determine a more precise composition value. These latter methods can also serve as a calibrant to the former ones.

5.2. Structural Evaluation

In addition to good control and measurement techniques of composition, it is necessary to be able to evaluate the quality of the films structurally. Many studies used only XRD to determine the structure of the films. While XRD statistically is better than TEM to evaluate the film structurally, it is not always straightforward to assure the phase purity of the films. For example, in studies of Al-Cu-Fe films, XRD was used to characterize the phases, however, the Al-Cu-Fe phase diagram with the crystalline phases, the rhombohedral R-phase, the orthorhombic O-phase, pentagonal phases, modulated and perfect icosahedral phases is very complex (Quiquandon et al. 1996; Grushko et al. 1996; Gayle 1992; Gratias et al. 1993; Bancel 1993). These phases show only small differences in their XRD patterns (Gratias et al. 1993; Bancel 1993). These small differences are further complicated in thin films due to finite grain size, strains and other defects. To study the structure of quasicrystalline thin films, TEM is an indispensable tool.

A recent trend to evaluate the structure of the films is by property measurements. Conductivity has become a new standard to evaluate if quasicrystalline phases exist in the films (Haberkern et al. 1998, 2000). A phase transformation resulting in quasicrystalline phases will create samples with much higher resistivity. This high resistivity is often compared to the resistivity of a single grain quasicrystal, which is assumed to be single quasicrystal phase, as a standard. Moreover, the anti-metallic conductivity dependence on temperature for quasicrystals is also

another signature of their existence. Quasicrystals have a higher electrical conductivity at higher temperature[1].

This newer method of evaluating the structure is acceptable as an indicator of the existence of some quasicrystalline phases, however, it does not provide much information regarding the structure of the films. Additionally, a precise quantitative measurement of this property will depend on the prior knowledge of the samples, such as thickness, homogeneity, density, etc, which is not always readily available. The measured property will indirectly indicate the quality of the films but will not and should not substitute structural analyses. It is rather unconvincing to read papers that claim growth of high quality quasicrystalline thin films without any structural information of the quasicrystallinity of the films itself.

5.3. Growth Mechanism

Earlier methods of synthesizing quasicrystals, such as fast quenching and conventional casting, will result in a bulk product rendering it difficult to use in most applications due to the brittleness. Methods of producing coatings and thin films have come out to solve this problem: sputtering, evaporation, plasma spray, etc. Underlying all these different methods is the fundamental question of the growth mechanisms of the quasicrystalline phases. The phase formation mechanisms are

[1]Haberkern et al. (2000) shows that the temperature dependence of the conductivity is qualitatively very similiar for quasicrystalline and amorphous samples. The inverse Matthiessen rule which is thought to be peculiar to quasicrystals is also valid for amorphous samples of the same composition in their experiments.

different depending on the synthesis routes. Understanding the mechanism is extremely crucial.

Tsai et al. (1988a) reported a stable quasicrystal in the Al-Cu-Fe system in both a fully annealed state as well as in a conventionally solidified state. In their early experiment, the stable quasicrystal consisted of large grains with an average size of 0.2 mm after annealing for 48 hours at 845°C (0.98 of the melting point). Biggs et al. (1991) acquired a single icosahedral phase sample by annealing melt-spun ribbon at 760 °C for three hours. Annealing this sample further at 600 °C for 24-36 hours resulted in a rhombohedral phase. This phase went through a reversible icosahedral-rhombohedral transition via a different transient modulated icosahedral states (Janot et al. 1991; Audier et al. 1990, 1991). This transient modulated states have been observed to form by annealing treatments of the as-quenched icosahedral state in a low temperature range (about 520-650 °C). The structural relationships between the different crystalline phases and the icosahedral Al-Cu-Fe quasicrystalline phase have been studied (Gayle 1992; Faudot et al. 1991; Gratias et al. 1993). Also, investigations were carried out on the decomposition of this icosahedral phase (Rosas and Perez 2001; Liu et al. 1991; Gayle 1992).

We will not discuss the different transition and decomposition that exist in the bulk quasicrystalline samples produced via as-quenched, conventional solidified or high temperature annealing. However it is important to notice that in the papers reporting the production of a quasicrystalline phase, the temperature

ranges (by post annealing of as-deposited samples) are much lower. The temperatures vary from approximately 450 to 700 °C to produce the quasicrystalline phase. Chien and Lu (1992) reported the cubic phase by annealing at 450 °C will transform to the quasicrystalline phase at 600 °C. Their DSC studies reveal the cubic-icosahedral transformation temperature to be 515 °C. Weisbecker et al. (2001) reported the transformation of an atomized powder upon annealing at 500 °C in air or in vacuum into a nearly pure icosahedral compound within 2 hours. Yoshioka et al. (1995) reported after annealing at 400 °C, the amorphous structure changed to the icosahedral phase of poor quality with a considerable amount of crystalline second phase. After annealing at 500 °C, the quality of the icosahedral phase was improved but still with a slight amount of a second phase remaining. After annealing at above 600 °C the sample became a single icosahedral phase. In our study, the phase transformation temperature between cubic-β to icosahedral Al-Cu-Fe is around 440 °C. Moreover, we have observed the formation of Al-Cu-Fe-Cr decagonal phase at a temperature as low as 310 °C. Regardless of various transition temperatures reported in the literature, the temperatures to transform the amorphous/cubic phase into the icosahedral phase in thin films/coatings are lower than the temperatures to form the icosahedral phase in the bulk. These temperatures are even lower than the temperatures to decompose the icosahedral phase into crystalline phases in bulk sample.

One important issue that needs to be raised is the standardization of temperature measurements. There are discrepancies in reports of the transformation temperatures to form the icosahedral phase. These discrepancies can be attributed to the different compositions of the alloys. Additionally, the true thermodynamic transformation temperature may not be easily measured due to sluggish kinetics. Moreover, there might also be errors in the measurements due to inaccurate methodologies. For example, in our temperature measurement of the formation of decagonal Al-Cu-Fe-Cr, we utilized an infrared pyrometer with the emissivity calibrated to substrate (e.g. MgO). The precise transformation temperature, however, can deviate as much as 50 °C from the measurement. Another example of the need for temperature measurement standardization is in the furnace. Depending on the locations of the thermocouple and the sample, the recorded temperature may not reflect the true temperature.

Beside conventional thin film growth succeeded by annealing, it is desirable to grow quasicrystalline thin films directly on heated substrates. This technique will reduce the energy cost in the annealing process as well as time. While this is a very interesting topic and it has been shown by Eisenhammer and Trampert (1997) that at a temperature of 460°C one can grow Al-Cu-Fe quasicrystalline films directly, we have not been successful in doing so, however we have not pursued it systematically. The direct growth itself poses a more fundamental question of the mechanism of the phase formation.

Eisenhammer and Trampert (1997) reported a study on the crystalline state of a very thin Al-Cu-Fe film, sputter deposited at the relatively low substrate temperature of 460 °C. In their HRTEM studies, they show that the layer consists of isolated quasicrystalline nanoparticles and proposed a nucleation process of the quasicrystalline phase in terms of a liquidlike to solid transition of nanoclusters. This is based on the belief that at the given composition and deposition temperature, the quasicrystalline state is metastable.

In the paper, they stated: "We conclude that the formation of quasicyrstalline nanoparticles takes place by a direct nucleation process within a narrow temperature interval above about 410 °C and below about 520 °C. With a small change in T_D (deposition temperature) the formation of two different metastable phases, cubic and icosahedral, with completely different local order and crystal symmetry is favored. We speculate that this behavior can be explained with the particular properties of nanoparticles. While the number of atoms necessary for the formation of a cube is rather small, the building block of the i phase contains about 50 atoms [20], and a critical nucleus will probably be much larger. Thus, we suggest that the formation proceeds along the following three steps: (1) In the first stage of growth, extremely small clusters are formed which show structural [21] and shape fluctuations [22]. According to the literature, these fluctuations occur since the clusters may be in a 'liquidlike' or quasimolten state. (2) During further deposition the nuclei grow and, with increased size, a transition from the liquidlike

state to the truly solid state takes place. The deposition temperature T_D controls the size at which this transition occurs: At lower temperature the critical nuclei are small and the β phase is frozen in. At higher temperature larger nuclei include a sufficient number of atoms to form the more complicated i-phase structure. (3) The frozen-in nuclei act as seeds for continued growth resulting in larger particles which maintain the crystalline structure of the initial nucleus (Eisenhammer and Trampert 1997).

While Eisenhammer and Trampert (1997) present an interesting idea on the growth mechanism at higher temperature, it is not without difficulties. They admitted that "although the proposed mechanism for the phase selection of nanoparticles was not observed directly, we believe that the reported indirect evidence is convincing." A few of their assumptions required further investigation. We will talk more about the assumption of stability of the quasicrystalline phase later along with deposition at room temperature followed by annealing.

Eisenhammer and Trampert (1997) believe in the existense of "... two different metastable phases, cubic and icosahedral, with completely different local order and crystal symmetry ...". However, it has been shown that in many experiments the existence of a transformation from the icosahedral phase to the cubic phase at room temperature occurs with assistance from energetic particles. The most popular and plentiful examples are icosahedral-cubic transformations on quasicrystals surface due to ion bombardment (as discussed in Chap.4.). Steurer

(2000) proposed a geometrical relationship between quasiperiodic structures and the cubic β-phase (CsCl-type) formed in a continuous phase transformation. He demonstrated that the lattice of the periodic average structure of the quasiperiodic phases matches very well the lattice of the cubic β-phase. Additionally, Shen et al. (1998) showed the similarity of icosahedral-packed cluster and cubic-closed-packed cluster in its crystal symmetry. Eisenhammer and Trampert (1997) may have proposed an explanation to the nucleation of icosahedral clusters, but fail to explain their stabilities during growth, given the assumption that at the given temperature the icosahedral phase is metastable.

Size-stabilized phases have been observed in many cases. It is likely to happen in this case since the clusters observed are isolated nanoparticles with a mean diameter of about 15 nm. If this is the case, then growth of a thicker film (or larger clusters) will eventually lead to destabilization of this phase and transformation to a more stable phase: cubic β-phase. However, in an earlier paper, Eisenhammer et al. (1995) also showed the direct formation of the icosahedral phase in a film with thickness of approximately 160 nm. Furthermore, as it has been elaborated previously, post annealing of varieries of as-deposited thin films have achieved quasicrystalline phases at annealing temperatures lower than the expected temperature for bulk.

In our study, the phase transformation temperature between cubic-β to icosahedral Al-Cu-Fe is around 440 °C (Widjaja and Marks 2003c). Moreover, we have

observed the formation of the Al-Cu-Fe-Cr decagonal phase at temperatures as low as 310 °C (Widjaja and Marks 2002). The latter, however, is for a film with thickness less than 30 nm and the annealing time is on the order of a few minutes. It is not conclusive if the lower transformation tempeature is related to the size of cluster (thickness of the film). Difficulties also rises in trying to determine the effect of size on transformation temperature. A DSC requires enough sample (approximately minimum of 1-2 grams) to allow a detectable measurement. It is necessary to design an experiment to observe the phase transfomation and monitor the temperature in-situ for samples in a range of sizes. For small size, one can use a TEM coupled with an in-situ heating holder. Care needs to be taken to ensure that the result is governed by thermodynamics not kinetics. A complementary work by simulation, e.g. molecular dyanamic, will shed light into the matter.

While most research reports the production of icosahedral phases via crystalline phases (e.g. cubic phase) in post annealling in the time scale of a few hours, Haberkern et al. (1998) and Roth et al. (1999) reported crystallization of amorphous samples of Al-Cu-Fe (deposited on cooled substratres) to the icosahedral phase at 450° on a time scale of only a few minutes. They explain this by a conjecture that there is a similar short range order between the amorphous and the icosahedral phase, therefore only short range diffusion is necessary to form the quasicrystal. They believe that the metastable amorphous state (produced at low temperatures) has a liquidlike order, but the dynamics of any structural

change is governed by the temperature given by the experimental condition. In their analysis, a heating rate of 5 K/min applied to the amorphous samples avoids the formation of a relatively large portion of a cubic phase.

The growth mechanism and the governing factors in growing quasicrystalline thin films/coatings have not yet been determined conclusively. It has been shown that the growth of thin films requires a lower temperature range and smaller time scale than for bulk growth. There might be different growth mechanisms for different routes: annealing of the cubic phase, growth on heated substrate and transformation from an amorphous precursor. Additionally, ignoring the possibility of incorrect temperature measurements, the problem of kinetics versus thermodynamics should be explored further. In most cases, above a certain temperature, which we believe will depend on composition and size, the icosahedral phase will coexist with the crystalline phases upon annealing. Raising the annealing temperature will result in higher percentage of icosahedral phase, however it is not obvious that it is required. We conjecture that the low proportion of icosahedral phase to crystalline phases at lower temperature is governed by kinetics since all the annealing experiments are carried at time magnitudes of a few hours. However, it is also important to notice the requirement of the necessary energy to overcome the energy barrier for transformation.

We believe that the significant temperature difference between thin coatings and bulk is governed by the size. This leads to the dominance of surface energy

versus bulk energy. However no study has investigated the influence of cluster size on the stability of the icosahedral phase. Additionally, we believe that the contamination might play role in the stability of the system. Our film grown in a UHV system seems to have a lower transformation temperature. This might be similar to the suggestion by Weisbecker et al. (2001) that oxygen stabilized the cubic phase.

CHAPTER 6

Future Work

The future work described herein is of interest and continues logically from the results described in previous chapters. The description of the future work will be divided into two parts: experimental and theoretical. The experimental part will focus on the friction and interfacial dislocations in metallic thin films on a quasiperiodic surface. The theoretical part highlights the relationship of friction-sliding direction and friction-misfit orientation between two crystalline surfaces using an extended 3-dimensional Frenkel-Kontorova-Tomlinson model. It is also of interest to extend the theoretical work to include quasiperiodic surfaces, in real or reciprocal space. The former part is, to some extent, similar to the work being carried out by Arno Merkle and the latter by Peter Hsieh, a third-year and a first-year student in the research group, respectively.

6.1. Experimental: Metal Thin Films on Quasiperiodic Substrates

In an attempt to grow a single element quasicrystalline phase, Shimoda et al. (2000b, 2001, 2002) have grown epitaxial Au and Pt (in the form of $AuAl_2$ and $PtAl_2$) on Al-Ni-Co decagonal crystals. This discovery, along with the growth of

epitaxial quasicrystalline thin films on crystalline substrates, has been discussed extensively in Chapter 4.

6.1.1. Interfacial Dislocations

It is of interest to understand the nature of interfacial dislocations between crystalline and quasicrystalline grains. Only a few works have reported this type of interfacial dislocations (Zhang and Geng 1992; Zhang and Li 1990; Zhuang et al. 1993). Zhuang et al. (1993) reported the observation of misfit dislocations between a B2 surface layer and decagonal $Al_{75}Ni_{10}Fe_{15}$ that are parallel but less regularly spaced. They observed two types of spacing with a distance ratio of the golden mean of $(1+\sqrt{5})/2$, which were attributed to the quasi-periodic nature of the misfit strain field of the decagonal phase.

We conjecture that the dislocations will be quasiperiodic on the crystalline grains and periodic on quasiperiodic grains. This is a very reasonable hypothesis since dislocations are created to relieve strains at the interface in this epitaxy system. A periodic substrate will create a periodic strain in the quasiperiodic counterpart, and hence periodic dislocations will result. Quasiperiodic dislocations in crystalline grains have been observed in ion-bombarded samples. The strain, κ, as described in chapter 4.2.1 will be expected to correlate with the density of the dislocations.

Experiments could be conducted by preparing a single grain quasicrystalline TEM sample. We have acquired Al-Cu-Fe 2-fold and 5-fold single grain icosahedral samples from our collaborators in Ames Laboratory. Different quasicrystals system can be explored, including the decagonal system which provides atomically-flat surface termination along the ten-fold axis. Thinning, dimpling and ion milling to produce a TEM sample needs to be followed by in-situ ion sputtering and annealing in UHV environment. The sample preparation and evaluation processes are described in Section.2.2.3. Elemental metal can then be evaporated in SPEAR onto this TEM-ready sample. The first trial could mimic Shimoda's experiments by using Au and Pt, with or without an In surfactant (Shimoda et al. 2000b, 2001, 2002). The presence of indium on the sample may complicate the study of the interface. However since indium functions as a surfactant and will rise to the surface during further deposition, it can be sputtered off the surface after the growth. Annealing at different temperatures and times must be carried out to acquire a reasonable grain size to study the interface between the two systems.

A combination of TEM imaging (bright field and dark field) and diffraction will reveal the existence, density and location of the interfacial dislocations and their correlation with the strain due to epitaxy. It might also be very interesting to observe dislocation movement upon annealing, given the availability of an in-situ heating TEM holder.

6.1.2. Friction of Incommensurate Sliding Direction

Since it is possible to grow an epitaxial crystalline metal on quasicrystalline substrate, we can exploit the effect of substrate quasiperiodicity on the periodic film. The crystalline grains will grow with a special grain boundary: 72° with respect to each other. Statistically, for any given sliding directions of a crystalline counterpart, about 80% of the grains will have incommensurate directions with respect to the other sliding piece. In friction between atomically flat surfaces, the commensurability will determine the friction coefficient (see Section. 6.2).

An experiment can be designed to compare the friction coefficient values of the following specimens: single crystalline, polycrystalline, and epitaxial polycrystalline with incommensurate boundaries, of certain metallic element grown on quasiperiodic substrate. The sliding experiment can be carried out using an AFM (Atomic Force Microscopy) or in a relatively larger scale with a nanoindentor with the capacity of measuring friction force. Care should be taken to work in the wearless regime (i.e. low load). Sample preparation requires a rather flat surface finish and sliding distance should be in the range of the terrace width. This experiment requires extreme caution but is feasible.

Arno Merkle has carried out an exploratory experiment, similar to the one described above, for sodium chloride and strontium titanate single crystals. A more detailed description along with the preliminary results can be found in his qualifying exam paper (Merkle 2003). This type of experiment is based on the

assumption that, at the nanoscale and for flat surfaces, the friction is governed by interaction of atoms located at their lattice positions.

6.2. Theoretical: Friction and Incommensurability

As we approach a smaller scale, friction is no longer dominated by its traditional components such as roughness, third body particles and lubrication. This is especially true when we are working in the wearless regime. Pioneering work was formulated by Tomlinson, Frenkel, and Kontorova in their attempts to describe interactions between surface atoms and periodic rigid potentials (Tomlinson 1929; Frenkel and Kontorova 1939).

In Tomlinson's model, a surface atom is moved with respect to a 1-D periodic potential. This results in a characteristic plucking of atoms (Tomlinson 1929). In his construction, the surface atoms act independently and are modeled as harmonic oscillators. One of the assumptions is that dissipation occurs entirely in the bulk. Frenkel and Kontorova (FK) in their model took account the coupling effects between atoms. The surface atoms are connected by another set of springs allowing them to behave like harmonic oscillators. Much research has been performed since then, including Aubry's theoretical demonstration of the existence of a state of vanishing static friction, which is commonly known as the Aubry transition (Aubry 1983). This transition occurs for an incommensurate interface where the interaction between the two surfaces is below a certain threshold. More recently, Gyalog and Thomas (1997) extended the Frenkel-Kontorova-Tomlinson (FKT) model into

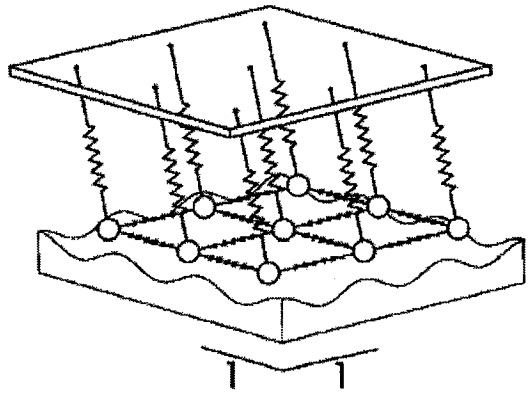

Figure 6.1. The two-dimensional Frenkel-Kontorova-Tomlinson model. The upper surface is rotated with respect to the lower surface by a misfit angle (Gyalog and Thomas 1997).

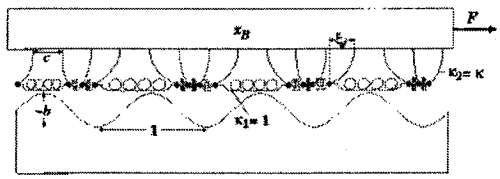

Figure 6.2. The one-dimensional Frenkel-Kontorova-Tomlinson model (Weiss and Elmer 1996).

a two-dimensional model (Fig. 6.1) from its original one-dimensional state as shown in Fig. 6.2. They showed, computationally, that friction depends on rotational angle between two square lattices for various sigma boundary configurations.

In their calculation, Gyalog and Thomas show that the friction at specific coincidence site lattice (sigma boundaries) to be discontinuous. Their model is a two-dimensional Frenkel-Kontorova-Tomlinson (FKT) model with an additional bending term which does not exist in 1D FKT model (Gyalog and Thomas 1997).

While there is a general trend that the friction decreases as the CSL gets larger (Fig. 6.3), it is not an analytical trend and the decrement is only correct in a general sense. They also showed that frictional force is, continuously, dependent on the sliding direction (Fig. 6.4).

It is of interest to relate the frictional force and the CSL area size, if there is any analytical relationship. Also of interest is the frictional value near the CSL. It is widely believed and intuitively correct that friction value at incommensurate angles are lower than at commensurate angles (i.e. CSL), however no study has calculated the frictional value near the CSL. We speculate that the friction force will increase discountinously near a CSL with a certain peak width which is dependent on the CSL area, with a peak FWHM larger for smaller CSL's. This peak width is believed to be highly related to the dislocations spacings, as widely known in the grain boundary community (Sutton and Balluffi 1995).

We proposed to expand the work similar to Gyalog's and Thomas' to include the frictional value at CSL's and near to CSL's. A few improvement should be made to their model to achieve a better calculation. In their model, Gyalog and Thomas define the frictional value at a given angle as the average value of the friction force component along the sliding direction. The average is taken over all possible relative arrangements of the two sliding pieces with fixed angle. Another possibility we propose is to calculate the frictional value for a given angle via energy minimization and atomic relaxations. The latter approach will calculate

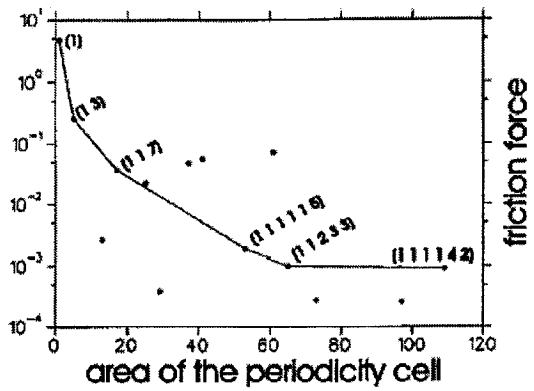

Figure 6.3. Result showing dependence of the friction force per particle on the area N of the periodicity cell. Plotted are the maximum values with respect to angle. The line connects values at misfit ratios a/b which have continued-fraction representations (shown as number sequences) coinciding in the two leading orders (Gyalog and Thomas 1997).

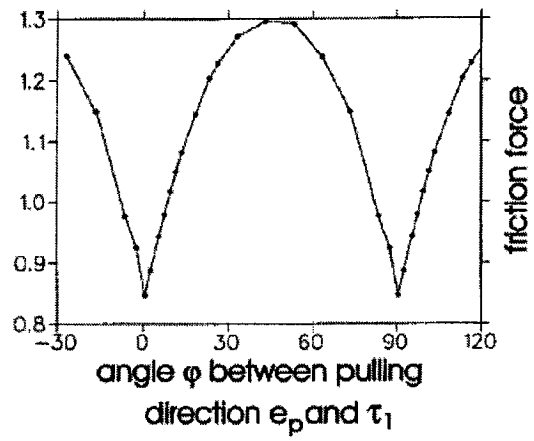

Figure 6.4. Result showing dependence of the friction force per particle on the pulling direction. (Gyalog and Thomas 1997)

only frictional force at an energy-minimized starting configuration as opposed to the expectation value of all possible configurations; this will lead to a better result.

In addition to that, our new model will take into account the third dimension of the system. While the basic framework is still a Frenkel-Kontorova-Tomlinson model with assumptions that only the first atomic layer will be relaxed and the bulk is rigid, we will now allow in the third dimension relaxation perpendicular to the surfaces. Each individual atom as well as the rigid bulk are allowed to relaxed along the Z direction by incorporating a Lennard-Jones like potential.

The FKT model is a 1D model with the upper body acting as a monolayer of a soft body (upper body in Fig. 6.2) sliding on a hard body (lower body in Fig. 6.2). The monolayer is constructed by a chain of N particles interacting with their nearest-neighbors harmonically, similar to replacing the atomic bondings with leaf springs. The lower body is described by a periodic external potential, which defines a hard surface, and is assumed to be fixed while the upper body slides. The atoms in the upper body relax to a minimum energy from the rigid original lattice configuration due to the interaction with the lower body and with their nearest neighbors. This relaxation occurs also during sliding and it is assumed that the relaxation is much faster than the sliding. This model also assumes only motions only parallel to the sliding surface (Weiss and Elmer 1996).

The potential energy of the FKT model is:

$$V(\xi_1, ..., \xi_N, x_B) = \frac{C_{fk}}{2}\sum_{j=1}^{N}(\xi_j - \xi_{j-1})^2 + \frac{C_t}{2}\sum_{j=1}^{N}\xi_j^2 + C_v\sum_{j=1}^{N} cos2\pi(x_B + c_j + \xi_j) \quad (6.1)$$

Here c is the lattice constant of the upper body, x_B is the position of the upper body relative to the lower surface and ξ_j is the position of particle j relative to the support $x_B + c_j$ of its leaf spring. C_{fk}, C_t and C_v are constants corresponding to the stiffness of the leaf springs of the nearest-neighbor coupling, stiffness of the leaf springs to the rigid bulk and the strength of the external potential that models the interaction with the lower body, respectively. All variables and parameters are measured in dimensionless units. They are based on the following independent basic units: the length unit is the surface lattice constant of the lower body, and the unit of the interaction strength is the stiffness of the nearest-neighbor coupling (therefore the C_t and C_v can be describe as C_{fk}). All other units can be expressed in terms of these basic units.

We will call the the first term in the Eqn. 6.1 the Frenkel Kontorova term (V_{fk}), the second the Tomlinson (V_t) and the third the Potential (V_v). We can now expand the equation into three dimension by expanding ξ_j into ξ_j^x, ξ_j^y and ξ_j^z, and V_v into a two dimensional spatially periodic external potential with a third

dimension a Lennard-Jones like potential. One of the trial potential is:

$$V_v(x) = C_v \sum_{j=1}^{N} C_z \left[cos(2\pi x_j) + cos(2\pi y_j) + \frac{1}{2} cos(2\pi x_j) cos(2\pi y_j) \right] \tag{6.2}$$

where C_z is the Lennard-Jones like potential for the perpendicular direction of the surface, and x_j and y_j are the positions in 2D of atom j:

$$\begin{aligned} C_z &= \frac{1}{4{z_j}^{12}} - \frac{1}{2{z_j}^{6}} \\ x_j &= x_B + c_j + \xi_j^x \\ y_j &= y_B + c_j + \xi_j^y \\ z_j &= z_B + \xi_j^y \end{aligned} \tag{6.3}$$

with x_B and y_B the position (sliding) in 2D of the upper body relative to the lower surface and z_B the upper rigid body translation due to relaxation or external force.

The calculation begins with x_B, y_B and z_B equal to zero (no external force) at a specific angle rotation. Minimization to find the lowest energy will result in a starting configuration prior to the sliding. This approach is more reasonable than Gyalog's averaging of all possible configuration. Energy minimization can be done by calculating the energies for all possible relative configurations and relaxing all individual atom positions at each configuration. One can let x_B and y_B vary (which will determine the local relaxation of atoms, ξ_j^x, ξ_j^y and ξ_j^z) until an energy minimum is achieved. One other technique is to raster through x_B and y_B in

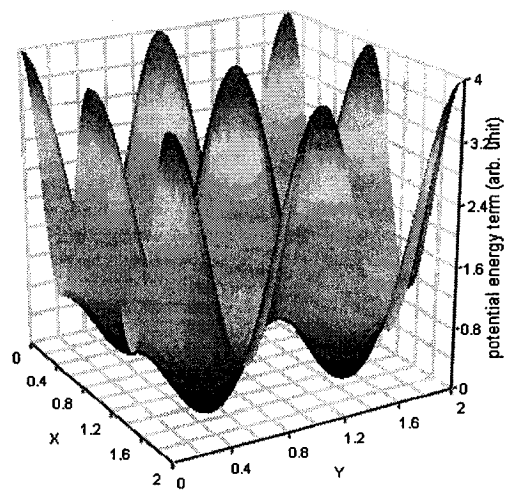

Figure 6.5. Schematic for the periodic potential representing the lower surface, as described in Eq.6.2.

one unit cell, which allows a quicker and certain method to arrive at the global minimum of the configurational energy, however is limited to the resolution of x_B and y_B. This can be further improved by letting x_B and y_B relax freely from the rastered solution.

Once an initial configuration corresponding to the lowest energy is found, the two pieces which have been oriented at a fixed angle are allowed to slide with a controlled sliding directions (fixed x_B and y_B). The value of x_B and y_B will define a vector that will determine the sliding angle. Care should be taken to choose the x_B and y_B step size in order to acquire a sufficient resolution to hit the minimum. An energy profile can be drawn as a function of sliding distance R, $\sqrt{x_B^2 + y_B^2}$, at the specific angle of θ, $\arctan(y_B/x_B)$. The frictional force, F, is defined as the first derivative of the energy E with respect to the distance R, this is the force

necessary to keep the relative bodies sliding with distance R with respect to the original configuration. However, upon the release of this force, it will return to the original configuration. From the phenomenological point of view the static friction F_S is defined as the smallest driving force F that initiates sliding. That is, any force F below F_S does not lead to a (meaningful) relative motion of the surfaces. Thus, the static friction is defined by the boundaries of F for which the stationary, motionless state is stable.

References

[1] Andersen, O. K., O. Jepsen, and D. Glotzel. 1985. *Highlights of condensed-matter theory*, 116–117. Amsterdam: North-Holland Physics Publishing.

[2] Anlage, S. M., B. Fultz, and K. M. Krishnan. 1988. Icosahedral phase formation in rapidly quenched aluminium-ruthenium alloys. *J. Mater. Res.* 3:421–425.

[3] Aubry, S. 1983. The twist map, the extended Frenkel-Kontorova model and the devils staircase. *Physica D* 7:240–258.

[4] Audier, M., Y. Brechet, M. Deboissieu, P. Guyot, C. Janot, and J. M. Dubois. 1991. Perfect and modulated quasi-crystals in the system Al-Fe-Cu. *Philos. Mag. B.* 63:1375–1393.

[5] Audier, M., and P. Guyot. 1990. *3rd international meetings on quasicrystals and incommensurate structures in condensed matter*, 288. Singapore: World Scientific.

[6] Audier, M., P. Guyot, and Y. Brechet. 1990. High-temperature stability and faceting of the icosahedral Al-Fe-Cu phase. *Philos. Mag. Lett.* 61:55–62.

[7] Bancel, P. A. 1993. Phason-induced transformations of icosahedral Al-Cu-Fe. *Phil. Mag. Lett.* 67:43–49.

[8] Bancel, P. A., and P. A. Heiney. 1986. Icosahedral aluminium-transition-metal alloys. *Phys. Rev. B.* 33:7917–7922.

[9] Bancel, P. A., P. A. Heiney, P. W. Stephens, A. I. Goldman, and P. M. Horn. 1985. Structure of rapidly quenched Al-Mn. *Phys. Rev. Lett.* 54:2422–2425.

[10] Bendersky, L. A. 1985. Quasicrystal with one-dimensional translational symmetry and a tenfold rotation axis. *Phys. Rev. Lett.* 55:1461–1463.

[11] Bengu, E. 2000. *Experimental and computational study of surfaces, interfaces and thin films*, Thesis (Ph.D., Materials Science and Engineering) - Northwestern University.

[12] Bengu, E., C. Collazo-Davila, D. Grozea, E. Landree, I. Widlow, and L.D. Marks M. Guruz. 1998. In situ growth and characterization of ultrahard thin films. *Microscopy Research and Technique* 42:295–301.

[13] Bengu, E., and L.D. Marks. 2001. Single-walled BN nanostructures. *Phys. Rev. Lett.* 86:2385–2387.

[14] Besser, M. F., and T. Eisenhammer. 1997. Deposition and applications of quasicrystalline coatings. *Mater. Res. Soc. Bull.* 22:59–63.

[15] Biggs, B. D., Y. Li, and S. J. Poon. 1991. Electronic properties of icosahedral, approximant, and amorphous phase of an Al-Cu-Fe alloy. *Phys. Rev. B.* 43:8747–8750.

[16] Black, P. J. 1955. The structure of $FeAl_3$. *Acta Cryst.* 8:43–48.

[17] Bolliger, B., V. E. Dmitrienko, M. Erbudak, R. Luscher, H. U. Nissen, and A. R. Kortan. 2001. Epitactic textures of fcc Al on icosahedral Al-Pd-Mn quasicrystal. *Phys. Rev. B* 63:052203.

[18] Bolliger, B., M. Erbudak, D. D. Vvedensky, and A. R. Kortan. 1999. Decagonal epilayers on the icosahedral quasicrystal $Al_{70}Pd_{20}Mn_{10}$. *Phys. Rev. Lett.* 82:763–766.

[19] Bolliger, B., M. Erbudak, D. D. Vvedensky, M. Zurkirch, and A. R. Kortan. 1998. Surface structural transitions on the icosahedral quasicrystal $Al_{70}Pd_{20}Mn_{10}$. *Phys. Rev. Lett.* 80:5369–5372.

[20] Bonasso, N., P. Pigeat, D. Rouxel, and B Weber. 2002. Effect of oxygen on the making of AlCuFe quasicrystalline coatings. *Thin Sol. Films* 409:165–171.

[21] Bonevich, J.E., and L.D. Marks. 1992. Ultrahigh vacuum electron microscopy of crystalline surfaces. *Microscopy: The Key Research Tool* March:95–101.

[22] Cai, T., F. Shi, Z. Shen, M. Gierer, A. I. Goldman, M. J. Kramer, C. J. Jenks, T. A. Lograsso, D. W. Delaney, P. A. Thiel, and M. A. Van Hove. 2001. Structural aspects of the fivefold quasicrystalline Al-Cu-Fe surface from STM and dynamical leed studies. *Surf. Sci.* 495:19–34.

[23] Chattopadhyay, K., S. Ranganathan, G. N. Subbanna, and N. Thangaraj. 1985. Electron-microscopy of quasi-crystals in rapidly solidified Al-14-percent Mn alloys. *Scr. Metall.* 19:767–771.

[24] Chen, H. S., and A. Inoue. 1987. Formation and structure of new quasicrystals of $Ga_{16}Mg_{32}Zn_{52}$ and $Al_{60}Si_{20}Cr_{20}$. *Scripta Metall.* 21:527–530.

[25] Chen, H. S., J. C. Phillips, P. Villars, A. R. Kortan, and A. Inoue. 1987. New quasicrystals of alloys containing s, p and d elements. *Phys. Rev. B.* 35:9326–9329.

[26] Chen, L. C., and F. Spaepen. 1988. Calorimetric evidence for the micro-quasicrystalline structure of amorphous Al-transition metal-alloys. *Nature* 336:366–368.

[27] Chien, C. L., and M. Lu. 1992. Three states of $Al_{65}Cu_{20}Fe_{15}$: Amorphous, crystalline, and quasi-crystalline. *Phys. Rev. B* 45:12793–12796.

[28] Clementi, E., and D. L.Raimondi. 1963. Atomic screening constants from SCF functions. *J. Chem. Phys.* 38:2686–2689.

[29] Clementi, E., D. L.Raimondi, and W.P. Reinhard. 1967. Atomic screening constants from SCF functions .2. atoms with 37 to 86 electrons. *J. Chem. Phys.* 47: 1300–.

[30] Collazo-Davila, C., E. Landree, D. Grozea, G. Jayaram, R. Plass, P.C. Stair, and L.D. Marks. 1995. *Journal of the Microscopy Society of America* 1:267.

[31] Conway, J.H., and K.M. Knowles. 1986. Quasi-periodic tiling in 2 and 3 dimensions. *J. Phys. A* 19:3645–3653.

[32] Cyrot-Lackman, F., T. Grenet, C. Berger, G. Fourcaudot, and C. Gignoux. 1995. *French Patent* No 9 503 938 .

[33] Dai, M., and R. Wang. 1990. Comparative investigation of microarea quasi-lattice parameters of Al-Si-Mn and Al-Cu-Fe icosahedral phases using HOLZ line patterns. *Acta Cryst. B* 46:455–458.

[34] Daniels, M.J., J. Maciejewski, J.S. Zabinski, Z.U. Rek, S.M. Yalisove, and J.C. Bilello. 2000. An investigation of sputtered Al-Cu-Fe-Cr quasicrystalline films via synchrotron diffraction. *Mat. Res. Soc. Proc.* 643:K.8.4.1.–K.8.4.6.

[35] Daulton, T. L., K. F. Kelton, and P. C. Gibbons. 1991. Decagonal and related phases in Al-Mn alloys - electron-diffraction and microstructure. *Philos. Mag. B* 63:687–714.

[36] Ding, Y., D. O. Northwood, and A. T. Alpas. 1997. Fabrication by magnetron sputtering of Al-Cu-Fe quasicrystalline films for tribological applications. *Surf. Coat. Tech.* 96:140–147.

[37] Dong, C. 2001. Private communication.

[38] Dong, C., and J.M. Dubois. 1991. Quasi-crystals and crystalline phases in $Al_{65}Cu_{20}Fe_{10}Cr_5$ alloy. *J. Mater Sci.* 26:1647–1654.

[39] ——. 1993. 2d geometrical model of the decagonal phase - tiling units and formation. *J. Non. Cryst. Solids* 159:107–120.

[40] Dong, C., J.M. Dubois, S.S. Kang, and M. Audier. 1992. *Phil. Mag. B.* 65:107.

[41] Dong, C., Z. K. Hei, L. B. Wang, Q. H. Song, Y. K. Wu, and K. H. Kuo. 1986. A new icosahedral quasicrystal in rapidly solidified $FeTi_2$. *Scripta Metall.* 20: 1155–1158.

[42] Dubois, J. M. 2000. New prospects from potential applications of quasicrystalline materials. *Mater. Sci. Eng.* 294:4–9.

[43] Dubois, J.M., S.S. Kang, and Y. Massiani. 1993. Application of quasicrystalline alloys to surface coating of soft metals. *J. Non-Crystalline Solids* 153:443–445.

[44] Dubois, J.M., S.S. Kang, and A. Perrot. 1994a. Towards applications of quasicrystals. *Mater. Sci. Eng. A* 179:122–126.

[45] Dubois, J.M., S.S. Kang, and J. Von Stebut. 1991. Quasi-crystalline low-friction coatings. *J. Mater. Sci. Lett.* 10:537–541.

[46] Dubois, J.M., A. Proner, B. Bucaille, Ph. Cathonnet, C. Dong, V. Richard, A. Pianelli, Y. Massiani, S. Ait-Yaazza, and E. Belin-Ferre. 1994b. *Ann. Chim. Sco. Mater.* 19:3–25.

[47] Duneau, M., and A. Katz. 1985. Quasiperiodic patterns. *Phys. Rev. Lett.* 54: 2688–2691.

[48] Ebalard, S., and F. Spaepen. 1989. The body-centered-cubic-type icosahedral reciprocal lattice of the Al-Cu-Fe quasi-periodic crystal. *J. Mater. Res.* 4:39–43.

[49] Eisenhammer, T., and M. Lazarov. 1994. *German patent* no 4 425 140.

[50] Eisenhammer, T., A. Mahr, A. Haugeneder, W. Assmann, and T. Reichelt. 1995.

[51] Eisenhammer, T., and A. Trampert. 1997. Formation of quasicrystalline Al-CuFe by physical deposition: Phase selection via nanocluster nucleation. *Phys. Rev. Lett.* 78:262–265.

[52] Elser, V. 1985. Indexing problems in quasicrystal diffraction. *Phys. Rev. B* 32: 4892–4898.

[53] ——. 1986. The diffraction pattern of projected structures. *Acta. Crys. A* 42: 36–43.

[54] Faudot, F. 1993. The Al-Cu-Fe phase-diagram - aluminum-rich corner and icosahedral region. *Ann. Chim. Sci. Mat.* 18:445–456.

[55] Faudot, F., A. Quivy, Y. Calvayrac, D. Gratias, and M. Harmelin. 1991. About the Al-Cu-Fe icosahedral phase formation. *Mater. Sci. Eng. A.* 133:383–387.

[56] Fletcher, N. H. 1964. Crystal interfaces. *J. Appl. Phys.* 35:234–240.

[57] ——. 1967. Structure and energy of crystal interfaces. II. a simple explicit calculation. *Philos. Mag.* 16:159–164.

[58] Fletcher, N. H., and P. L. Adamson. 1966. Structure and energy of crystal interfaces. I. formal development. *Phil. Mag.* 14:99–110.

[59] Fletcher, N. H., and K. W. Lodge. 1975. *Epitaxial growth, part B,* chap. 7, 529–557. New York: Academic Press.

[60] Follstaedt, D. M., and J. A. Knapp. 1986. Icosahedral-phase formation by solid-state interdiffusion. *Phys. Rev. Lett.* 56:1827–1830.

[61] Fortes, M. A. 1983. N-dimensional coincidence-site-lattice theory. *Acta. Cryst. A* 39:351–357.

[62] Franke, K. J., H. R. Sharma, W. Theis, P. Gille, Ph. Ebert, and K. H. Rieder. 2002. Quasicrystalline epitaxial single element monolayers on icosahedral Al-Pd-Mn and decagonal Al-Ni-Co quasicrystal surfaces. *Phys. Rev. Lett.* 89:156104.

[63] Frenkel, Y. I., and T. Kontorova. 1939. *Phys. Z. Sowjetunion* 13:1.

[64] Friedel, G. 1926. *Lecon de cristallographie.* Paris: Berger Levrault.

[65] Gahler, F., P. Kramer, H. Trebin, and K. Urban. 2000. ICQ7, proceedings of the 7th International Conference on Quasicrystals, 20-24 September, 1999, Stuttgart, Germany - preface. *Mater. Sci. Eng.* 294:1–3.

[66] Gahler, F., and J. Rhyner. 1986. Equivalence of the generalized grid and projection methods for the construction of quasi-periodic tilings. *J. Phys. A* 19:267–277.

[67] Gayle, F. W. 1992. Phase equilibria at 550°C in the Al-Cu-Fe system: 50 to 70 at. % Al, 0 to 9 at. % Fe. *J. Phase Equilib.* 13:619–622.

[68] Giacovazzo, C. 1998. *Direct phasing in crystallography,* 2, 18–20. Oxford University Press.

[69] Gratias, D., J. W. Cahn, and B. Mozer. 1988. Six-dimensional fourier analysis of icosahedral $Al_{73}Mn_{21}Si_6$ alloy. *Phys. Rev. B.* 38:1643–1646.

[70] Gratias, D., Y. Calvayrac, J. Devaud-Rzepski, F. Faudot, M. Harmelin, A. Quivy, and P.A. Bancel. 1993. The phase-diagram and structures of the ternary AlCuFe system in the vicinity of the icosahedral region. *J. Non-Cryst. Solids* 153:482–488.

[71] Grimmer, H. 1974a. Disorientations and coincidence rotations for cubic lattices. *Acta. Cryst. A* 30:685–688.

[72] ——. 1974b. A method of determining the coincidence site lattices for cubic crystals. *Acta. Cryst. A* 30:680.

[73] ——. 1976. Coincidence-site lattices. *Acta. Cryst. A* 32:783–785.

[74] ——. 1984. The generating function for coincidence site lattices in the cubic system. *Acta. Cryst. A* 40:108–112.

[75] ——. 1989. Systematic determination of coincidence orientations for all hexagonal lattices with axial-ratio c/a in a given interval. *Acta. Cryst. A* 45:320–325.

[76] Grimmer, H., W. Bollmann, and D. H. Warrington. 1974. Coincidence-site lattices and complete pattern-shift lattices in cubic crystals. *Acta. Cryst. A* 30:197–207.

[77] Grushko, B., R. Wittenberg, and D. Holland-Moritz. 1996. Solidification of Al-Cu-Fe alloys forming icosahedral phase. *J. Mater. Res.* 11:2177–2185.

[78] Gyalog, T., and H. Thomas. 1995. Friction between atomically flat surfaces. *Europhys. Lett.* 37:195–200.

[79] ——. 1997. Atomic friction. *Z. Phys. B* 104:669–674.

[80] Haberkern, R., K. Khedhri, C. Madel, and P Haussler. 2000. Electronic transport properties of quasicrystalline thin films. *Mat. Sci. Eng. A* 294:475–480.

[81] Haberkern, R., C. Roth, R. Knofler, F. Zavaliche, and P. Haussler. 1998. *Proceedings of the 6th International Conference on Quasicrystals*, 643–646. Singapore.

[82] He, L. X., Y. K. Wu, and K. H. Kuo. 1988a. Decagonal quasicrystals with different periodicites along the tenfold axis in rapidly solidified $Al_{65}Cu_{20}M_{15}$ (M = Mn, Fe, Co, or Ni). *J. Mater. Sci.* 7:1284–1286.

[83] He, L.X., Z. Zhang, Y.K. Wu, and K.H. Kuo. 1988b. Stable decagonal quasicrystals with different periodicities along the tenfold axis in $Al_{65}Cu_{20}Co_{15}$. *Inst. Phys. Conf. Ser.* 93:501–502.

[84] Heiney, P. A., P. A. Bancel, A. I. Goldman, and P. W. Stephens. 1986. Extended x-ray absorption fine-structure study of Al-Mn-Ru-Si icosahedral alloys. *Phys. Rev. B.* 34:6746–6751.

[85] Henley, C. L., and V. Elser. 1986. Quasicrystal structure of $(Al, Zn)_{49}Mg_{32}$. *Philos. Mag. B.* 53:L59–L66.

[86] Hiraga, K. 1991. *Quasicrystals the state of the art, directions in condensed matter physics*, 95. Singapore: World Scientific.

[87] Ikuhara, Y., and P. Pirouz. 1996. Orientation relationship in large mismatched bicrystals and coincidence of reciprocal lattice points (CRLP). *Mater. Sci. Forum* 207:121–124.

[88] Inoue, A., H. Kimura, T. Masumoto, A. P. Tsai, and Y. Bizen. 1987a. Al-Ge-(Cr or Mn) and Al-Si-(Cr or Mn) quasicrystal with high metalloid concentration prepared by rapid quenching. *J. Mater. Sci. Lett.* 771–774.

[89] Inoue, A., H. M. Kimura, and T. Masumoto. 1987b. Formation, thermal stability and electrical resistivity of quasicrystalline phase in rapidly quenched Al-Cr alloys. *J. Mater. Sci* 22:1758–1768.

[90] Inoue, Bizen, and Masumoto. 1988. Quasicrystalline phase in Al-Si-Mn system prepared by annealing of amorphous phase. *Metall. Trans. A.* 19:383–386.

[91] Janot, C. 1992. *Quasicrystals: A primer in monograph on the physics and chemistry of materials*, 21–49. New York.

[92] Janot, C., M. Audier, M. Deboissieu, and J. M. Dubois. 1991. Al-Cu-Fe quasicrystals - low-temperature unstability via a modulation mechanism. *Europhys. Lett.* 14:355–360.

[93] Janot, C., J. Panneteir, J. M. Dubois, J. P. Houin, and P. Weinland. 1988. Stoichiometry in Al-Mn-based icosahedral phases. *Philos. Mag. B.* 58:59–67.

[94] Jaric, M. V. 1986. Diffraction from quasi-crystals - geometric structure factor. *Phys. Rev. B* 34:4685–4698.

[95] 95 Kalugin, P.A., A.Y. Kitaev, and L.S. Levitov. 1985. $Al_{0.86}Mn_{0.14}$ - a 6-dimensional crystal. *JETP Lett.* 41:145–149.

[96] Kelton, K. F., P. C. Gibbons, and P. N. Sabes. 1988. New icosahedral phases in ti-transition metal alloys. *Phys. Rev. B.* 38:7810–7813.

[97] Kelton, K.F. 1993. Quasi-crystals - structure and stability. *Int. Mater. Rev.* 38: 105–137.

[98] Khoukaz, C., R. Galler, H. Mehrer, P. C. Canfield, I. R. Fisher, and M. Feuerbacher. 2000. Diffusion of Co-57 in decagonal Al-Ni-Co-quasicrystals. *Mater. Sci. Eng. A* 294:697–701.

[99] Kim, Y., and T. Hsu. 1991. A reflection electron-microscopic (REM) study of alpha-Al_2O_3(0001) surfaces. *Surf. Sci.* 258:131–146.

[100] Kittel, C. 1976. *Introduction to solid state physics*, Chap. 1. New York: Wiley.

[101] Knapp, J. A., and D. M. Follstaedt. 1985. Formation of icosahedral Al(Mn) by directed energy processes. *Phys. Rev. Lett.* 55:1591–1594.

[102] Ko, J. S., and A. J. Gellman. 2000. Friction anisotropy at Ni(100)/Ni(100) interfaces. *Langmuir* 16:8343–8351.

[103] Kreider, K. G., F. S. Biancaniello, and M. J. Kaufman. 1987. Sputter deposition of icosahedral Al-Mn and Al-Mn-Si. *Scripta Metall. Mater.* 21:657–662.

[104] Kuo, K. H. 1987. Some new icosahedral and decagonal quasicrystals. *Mater. Sci. Forum* 22-24:131–140.

[105] Kuo, K. H., C. Dong, D. S. Zhou, X. Y. Guo, Z. K. Hei, and D. X. Li. 1986. A Friauf-Laves (Frank-Kasper) phase related quasicrystal in a rapidly solidified Mn_3Ni_2Si alloy. *Scripta Metall.* 20:1695–1698.

[106] Kuo, K. H., D. S. Zhou, and D. X. Li. 1987. Quasicrystalline and Frank-Kasper phases in a rapidly solidified $V_{41}Ni_{36}Si_{23}$ alloy. *Philos. Mag. Lett.* 55:33–37.

[107] Levine, D., and P. J. Steinhardt. 1984. Quasicrystals - a new class of ordered structures. *Phys. Rev. Lett.* 53:2477–2480.

[108] Li, G. H., D. L. Zhang, H. W. Jiang, W. Y. Lai, W. Liu, and Y. P. Wang. 1997. Fully oriented decagonal quasicrystalline thin films on crystalline substrates. *Appl. Phys. Lett.* 71:897–899.

[109] Li, X.Z., C. Dong, and J.M. Dubois. 1995. Structural study of crystalline approximants of the Al-Cu-Fe-Cr decagonal quasi-crystal. *J. Appl. Cryst* 28:96–104.

[110] Li, X.Z., L.D. Marks, J. Maciejewski, L. Fehrenbacher, J. Zabinski, and J. ONeil. 2002. Stable quasicrystalline phase in Al-Cu-Fe-Cr coating materials. *Metal. Mater. Trans. A.* 33:675–679.

[111] Liu, W., U. Koster, and A. Zaluska. 1991. Continuous decomposition of icosahedral quasi-crystals in Al-Cu-Fe alloys. *Phys. Stat. Sol. A.* 126:K9–K14.

[112] Ma, Y., and E. A. Stern. 1988. Short-range stucture of Al-Mn and Al-Mn-Si aperiodic alloys. *Phys. Rev. B.* 38:3754–3765.

[113] Mai, Z., B. Zhang, M. Hui, Z. Huang, and X. Chen. 1987. Study of large size quasicrystal in Al_6Li_3Cu alloy. *Mater. Sci. Forum* 22-24:591–600.

[114] Mandal, R. K., and S. Lele. 2000. Interfaces in quasicrystals: problems and prospects. *Mater. Sci. Eng.* 294:813–817.

[115] Marks, L. D., M. Kubozoe, M. Tomita, M. Ukiana, T. Furutsu, and I. Matsui. 1988. *Design and initial performance of a UHV-HREM.* San Fransisco: San Fransisco Press.

[116] Menguy, N., M. Audier, M. DeBoissieu, P. Guyot, M. Boudard, and C. Janot. 1993. Phason-phonon-assisted epitaxy at icosahedral-decagonal interfaces in Al-Pd-Mn quasicrystals. *Philos. Mag. Lett.* 67:35–41.

[117] Merkle, A. P. 2003. *Atomic-scale friction: Incommensurate interfaces, coincidence and quasiperiodicity*, Proposal for Ph.D. Candidacy.

[118] Moulder, J. F., W. F. Stickle, P. E. Sobol, and K. D. Bomben. 1992. *Handbook of x-ray photoelectron spectroscopy*, 25. Eden Prairie.

[119] Mukhopadhyay, N. K., K. Chattopadhyay, and S. Ranganathan. 1988. Synthesis and structural aspects of quasicrystals in Mg-Al-Ag system - Mg_4Al_6Ag. *Metall. Trans. A.* 20:805–812.

[120] Mukhopadhyay, N. K., N. Thangaraj, K. Chattopadhyay, and S. Raganathan. 1987. A comparative electron microscopy study of Al-based and Mg-based quasicrystals. *J. Mater. Res.* 2:299–304.

[121] Mukhopadhyay, N.K., and G.C. Weatherly. 2001. Formation of quasicrystalline and vacancy ordered phases in vapour deposited thin films of Al-Cu-Co alloys. *Mat. Sci. Eng. A* 304:855–859.

[122] Nanao, S., W. Dmowski, T. Egami, J. W. Richardson, and J. D. Jorgensen. 1987. Structure of Al-Mn-Cr-Si quasicrystals studied by pulsed neutron scattering. *Phys. Rev. B.* 35:435–440.

[123] Naumovic, D., P. Aebi, L. Schlapbach, C. Beeli, K. Kunze, T. A. Lograsso, and D. W. Delaney. 2001. Formation of a stable decagonal quasicrystalline Al-Pd-Mn surface layer. *Phys. Rev. Lett.* 87:195506.

[124] Nelson, D. R., and B. I. Halperin. 1985. Pentagonal and icosahedral order in rapidly cooled metals. *Science* 229:233–238.

[125] Ohashi, W., and F. Spaepen. 1987. Stable Ga-Mg-Zn quasi-periodic crystals with pentagonal dodecahedral solidification morphology. *Nature* 330:555–556.

[126] Ohring, M. 1992. *The materials science of thin films*, 235. London: Academic Press Ltd.

[127] Perry, S.S., and P.B. Merrill. 1997. Preparation and characterization of MgO(100) surfaces. *Surf. Sci.* 383:268–276.

[128] Poon, S. J., A. J. Drehmann, and K. R. Lawless. 1985. Glassy to icosahedral phase transformation in Pd-U-Si alloys. *Phys. Rev. Lett.* 55:2324–2327.

[129] Qin, Y. L., R. H. Wang, Q. L. Wang, Y. M. Zhang, and C. X. Pan. 1995. Ar+ ion-irradiation-induced phase-transformations in an $Al_{70}Co_{15}Ni_{15}$ decagonal quasicrystal. *Philos. Mag. Lett.* 71:83–90.

[130] Quiquandon, M., A. Quivy, J. Devaud, F. Faudot, S. Lefebvre, M. Bessiere, and Y. Calvayrac. 1996. Quasicrystal and approximant structures in the Al-Cu-Fe system. *J. Phys. Condens. Matter* 8:2487–2512.

[131] Rabson, D. A., N. D. Mermin, D. S. Rokshar, and D. C. Wright. 1991. The space-groups of axial crystals and quasi-crystals. *Rev. Mod. Phys.* 63:699–733.

[132] Ranganathan, S. 1966. On the geometry of coincidence-site lattices. *Acta. Cryst.* 21:197–199.

[133] Rosas, G., and R. Perez. 2001. On the transformations of the ψ-AlCuFe icosahedral phase. *Mater. Lett.* 47:225–230.

[134] Roth, C., G. Schwalbe, R. Knofler, F. Zavaliche, O. Madel, R. Haberkern, and P. Haussler. 1999. A detailed comparison between the amorphous and the quasicrystalline state of Al-Cu-Fe. *J. Non-Cryst. Sol.* 252:869–873.

[135] Saadi, N., F. Faudot, D. Gratias, and B. Legendre. 1996. *5th International Conference on Quasicrystals.* Singapore: World Scientific.

[136] Saintfort, P., and B. Dubost. 1986. The T2 compound: a stable quasi-crystal in the system Al-Li-Cu-(Mg). *J. Phys. France* 47:C3321–330.

[137] Sanchez-Pascual, A., F.J. Garcia de Blas, J.M. Algaba, J. Alvarez, P. Valles, M.C. Garcia-Poggio, and A. Aguero. 1999. Application of quasicrystalline materials as thermal barriers in aeronautics and future perspectives of use for these materials. *Mater. Res. Soc. Symp. Proc.* 553:447.

[138] Sastry, G. V., C. Suryanarayana, M. Van Sande, and G. Van Tendeloo. 1978. New ordered phase in Al-Pd system. *Mater. Res. Bull.* 13:1065–1070.

[139] Sastry, G. V. S., V. V. Rao, P. Ramachandrarao, and T. R. Anantharaman. 1986. A new quasicrystallline phase in rapidly Mg_4CuAl_6. *Scripta Metall.* 20:191–193.

[140] Schurer, P. J., B. Koopmans, and F. van der Woude. 1988. Structure of icosahedral Al-($M_{1-x}Fe_x$) alloys (M=Cr, Mn, or Fe). *Phys. Rev. B.* 37:507–510.

[141] Senechal, M. 1995. *Quasicrystals and geometry.* New York : Cambridge University Press.

[142] Shechtman, D. 1990. The role of TEM in discovering and understanding quasicrystals. *Ultramicroscopy* 32:187.

[143] Shechtman, D., I. Blech, D. Gratias, and J.W. Cahn. 1984a. Metallic phase with long-range orientational order and no translational symmetry. *Phys. Rev. Letts.* 53:1951–1953.

[144] Shechtman, D., and C. I. Lang. 1997. Quasiperiodic materials: Discovery and recent developments. *Mater. Res. Bull.* 22:40–42.

[145] Shechtman, D., R. J. Schaefer, and F.S. Biancaniello. 1984b. Precipitation in rapidly solidified Al-Mn alloys. *Metall. Trans. A.* 15:1987–1997.

[146] Shen, Y., G. J. Shiflet, and S. J. Poon. 1988. Stability and formation of Al-Cu-(Li, Mg) icosahedral phases. *Phys. Rev. B.* 38:5332–5337.

[147] Shen, Z., M. J. Kramer, C. J. Jenks, A. I. Goldman, T. Lograsso, D. Delaney, M. Heinzig, W. Raberg, and P. A. Thiel. 1998. Crystalline surface structures induced by ion sputtering of Al-rich icosahedral quasicrystals. *Phys. Rev. B* 58: 9961–9971.

[148] Shen, Z., W. Raberg, M. Heinzig, C. J. Jenks, V. Fournee, M. A. Van-Hove, T. A. Lograsso, D. Delaney, T. Cai, P. C. Canfield, I. R. Fisher, A. I. Goldman, M. J. Kramer, and P. A. Thiel. 2000. A LEED comparison of structural stabilities of the three high-symmetry surfaces of Al-Pd-Mn bulk quasicrystals. *Surf. Sci.* 450: 1–11.

[149] Shimoda, M., J. Q. Guo, T. J. Sato, and A. P. Tsai. 2000a. Surface structure and structural transition of decagonal Al-Ni-Co quasicrystal. *Surf. Sci.* 454:11–15.

[150] ——. 2001. Surfactant-mediated growth of $AuAl_2$ film on a decagonal $Al_{72}Ni_{12}Co_{16}$ quasicrystal. *Surf. Sci.* 482:784–788.

[151] Shimoda, M., T. J. Sato, A. P. Tsai, and J. Q. Guo. 2000b. Epitaxial crystalline film with psuedo-tenfold symmetry formed by Au-deposition on a decagonal $Al_{72}Ni_{12}Co_{16}$ quasicrystal. *Phys. Rev. B* 62:11288–11291.

[152] ——. 2002. Epitaxial film growth on a decagonal $Al_{72}Ni_{12}Co_{16}$ quasicrystal. *Surf. Sci.* 507:276–280.

[153] Sonsky, J., M. Jelinek, L. Jastrabik, V. Studnicka, D. Chvostova, and Z. Bryknar. 1997. Study of quasicrystalline thin films based on Al-Pd-Mn and Al-Cu-Fe prepared by PLD. *Czechoslovak J. Phys.* 47:1019–1024.

[154] Sordelet, D. J., S. D. Widener, Y. Tang, and M. F. Besser. 2000. Characterization of a commercially produced Al-Cu-Fe-Cr quasicrystalline coating. *Mater. Sci. Eng. A* 294:834–837.

[155] Steinhardt, P. J., H. C. Jeong, K. Saitoh, M. Tanaka, E. Abe, and A. P. Tsai. 1998. Experimental verification of the quasi-unit-cell model of quasicrystal structure. *Nature* 396:55–57.

[156] Stemmer, S., P. Pirouz, and Y. Ikuhara. 1996. Film/substrate orientation relationship in the AlN/6H-SiC epitaxial system. *Phys. Rev. Lett.* 77:1797–1800.

[157] Steurer, W. 1990. The structure of quasi-crystals. *Z. Kristallogr.* 190:179–234.

[158] ——. 2000. Geometry of quasicrystal-to-crystal transformations. *Mater. Sci. Eng. A* 294-296:268–271.

[159] Steurer, W., T. Haibach, B. Zhang, S. Kek, and R. Luck. 1993. The structure of decagonal $Al_{70}Ni_{15}Co_{15}$. *Acta Cryst. B* 49:661–675.

[160] Steurer, W., and K. H. Kuo. 1990. 5-dimensional structure-analysis of decagonal $Al_{65}Cu_{20}Co_{15}$. *Acta Cryst B* 46:703–712.

[161] Sun, W., and K. Hiraga. 1993. Interface structure between decagonal and icosahedral quasi-crystals in Al-Pd-Mn alloy. *Philos. Mag. Lett.* 67:159–164.

[162] Susnitzky, D. W., and C. B. Carter. 1992. Surface-morphology of heat-treated ceramic thin-films. *J. Am. Ceram. Soc.* 75:2463–2478.

[163] Sutton, A. P. 1992. Irrational interfaces. *Progr. Mater. Sci.* 36:167–202.

[164] Sutton, A. P., and R. W. Balluffi. 1995. *Interfaces in crystalline materials.* Oxford: Clarendon Press.

[165] Symko, O. G. 2002. Private communication.

[166] Tomlinson, G. A. 1929. A molecular theory of friction. *Phil. Mag.* 7:905–939.

[167] Tsai, A. P., A. Inoue, and T. Masumoto. 1988a. A new icosahedral Al-Fe-Ta alloy prepared by rapid solidification. *Jpn. J. Appl. Phys.* 27:L1587–L1590.

[168] ——. 1988b. New quasicrystals in $Al_{65}Cu_{20}M_{15}$ (M = Cr, Mn or Fe) system prepared by rapid solidification. *J. Mater. Sci. Lett.* 7:322–326.

[169] ——. 1988c. New stable quasicrystals in Al-Cu-M (M = V, Cr or Fe) systems. *Trans. JIM* 29:521–524.

[170] Tsai, A.P., A. Inoue, and T. Masumoto. 1988d. New stable icosahedral Al-Cu-Ru and Al-Cu-Os alloys. *Jpn. J. Appl. Phys.* 27:L1587–L1590.

[171] Tsai, A.P., A. Inoue, and T. Matsumoto. 1987. A stable quasi-crystal in Al-Cu-Fe system. *Jpn. J. Appl. Phys.* 26:1505–1507.

[172] Urban, K., N. Moser, and H. Kronmuller. 1985. Phase-transitions between the quasicrystalline, crystalline, and amorphous phases in Al-14 at percent-Mn. Phys. *Status Solidi A* 91:411–422.

[173] Vainshtein, B. K. 1981. *Modern crystallography I*, chap. 2. Berlin: Springer-Verlag.

[174] Wagner, C.D., L.E. Davis, M.V. Zeller, J.A. Taylor, R.H. Raymond, and L.H. Gale. 1981. Empirical atomic sensitivity factors for quantitative-analysis by electron-spectroscopy for chemical-analysis. *Surf. Interface. Anal.* 3:211–225.

[175] Wang, Z. G., X. X. Yang, and R. H. Wang. 1993. Ar+ion-irradiation-induced phase-transformation in an $Al_{62}Cu_{25.5}Fe_{12.5}$ icosahedral quasi-crystal. *J. Phys. Cond. Mat.* 5:7569–7576.

[176] Warrington, D. H., O. Radulescu, and R. Luck. 1997. Coincidence lattices and quasilattices for icosahedral quasicrystals. *Acta. Cryst. A* 53:314–328.

[177] Weber, S. 2000. Computer code QUAREF, private communication.

[178] Weber, S., and A. Yamamoto. 1998. Noncentrosymmetric structure of a decagonal $Al_{70}Mn_{17}Pd_{13}$ quasicrystal. *Acta Cryst. A* 54:997–1005.

[179] Weisbecker, P., G. Bonhomme, A. Cael, L. Zhang, and J. M. Dubois. 2001. Xray diffraction study of the transformation of an Al-Cu-Fe atomized powder upon annealing at 500c. *Mater. Res. Soc. Sym.* 643:K9.2.1.–K9.2.5.

[180] Weiss, M., and F. J. Elmer. 1996. Dry friction in the Frenkel-Kontorova-Tomlinson model: Static properties. *Phys. Rev. B* 53:7539–7549.

[181] Whittaker, E.J., and R.M. Whittaker. 1988. Some generalized penrose patterns from projections of normal-dimensional lattices. *Acta Crys. A* 44:105–112.

[182] Widjaja, E. J., and L. D. Marks. 2002. *Thin Sol. Films* 420:295–299.

[183] ——. 2003a. *Philos. Mag. Lett.* 83:47–55.

[184] ——. 2003b. Coincidence of reciprocal lattice planes model for quasicrystal-crystal epitaxy. *Phys. Rev. B* 68:134211–134220.

[185] ——. 2003c. Microstructural evolution in Al-Cu-Fe quasicrystalline thin films. *Thin Sol. Films* 441:63–71.

[186] Wolf, D., and S. Yip. 1992. *Material interfaces.* London: Chapman and Hall.

[187] Xu, P., G. Jayaram, and L. D. Marks. 1994. Cross-correlation method for intensity measurement of transmission electron-diffraction patterns. *Ultramicroscopy* 53: 15–18.

[188] Yamamoto, A. 1996. Crystallography of quasiperiodic crystals. *Acta Cryst. A* 52: 509–560.

[189] Yamamoto, A., and K. Hiraga. 2000. Six-dimensional model of an i-Al-Pd-Mn quasicrystal compatible with its 2/1 approximant. *Mater. Sci. Eng.* 294:228–231.

[190] Yang, X. X., R. H. Wang, and X. J. Fan. 1996. Phase transitions in $Al_{62}Cu_{25.5}Fe_{12.5}$ quasicrystal induced by low-temperature Ar_2+ irradiation. *Philos. Mag. Lett.* 73:121–127.

[191] Yoshioka, A., K. Edagawa, K. Kimura, and S. Takeuchi. 1995. Production of high quality thin-film samples of Al-Cu-Fe icosahedral quasicrystal. *Jpn. J. Appl. Phys.* 34:1606–1609.

[192] Zhang, H., D. H. Wang, and K. H. Kuo. 1988. Quasicrystalline, crystalline phases and multiple twins in rapidly solidified Al-Cr alloys. *Phys. Rev. B.* 37:6220–6225.

[193] Zhang, J. P., A. K. Cheetam, K. Sun, J. S. Wu, K. H. Kuo, J. Shi, and D. D. Awschalom. 1997. Submicron GaMn quasicrystals in ferromagnetic GaAs. *Appl. Phys. Lett.* 71:143–145.

[194] Zhang, Z., and W. Geng. 1992. Direct observation of misfit dislocations at the interface between a decagonal quasi-crystal and its epitaxial crystalline layers. *Philos. Mag. Lett.* 65:211–218.

[195] Zhang, Z., and N. C. Li. 1990. Orientation relationship between the icosahedral quasicrystalline and the B2-based crystalline phases in $Al_{65}Cu_{20}Fe_{15}$ alloys. *Scripta Metall.* 24:1329–1334.

[196] Zhang, Z., and K. Urban. 1989. Dislocations and planar faults in decagonal Al-Cu-Co alloy. *Scripta Metall. Mater.* 23:1663–1668.

[197] Zhang, Z., H. Q. Ye, and K. H. Kuo. 1985. A new icosahedral phase with m35 symmetry. *Philos. Mag. A.* 52:L49–L52.

[198] Zhuang, Y., Z. Zhang, and D. B. Williams. 1993. A transmission electronmicroscopy study of interphase dislocations between decagonal quasi-crystalline and crystalline phases in $Al_{75}Ni_{10}Fe_{15}$ alloy. *J. Non-Cryst. Sol.* 153:119–122.

[199] Zumkley, T., and H. Nakajima. 2000. Solute diffusion of Ni in icosahedral Al-Pd-Mn quasicrystals. *Philos. Mag. A* 80:1065–1074.

[200] Zurkirch, M., B. Bolliger, M. Erbudak, and A. R. Kortan. 1998. Structural transformations at the surface of the decagonal quasicrystal $Al_{70}Co_{15}Ni_{15}$. *Phys. Rev. B* 58:14113–14116.

APPENDICES

A. Quasicrystalline Cooking Pan

One potential application of the quasicrystalline coatings is to exploit its non-stick surface property combined with the relatively high hardness. A French company, Sitram, produced Cyberbox, a patented stick-resistant pan, which utilized the Al-Cu-Fe-Cr plasma sprayed coatings as the non-stick coatings. With a slightly lower quality in non-stick performace compared to traditional teflon coatings, it surpasses the older technology with its durability. Its claims of superiority are shown on Fig. A.1. One of many website links that provide commercial information on this cooking pan is: http://www.chefsresource.com/sitramcybernox.html. The streaming video gives information on this product, which claims to be a new generation non-stick high-durability cooking pan.

While this product is still available in the market under the same brand [1], one set of pans we bought two years ago no longer used the quasicrystalline technology as the non-stick coating. In place of Al-Cu-Fe-Cr coating, the coating specimens reveal the utilization of chromium coating on top of a stainless steel substrate.

[1]The quasicrystalline technology is not explicitly mentioned in the many sources that provide the information on the product (including on the box of the product).

Figure A.1. Product information as shown on the container box of Cybernox by Sitram.

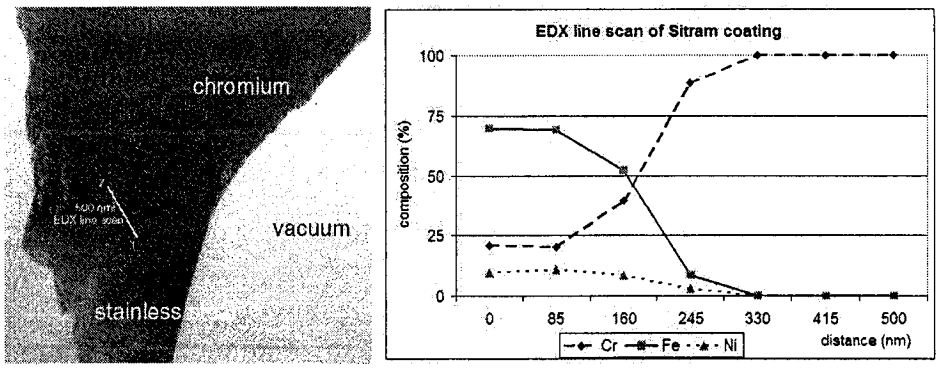

Figure A.2. Analyses of cross-section sample of Cybernox cooking pan. a) STEM bright field showing the stainless steel substrate and the chromium coating. Superimposed on the image is a line showing where EDX line-scan (b) was conducted.

STEM bright field (Fig. A.2.a) combined with EDX line-scan (Fig. A.2.b) conclusively shows the content of the coatings, in addition to EDX from a SEM showing a pure Cr coating.

The reason for this technology shift to a less suitable chromium coatings in unknown, but highly believable due to the inability to control the quality of the coatings (Dong 2001). It has been discussed in the text that the result of plasma spray is a composite materials - which not only contains the desired quasicrystalline phases but also others. There is one paper which studied the coatings of this pan, which was still quasicrystalline at that time (Sordelet et al. 2000). This failure to continue production of the non-stick coatings is not only due to the nature of the plasma sprayed coating, but it is also the difficult in a sputtering system to control the composition as discussed in chapter 3.2.

B. SINBAD

The modified chamber, equipped with a magnetron sputtering chamber for quasicrystalline thin films deposition continues to have its old name SINBAD, which stands for Stabilized Ion and Neutral Beam Assisted Deposition. While SINBAD has been modified from its original deposition source, the rest of the system (i.e. vacuum chamber, pumping system, vacuum gauges) remains the same. Documentation of the system have been given elsewhere in a previous thesis of a student from this research group (Bengu 2000).

The magnetron sputtering gun is the new modification. The magnetron gun allows an adjustable distance between the target and sample by a compressible bellow. It can hold a single target with a dimension 1.5" in diameter and thickness between 1/8"-1/4" inch. The target is held mechanically (and also magnetically for a magnetic target) and can be of single or multiple elements (e.g. vacuum alloying or powder metallurgy target). The original magnetron system has been altered slightly to simplify the process. The argon inlet line, which was an integral part of the gun, has been blanked and another flange near the target is used to feed the inert gas. This modification is related due to design of the gun which due to the lack of available space it was difficul to tighten the inlet line to the gun.

Target conditioning is carried out by sputtering for 45-60 minutes to clean the target; this procedure is carried out for a new target and everytime the target is exposed to contaminants (e.q. air). A shorter conditioning, approximately 10-15 minutes, is conducted prior to deposition when the system is kept under UHV. A shutter can be used to prevent deposition on the substrate while target is being conditioned. Another alternative is to bring the substrate from the sample transfer chamber (STC) after the target conditioning. Care needs to be taken to ensure that the pressure in SINBAD is near the pressure of the STC before opening the valve between them.

A continuous water flow from a chiller is required to cool down the rare earth magnets, located right behind the target, during deposition. Currently, the water cooling line is a continuous line from the line to cool the Turbo Molecular Pump (TMP).

During deposition, the chamber pressure is maintained at 2-3 x 10^{-3} Torr of Argon. The ion pump needs to be turned off prior to the deposition and given sufficient time to cool down. Pumping is solely carried out by the TMP, backed by the mechanical rotary pump. A valve between the TMP and the chamber can be partially closed to reduce the pumping rate by limiting the conductance. A better alternative is to change the speed of the TMP. A typical setting is to have the TMP in low speed mode (2/3 of the maximum speed) with a fully open valve,

and to have the Mass Flow Controller (MFC) set to mantain the desire pressure for deposition.

C. CRLP Program

C.1. Quaref

The program QuaRef simulate the 3D reciprocal lattice coordinates with theoretical structure factors (which relate to the intensity, which was used to calculate the interfacial energy in the CRLP model). The simulation for the quasicrystal reciprocal lattice (diffraction pattern) was developed by Steffen Weber. [1]

QuaRef is a stand-alone software for Windows95/98/ME/2000/NT. It creates lists of reflections for dihedral (octagonal, decagonal, dodecagonal) and icosahedral quasicrystals. It displays the 0^{th} layer as a static image and the the whole set of reflections in an interactive 3D viewer. The reflections can be rotated by dragging the mouse over the display area. For the simulation the user can choose between lattice matrices as used by Dr. Akiji Yamamoto or Prof. Walter Steurer (Yamamoto 1996; Steurer 1990). QuaRef observes the extinction rules for the chosen space groups. The encoded extinction rules are based on the paper by Rabson et al. (1991).

[1]Details of this program can be found at this link: http://jcrystal.com/products/quaref/index.html

C.2. C Code for CRLP Model

The CRLP code was written in C. The detail of the code is attached in this appendix as documentation.

(1) crystal.c: program to generate reflections in crystal, given two non-linear **u** and **v** vectors. It will limit the reciprocal space to q value and output the reflections in **crystal1.txt**.

(2) quaref.c: program to reduce the search in reciprocal lattice for quasicrystalline reflections up to certain q value. Input: Value for q as an arguments and output of Quaref as **quaref.hkl**. Argument 1 is for the value of q-space cutoff. Output: **quaref1.txt** as q-space cutoff reciprocal space of quasicrystalline reflections.

(3) quaref1.c: program to reduce the 3D reciprocal reflections into 2D. Input: **quaref1.txt**. Output: **quaref2.txt**. Change the values of tethadegree and phidegree for determining the 2D plane-section.

(4) rotating.c: program to reorient the 2D reflections into the reference coordinate system. Input: **quaref2.txt**. Output: **quaref3.txt**. Change the values of tethadegree and phidegree to set the rotation of coordinate axes - the value should be the same with the ones in quaref1.c.

(5) quaref2.c: program to reduce the reciprocal lattice up to certain reciprocal matching between the quasicrystalline and nearby crystalline spots, with set tolerance. Reflections beyond certain tolerance value are removed since

the reciprocal values of their κ vectors are negligible. Input: **crystal1.txt** and **quaref3.txt**. Output: **quaref4.txt** as reduced quasicrystalline reflections after matching with crystalline reflections.

(6) crystal1.c: similar to quaref2.c for crystalline reflections. Input: **quaref4.txt** and **crystal1.txt**. Output: **crystal2.txt**.

(7) run *uniq quaref4.txt >quaref5.txt* and *cp quaref5.txt quaref4.txt*, run *uniq crystal2.txt >crystal3.txt* and *cp crystal3.txt crystal2.txt* to take only uniqe reflections.

(8) eneralpha180.c: program to calculate the energy using Eg.4.13. by rotating the two interfaces. Rotation depends on the number of steps and resolution (change res and sym values). Input: **crystal2.txt** and **quaref4.txt**, argument 1 is the α value (look at table 4.1) and argument 2 is for icosahedral/decagonal. Output: **energy.txt** is the energy value as a function of rotation.

crystal.c

```
#include <stdio.h>
#include<string.h>
#include<stdlib.h>
#include<math.h>

main ()
{
   float xu,yu,xv,yv, x,y,q, maxq;
   int i,j, hk;
   FILE *fp;

/* maximum hk to list, later truncate with maxq */
   hk=10;

/* put file name here, output */
   fp=fopen("/usr1/edy/3D/crystal1.txt","wt");
   fprintf(fp," i   j     q          x         y \n");
   printf("Input u vector, xu, yu:  ");
   scanf("%f %f", &xu, &yu);
   printf("Input v vector, xv, yv:  ");
   scanf("%f %f", &xv, &yv);
   printf("Maximum q to consider :  ");
   scanf("%f", &maxq);
   for (i=-hk; i<=hk; i++)
   {
      for (j=-hk; j<=hk; j++)
      {
         x=i*xu+j*xv;
         y=i*yu+j*yv;
         q=sqrt(x*x+y*y);
      if (q<(maxq))
         fprintf( fp, "%3i %3i %9.6f %9.6f %9.6f \n", i, j,
q, x, y);
      }
   }
   fputs("x", fp);
   fclose(fp);
}
```

quaref.c

```
#include <stdio.h>
#include<string.h>
#include<stdlib.h>

main (int dd, char *argv[])

{
   int c;
   char temp[101], line[101];
   char dummy[30];
   int i,j, deca, dec;
   float float_dummy, rest;


   FILE *fp;
   FILE *fpp;

rest=atof(argv[1]);

/* for decagonal add deca=4 */
   printf("decagonal? yes=1: ");
   deca=0;
   scanf("%i", &dec);
   if(dec==1)
      deca=-4;

/* put file name here, input and output */
   fpp=fopen("/usr1/edy/3D/quaref1.txt","w");
   if( fp=fopen("/usr1/edy/3D/quaref.hkl", "rt"))
   {
      for(j=1; j<8; j++)
      {
         strcpy(line, fgets(temp, 101, fp));
      fputs(line, fpp);
      }

      while (temp[0]!='x')
      {
            strcpy(line,fgets (temp,101, fp));
/*          printf( "%s", line); */
```

```
            for ( i=0; i<7; i=i+1)
                dummy[i]=temp[i+52+deca];

/*          printf("%s \n", dummy); */
              float_dummy=atof(dummy);
/*       printf("%f \n", float_dummy);  */

/* putting in a new file refections with certain range of
qe */

         if(float_dummy<=rest)
          fputs(line, fpp);
      }
   }
   else
   printf("Error in opening file\n");

   fputs("x", fpp);
   fclose(fp);
   fclose(fpp);
}
```

quaref1.c

```
#include <stdio.h>
#include<string.h>
#include<stdlib.h>
#include<math.h>
#define PI 3.1415926535898

main ()

{
   int c;
   char temp[101], line[101];
   char dummy1[30], dummy2[30], dummy3[30];
   int i,j, deca, dec;
   float float_dummy1, float_dummy2, float_dummy3;
   float a1 ,a2 ,a3, dot, tolerance;
   double tetha, phi, tetha_degree, phi_degree, sint, sinp,
cost, cosp;
   FILE *fp;
   FILE *fpp;

       tetha_degree=0;
       phi_degree=0;

/* for decagonal add deca=4 */
   printf("decagonal? yes=1: ");
   deca=0;
   scanf("%i", &dec);
   if(dec==1)
      deca=-4;


/* put file name here, input and output */
   fpp=fopen("/usr1/edy/3D/quaref2.txt","w");
   if( fp=fopen("/usr1/edy/3D/quaref1.txt", "rt"))
   {
      for(j=1; j<8; j++)
      {
         strcpy(line, fgets(temp, 101, fp));
      fputs(line, fpp);
      }
```

```
      while (temp[0]!='x')
      {
            strcpy(line,fgets (temp,101, fp));
/*          printf( "%s", line);*/

            for ( i=0; i<8; i=i+1)
            {
                dummy1[i]=temp[i+71+deca];
                dummy2[i]=temp[i+81+deca];
                dummy3[i]=temp[i+91+deca];
            }

/*          printf("%s %s %s \n", dummy1, dummy2,
dummy3);*/
              float_dummy1=atof(dummy1);
              float_dummy2=atof(dummy2);
              float_dummy3=atof(dummy3);
/*          printf("%f %f %f \n", float_dummy1,
float_dummy2, float_dummy3);*/

/* constraint of zone axis */

       phi=phi_degree*PI/180;
       tetha=tetha_degree*PI/180;

       a1=sin(tetha)*cos(phi); a2=sin(tetha)*sin(phi);
a3=cos(tetha);
       dot=a1*float_dummy1+a2*float_dummy2+a3*float_dummy3;
/*     printf("%f \n", dot );*/
       tolerance=0.005;
       if(dot<tolerance & dot>-tolerance)
          {
          fputs(line, fpp);
/*        printf("%f \n", dot);*/
          }
      }
   }
   else
   printf("Error in opening file\n");

   fputs("x", fpp);
   fclose(fp);
   fclose(fpp);
}
```

rotating.c

```
#include <stdio.h>
#include<string.h>
#include<stdlib.h>
#include<math.h>
#include<float.h>
#define PI 3.1415926535898

main ()

{

   int c;
   char temp[101], line[101];
   char dummy1[30], dummy2[30], dummy3[30];
   int i,j, deca, dec;
   float float_dummy1, float_dummy2, float_dummy3;
   float a1 ,a2 ,a3, dot, tolerance;
   double phi_degree, tetha_degree, phi, tetha;
   double l11, l12, l13, l21, l22, l23, l31, l32, l33;
   double sint, sinp, cost, cosp;
   double x1,y1,z1, newq_original, newq, delta;
   char linedummy[80];

   FILE *fp;
   FILE *fpp;

        tetha_degree=90;
       phi_degree=18;

/* for decagonal add deca=4 */
   printf("decagonal? yes=1: ");
   deca=0;
   scanf("%i", &dec);
   if(dec==1)
      deca=-4;

   phi=phi_degree*PI/180;
   tetha=tetha_degree*PI/180;
   sint=sin(tetha);
   cost=cos(tetha);
   sinp=sin(phi);
```

```
   cosp=cos(phi);
   l11=cosp*cosp*cost+sinp*sinp;
   l12=cosp*sinp*cost-sinp*cosp;
   l13=-1*cosp*sint;
   l21=sinp*cosp*cost-cosp*sinp;
   l22=sinp*sinp*cost+cosp*cosp;
   l23=-1*sinp*sint;
   l31=sint*cosp;
   l32=sint*sinp;
   l33=cost;
/* printf("%f %f %f\n", l11, l12, l13);
   printf("%f %f %f\n", l21, l22, l23);
   printf("%f %f %f\n", l31, l32, l33);*/


/* put file name here, input and output */
   fpp=fopen("/usr1/edy/3D/quaref3.txt","w");
   if( fp=fopen("/usr1/edy/3D/quaref2.txt", "rt"))
   {
      for(j=1; j<8; j++)
      {
         strcpy(line, fgets(temp, 101, fp));
      fputs(line, fpp);
      }

      while (temp[0]!='x')
      {
            /*printf("%s", temp);*/
            strcpy(line,fgets (temp,101, fp));
/*          printf( "%s", line);*/

            for ( i=0; i<8; i=i+1)
            {
                dummy1[i]=temp[i+71+deca];
                dummy2[i]=temp[i+81+deca];
                dummy3[i]=temp[i+91+deca];
            }

/*          printf("%s %s %s \n", dummy1, dummy2,
dummy3);*/
              float_dummy1=atof(dummy1);
              float_dummy2=atof(dummy2);
              float_dummy3=atof(dummy3);
```

```
/*          printf("%f %f %f \n", float_dummy1,
float_dummy2, float_dummy3);*/

/* changing cartesian reference */

x1=float_dummy1*l11+float_dummy2*l12+float_dummy3*l13;

y1=float_dummy1*l21+float_dummy2*l22+float_dummy3*l23;

z1=float_dummy1*l31+float_dummy2*l32+float_dummy3*l33;
       newq=sqrt(x1*x1+y1*y1);
       newq_original=sqrt(x1*x1+y1*y1+z1*z1);
       delta=(newq-newq_original)*10000/newq_original;
/*     printf("%f %f %f\n", x1,y1,z1 );*/
       for ( i=0; i<70+deca; i=i+1)
           linedummy[i]=temp[i];
     if (temp[0]!='x')
/*     fprintf(fpp, "%s %9.6f %9.6f %9.6f %9.6f\n",
linedummy, x1, y1, z1, delta);       */
       fprintf(fpp, "%s %9.6f %9.6f %9.6f \n", linedummy,
x1, y1, z1);
           }

   }
   else
   printf("Error in opening file\n");

   fputs("x", fpp);
   fclose(fp);
   fclose(fpp);
}
```

quaref2.c

```
#include <stdio.h>
#include<string.h>
#include<stdlib.h>

main ()

{
   int c;
   char temp[111], line[111], linec[40];
   char dummy[30], dummyc[30];
   int i,j, crys, k, ind, l, dec, deca;
   float float_dummy, delta, tolerance, float_dummyc, qc;
   float cryst_q[50], qcc[150], junk;

   FILE *fp;
   FILE *fpp;
   FILE *fpc;


/* for decagonal add deca=4 */
   printf("decagonal? yes=1: ");
   deca=0;
   scanf("%i", &dec);
   if(dec==1)
      deca=-4;
   tolerance=0.01;
   qcc[0]=0; k=1; ind=1;
/* read q-s from crystal.txt */
   fpc=fopen("/usr1/edy/3D/crystal1.txt","rt");
   strcpy(linec,fgets (temp,40, fpc));
   while (temp[0]!='x')
   {
      strcpy(linec,fgets (temp,40, fpc));
      for ( i=0; i<8; i=i+1)
         dummyc[i]=temp[i+9];
      float_dummyc=atof(dummyc);
/*      printf("%f \n", float_dummyc); */
      for (l=0; l<k; l++)
      {
         if(float_dummyc==qcc[l])
            ind=ind*0;
```

```
/*      printf("%i %f \n", ind, qcc[l]);*/
      }
      if (ind>0)
      {
/*              printf("%f \n", float_dummyc);*/
      qcc[k]=float_dummyc; k++;
      }
      ind=1;
   }
   for (l=1; l<k; l++)
      printf("crystal q: %i %f \n", l, qcc[l]);

/*   printf("Number of crystalline reflections to consider:
");
   scanf("%i", &crys);
      for (i=0; i<crys; i++)
         {
         printf("Enter q value: ");
         scanf("%f", &cryst_q[i]);
         }
*/
/* put file name here, input and output */
   fpp=fopen("/usr1/edy/3D/quaref4.txt","w");
   if( fp=fopen("/usr1/edy/3D/quaref3.txt", "rt"))
   {
      for(j=1; j<8; j++)
      {
         strcpy(line, fgets(temp, 110+deca, fp));
      fputs(line, fpp);
      }

      while (temp[0]!='x')
      {
            strcpy(line,fgets (temp,110+deca, fp));
/*          printf( "%s", line); */

            for ( i=0; i<7; i=i+1)
                dummy[i]=temp[i+52+deca];

/*          printf("%s \n", dummy); */
              float_dummy=atof(dummy);
/*       printf("%f \n", float_dummy);  */
```

```
                for (l=1; l<k; l++)
            {
                delta=qcc[l]-float_dummy;
                if (delta<tolerance & delta>-tolerance)
                    fputs(line, fpp);
            }
        }
}
    else
    printf("Error in opening file\n");

    fputs("x", fpp);
    fclose(fp);
    fclose(fpp);
    fclose(fpc);
}
```

crystal1.c

```
#include <stdio.h>
#include<string.h>
#include<stdlib.h>

main ()

{
   int c;
   char temp[111], line[111], linec[111];
   char dummy[30], dummyc[30];
   int i,j, crys, k, ind, l, deca, dec;
   float float_dummy, delta, tolerance, float_dummyc, qc;
   float cryst_q[15], qcc[150], junk;

   FILE *fp;
   FILE *fpp;
   FILE *fpc;

/* for decagonal add deca=4 */
   printf("decagonal? yes=1: ");
   deca=0;
   scanf("%i", &dec);
   if(dec==1)
      deca=-4;

   tolerance=0.01;
   qcc[0]=0; k=1; ind=1;
   fpc=fopen("/usr1/edy/3D/quaref4.txt","r");
   for(j=1; j<8; j++)
         strcpy(linec, fgets(temp, 111, fpc));

   while (temp[0]!='x')
   {
      strcpy(linec,fgets (temp,111, fpc));
      for ( i=0; i<7; i=i+1)
         dummyc[i]=temp[i+52+deca];
      float_dummyc=atof(dummyc);
      for (l=0; l<k; l++)
      {
         if(float_dummyc==qcc[l])
            ind=ind*0;
```

```
      }

      if (ind>0)
        { qcc[k]=float_dummyc; k++;  }

      ind=1;
   }

   for (l=1; l<k; l++)
      printf("quasicrystal q: %i %f \n", l, qcc[l]);

/* put file name here, input and output */
   fpp=fopen("/usr1/edy/3D/crystal2.txt","w");
   if( fp=fopen("/usr1/edy/3D/crystal1.txt", "rt"))
   {
         strcpy(line, fgets(temp, 101, fp));
      fputs(line, fpp);

      while (temp[0]!='x')
      {
            strcpy(line,fgets (temp,40, fp));
/*            printf("%s", line);*/
            for ( i=0; i<8; i=i+1)
                dummy[i]=temp[i+9];

              float_dummy=atof(dummy);


                for (l=1; l<k; l++)
          {
             delta=qcc[l]-float_dummy;
             if (delta<tolerance & delta>-tolerance)
                fputs(line, fpp);
          }
      }

   }

   fputs("x", fpp);
   fclose(fp);
   fclose(fpp);
   fclose(fpc);
}
```

eneralpha180.c

```
#include <stdio.h>
#include<string.h>
#include<stdlib.h>
#include<math.h>
#define PI 3.1415926535898

main (int dd, char *argv[])

{
   int c,dec, wei;
   char temp[101], tempp[130], line[130], linep[40];
   char dummypx[30], dummypy[30], dummyc[30], dumqi[30],
dumqidec[30], dummyint[30];
   int i, ii, j, ll,  crys, k, ind, l, m, n, jmin, imin,
angle, o, sym, jj, deca, res, mm;
   float float_dummy, delta, tolerance,
float_dummypx[50000], float_dummyint[50000],
float_dummypy[50000], qc;
   float cryst_q[10000], qcc[10000], junk, length,
realangle;
   float float_dummyppx[50000], float_dummyppy[50000],
float_dumqi[50000], float_dumqidec[50000];
   float deltax, deltay, ks, ksmin, kmin[36000], total,
dumppx, dumppy, total_angle[36000], alpha;
   double l11, l12, l21, l22, angle_rad, en, qqq, weigh;

   FILE *fp;
   FILE *fpp;
   FILE *fpc;

   fp=fopen("/usr1/edy/3D/crystal2.txt","rt");
   fpp=fopen("/usr1/edy/3D/quaref4.txt","rt");
   res=40;
   sym=190*res;

alpha=atof(argv[1]);
   dec=atoi(argv[2]);
   /* for decagonal add deca=4 */
/*  scanf("%i", &dec);  */
   deca=0;
      if(dec==1)
```

```
      deca=-4;

   /*weight-ing (v(q)) */
    /*v(q) = 1/(exp(7.5*q-4)+1) */
    printf("v(q) = 1/(exp(alpha*q-4)+1) \n");

/* get rid of file explanation */
      for(j=1; j<8; j++)
      strcpy(line, fgets(temp, 101, fpp));

      strcpy(line,fgets (temp,40, fp));

/* reading crystal2.txt */
   k=0;
   while (temp[0]!='x')
   {
      strcpy(linep,fgets (temp,40, fp));
      for ( i=0; i<9; i=i+1)
      {
         dummypx[i]=temp[i+18];
         dummypy[i]=temp[i+28];
      }

      float_dummypx[k]=atof(dummypx);
      float_dummypy[k]=atof(dummypy);

   k++;
   }

/* reading quaref4.txt */
   l=0;
   while (tempp[0]!='x')
   {
   strcpy(line,fgets (tempp,130, fpp));

      for (mm=0; mm<7; mm=mm+1)
         {dumqi[mm]=tempp[mm+62+deca];}

      for ( m=0; m<9; m=m+1)
      {
         dummypx[m]=tempp[m+71+deca];
         dummypy[m]=tempp[m+81+deca];
      }
```

```
      float_dummyppx[l]=atof(dummypx);
      float_dummyppy[l]=atof(dummypy);
      float_dumqi[l]=atof(dumqi);

            l++;
   }

/* energy calculation with rotation */
   fpc=fopen("/usr1/edy/3D/energy.txt","w");
fputs("Angle          energy \n", fpc);
o=0;
n=0;

for (angle=0; angle<sym; angle++)
{

/* printf("%i %i \n", angle, o);*/
angle_rad=(0+angle)*PI/(180*res);
total=0;
l11=cos(angle_rad);
l12=sin(angle_rad);
l21=-1*l12;
l22=l11;

   for (j=0; j<l-1; j++)

   {
   ksmin=1000;

      for (i=0; i<k-1; i++)
      {
        dumppx=l11*float_dummyppx[j]+l21*float_dummyppy[j];
        dumppy=float_dummyppx[j]*l12+float_dummyppy[j]*l22;

qqq=sqrt(float_dummyppx[j]*float_dummyppx[j]+float_dummyppy
[j]*float_dummyppy[j]);

         deltax=dumppx-float_dummypx[i];
         deltay=dumppy-float_dummypy[i];

         ks=sqrt(deltax*deltax+deltay*deltay);
/*        printf("%i %i %f \n", j, i, ks);
*/
```

```
            if (ks<ksmin)
            {
               ksmin=ks;
               jmin=j;
               imin=i;
            }
         }

        /* length=sqrt(dumppx*dumppx+dumppy*dumppy);
          printf("%i %f %f %f \n", j, dumppx, dumppy, length);
          */

         weigh=exp((alpha*qqq)-4)+1;

      kmin[n]=ksmin;
/*     en=(0.01/(float_dumqi[j]*kmin[n])) ;*/
       en=(0.1/(float_dumqi[j]*kmin[n]*weigh*weigh));

/* printf("qi= %i %f %f %f %f\n", j, float_dumqi[j],
float_dumqidec[imin], kmin[n], en);*/
/*     printf("%f", float_dumqi[j]); */

      total=total+en;
      }

      total_angle[n]=-total;
      o++;

      realangle=((float)angle)/((float)res);
      fprintf( fpc, "%f  %15.7f \n", realangle,
total_angle[n]);

      n++;
}

fputs("x", fpc);

fclose(fp);
fclose(fpp);
fclose (fpc);

}
```